DISSERTATION

DOCTOR OF PHILOSOPHY

EFFECT OF ATOMIC OXYGEN EXPOSURE ON SPACECRAFT CHARGING PROPERTIES

NOOR DANISH AHRAR MUNDARI

STUDENT NO.: 07586406

DEPARTMENT OF ELECTRICAL ENGINEERING

KYUSHU INSTITUTE OF TECHNOLOGY

2011

DISSERTATION

EFFECT OF ATOMIC OXYGEN EXPOSURE ON SPACECRAFT CHARGING PROPERTIES

SUBMITTED

IN PARTIAL FULFILLMENT OF THE REQUIREMENTS

FOR THE DEGREE OF

DOCTOR OF PHILOSOPHY

BY

NOOR DANISH AHRAR MUNDARI

SUPERVISED BY

PROFESSOR MENGU CHO

DEPARTMENT OF ELECTRICAL ENGINEERING

KYUSHU INSTITUTE OF TECHNOLOGY

2011

Dissertation

EFFECT OF ATOMIC OXYGEN EXPOSURE ON SPACECRAFT CHARGING PROPERTIES

By

Noor Danish Ahrar Mundari

(Student Number: 07586406)

Supervisor:

Professor Mengu Cho

Member of Dissertation committee:

Professor Mengu Cho

Professor Kazuhiro Toyoda

Professor Masayuki Hikita

Professor Yasuhiro Akahoshi

Kyushu Institute of Technology

Department of Electrical Engineering

I certify that I have read this dissertation and that in my opinion it is fully adequate, in scope and in quality, as a dissertation for the degree of Doctor of Philosophy.

……

Mengu Cho

(Professor, Electrical Engineering, Principal Advisor)

I certify that I have read this dissertation and that in my opinion it is fully adequate, in scope and in quality, as a dissertation for the degree of Doctor of Philosophy.

……

Kazuhiro Toyoda

(Professor, Electrical Engineering, KIT)

I certify that I have read this dissertation and that in my opinion it is fully adequate, in scope and in quality, as a dissertation for the degree of Doctor of Philosophy.

……

Masayuki Hikita

(Professor, Electrical Engineering, KIT)

I certify that I have read this dissertation and that in my opinion it is fully adequate, in scope and in quality, as a dissertation for the degree of Doctor of Philosophy.

……

Yasuhiro Akahoshi

(Professor, Mechanical Engineering, KIT)

Contents

Illustrations

Tables

Abstract

Spacecraft surface charging can lead to arcing and a loss of electrical power generation capability of solar panel, or even loss of a satellite. The charging problem may be further aggravated by the atomic oxygen (AO) exposure in Low Earth Orbit (LEO), which modifies the surface of materials like, Polyimide, Teflon, anti-reflective coating, cover glass, etc., used on satellite surface. These affect material properties, such as resistivity, secondary electron emissivity, photo emission, which govern the charging behaviour. These properties are crucial input parameters for spacecraft charging analysis.

This research develops a new facility at KIT, based on a novel technique for generating atomic oxygen flux involving laser induced breakdown of molecular oxygen. High velocity AO in an evacuated nozzle is formed, where laser beam breakdowns molecular oxygen into AO injected through a pressurized pulse valve into the nozzle. The energy of AO is measured using Time of flight (TOF) technique. The generated AO flux is measured using Quartz Crystal Microbalance (QCM). The Mass Flow Controller (MFC) inserted in oxygen gas supply line measures the net amount of gas being injected through pulse valve. The spectral analysis of AO production wavelength (777.6nm) is detected using a spectrometer. The relative abundance of generated species is observed using a Quadrupole Mass Analyzer System (QMAS). The developed facility produces AO of velocity 8~14 kms^{-1} having the flux in the order of 10^{18} $atoms/m^2/shot$. This flux is used to expose spacecraft surface materials for extended period of 10 years at 800 km, equivalent to exposure of satellite surface materials to atomic oxygen fluence for the normal lifetime of the satellite in orbit.

This thesis develops a new method and facility for the measurement of resistivity of atomic oxygen exposed polyimide by using surface charge decay method. The resistivity measurement is performed in vacuum using the charge storage decay method at room temperature, which is considered most appropriate for measuring the resistivity for space

application. The mathematical formulation and experimental facility are indigenously developed to measure resistivity as per space requirement. We introduce a new method to measure surface and volume resistivity together, which can be further improved to measure the secondary electron characteristics. The results show that the surface resistivity increases and the volume resistivity remains almost the same for the AO exposure fluence of 5.4x 10^{18}atoms cm^{-2} on polyimide film.

Acknowledgements

I would like to thank everyone who has supported me and assisted my academic carrier at Kyushu Institute of Technology for the last three and half years since July 2007.

First of all, I am thankful to almighty Allah for His blessings and Prophet Mohammad SAW for his guidance in my life.

The research described in this dissertation would not have been possible without the efforts of the many people who contributed to the development of atomic oxygen exposure facility, resistivity measurement facility and material analysis facility.

I would like to specifically thank my advisor Professor Mengu Cho for his encouragement, support and guidance during the course of this research. I would also like to specifically thank Professor Kazuhiro Toyoda for his participation in this research endeavour and his participation in my defence committee. His commitment to my dissertation is greatly appreciated, and his guidance and involvement in my doctoral program have been very educational. I would also like to thank Professor Masayuki Hikita and Professor Yashuhiro Akahoshi for their participations in my defence committee and their parts in reading and verifying this dissertation. I would like to thank Professor M. Tagawa, Kobe University for suggesting the solution of many difficulties in realising AO facility.

Since I cannot possibly list all persons who have helped me in some way during the course of these last three and half years, I would like to extend my appreciation to several groups of people. These include all members of the Kyushu Institute of Technology administrative and support staff that have assisted me in overcoming the hurdles of academia and my fellow students' friends who have helped in the course of this long engagement. In particular, I would like to thank several KIT Faculty & Staff, students, and friends for their encouragement and support, including Dr. Minoru Iwata, Dr. Arifur Rahaman Khan, Dr. Teppei Okumrua, Dr. Hirokazu Masui, Ms. Kumiko Shirakawa, Ms. Gotou Minako, Ms.

Matsuki Reiko, Mr. Yuta Sakamoto, Mr. Musasi Sakamoto, Mr. Yasunori Furukawa, Mr. Kyano, Mr. Takuya Hisashiba. I would like to extend very special thanks to Mr. Masaru Chiga, Master student of KIT, for his contribution in this research.

Special thanks to my friends at KIT, Dr. Hendra, Dr. Md. Atiqur Rahman Ahad, Dr. Ahmed Mohammed Galal, Dr. Umar Khayam, Dr. Nurkholis Hamidi, Dr. Mazen Zaqout , Dr. Li Changsong, Mr. Subhkan family, Mr. Budi Sugandi family, Mr. S.M.Ashik Eftakhar family, Mr. Cao Trueng Tue, Mr. Nguyen Duc Long, Mr. Myo Min Thein, Mr. Touamoua Nhialue , Mr. Chinda Rokhamsay, Ms. Shahera Hossain, Ms. Quynh Nga Pham, Ms. Zhang Yu, , Ms. Doan Thi Phuong, Ms. Chanpheng Lor for always making friendly environment.

Finally, I would like to express my special thank to my Late grandfather Professor Syed Salauddin Ahmad Ahrar and my Late grandmother Ms. Saleha Ahrar for all the inspiration which I derived from them to this stage. Special thanks are deserved for my parents Mr. Zayauddin Ahrar & Ms. Zohra Ahrar and sibling for their support and understanding throughout my graduate career. I would like to thanks Ms. Salma Ahrar for inspiring me to peruse overseas student life in Japan. I would specially like to thanks my brother Dr. Noor Aman Ahrar Mundari for his personal support and help with this dissertation and keeping me motivated. To my parents, I am indebted for their continuous support and faith in my success in many ways this degree would not have been possible without their assistance and love.

This research and my academic career have been supported by Japanese Ministry of Education, Sport, Culture, Science and Technology for providing fund to this research. Finally I would like to acknowledge, that financial support given to me by my thesis principal advisor Professor Mengu Cho was instrumental to carry out this research for so long at KIT.

Kitakyushu, February 2010

Noor Danish Ahrar Mundari

Chapter 1: Introduction

1.1 Statement of the problem

Spacecraft charging causes anomalous behavior on satellites, which in recent years became more severe due to increase in satellite power requirements[(1)-(3)]. The potential of the spacecraft, which is present in orbital plasma, is determined by a balance among various current sources to/from the spacecraft[(4)-(6).] A spacecraft placed in the plasma will assume a floating potential different from the plasma itself. Let's, analyze the situation of spacecraft in orbital environment by considering the Figure 1.1.

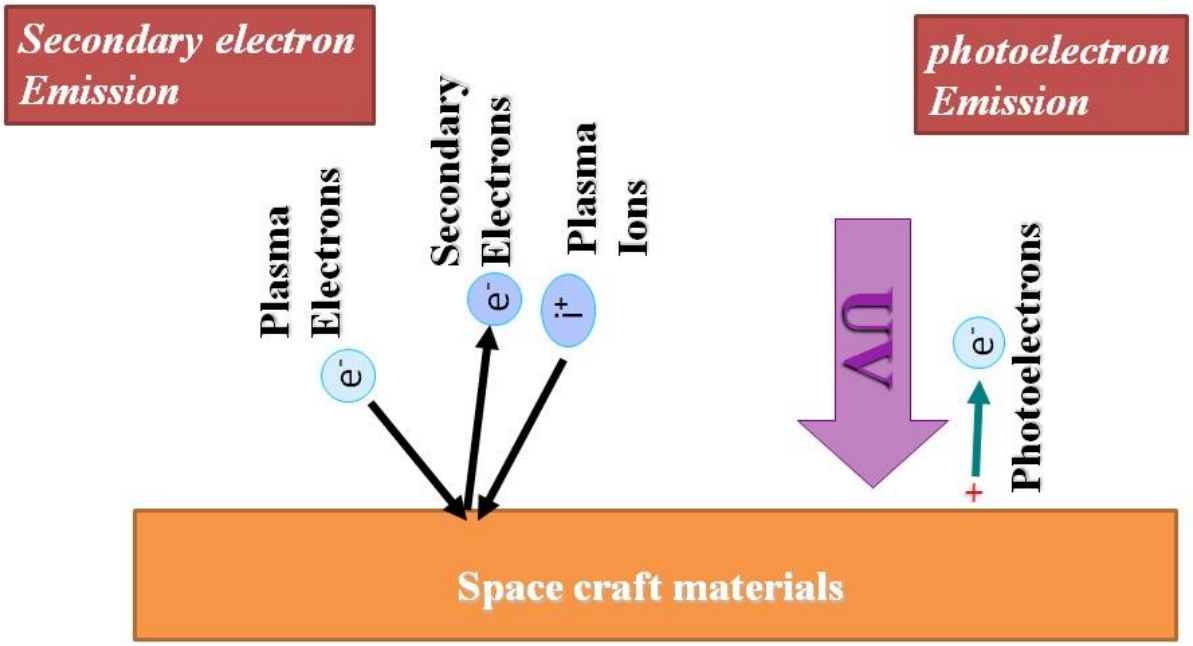

Figure 1.1: Spacecraft surface materials in orbital environment

In darkness, a spacecraft surface will tend to charge negatively from the ambient plasma electrons. The plasma is basically neutral, having equal numbers of electrons and ions; however, the electrons are much lighter particles, and therefore, move at higher velocities[(7:1)]. Hence the negative electron current to the spacecraft surface is greater than the positive ions. During sunlight, sunlight exposure provides photoemission, which can act as a charge drain

to neutralize the surface potential, or can act as a discharge trigger upon the emergence from the eclipse/shadow.

For geosynchronous orbit (GEO), the satellite surface exposed to sunlight charge to positive 2~3volt due to photoelectron current emitted from the surface. However, during eclipse, a negative surface potential is observed. Photoemission from the satellite surface is the principal source because of the presence of the extreme ultraviolet wavelength in the range (< 200A) in the same region where many materials have rather large photoelectric yields and the solar spectrum also has significant energy there. During eclipse, the spacecraft roughly charges to a negative potential equivalent to the electron temperature of the plasma. For shadowed dielectric or isolated surfaces, the potential may charge to negative 1 to 10kV from local electrons. Surface discharges are primarily caused by low energy electrons (up to a few tens of keV).

In low earth orbit (LEO), the thermal electron currents are the largest and satellites tend to be slightly negative. In addition, spacecraft charging is a function of the space environment characteristics like solar activity, geomagnetic storm, solar spectrum, etc[7:2,8]. The high voltage solar array is the primary cause for LEO charging.

In case of PEO, satellites are exposed to unique environment where the low energy ionosphere plasma (0.1~0.2eV) and particles of auroral zone (>1 keV) are mixed. This mixing of environment increases the possibility of charging severely, as observed in ADEOS-2 failure[2].

Spacecraft surfaces have insulators and conductors on its surface whose electrical properties are quite different. In general, all the metallic parts on spacecraft are interconnected. Insulator makes the major component of spacecraft surface exposed to orbital plasma environment. Where there is a boundary between insulator-conductor-space plasma

(called Triple junction) the phenomenon of Electrostatic discharge (EDS) is observed[9]. This ESD is dependent on the insulator potential, the spacecraft potential (metallic parts - connected to the spacecraft ground) and the thickness of the insulator. Although the potential difference between the spacecraft and the orbital plasma is important for the charging, it is the differential potential between insulator and the conductor that plays a significant role in surface discharge. The insulator surface develops a potential due to local balance of charge particle which is usually different from the conductor. When the insulator potential is positive with respect to spacecraft potential, it is called 'Inverted Potential Gradient' (IPG) and the opposite case is called 'Normal Potential Gradient' (NPG). These IPG or NPG will be determined by the orbital plasma and materials characteristics such as, surface resistivity, secondary electron and photoelectron which control the distribution or the development of surface potential of materials. In general, for LEO orbit with low inclination, IPG is usual condition; whereas, for high inclination orbits IPG or NPG can occur.

Thus we observe that, the potential of the spacecraft, that is present in orbital plasma, is determined by the photoelectron current, the secondary electron current and the current decay by surface or volume conductivity, which are material-dependent properties. Hence material's surface characteristics become very important factor in deciding the charging condition of spacecraft. Most of these properties of materials can be found in handbooks of materials for virgin materials. However, spacecraft charging analysis tool, e.g., NASCAP, MUSCAT simulate the charging condition for the entire life time of satellite or spacecraft. These tools need the material's parameters of not only the virgin materials but also of the aged materials. Here comes the effect of spacecraft environment and orbital environment which affect the surface of materials with the progress of time.

Atomic Oxygen (AO), predominant component of lower earth orbit (LEO) environment, is highly corrosive, combining with most materials they encounter[(10)-(12)]. In addition, a spacecraft's orbital velocity of 8km/sec has the effect of exposing a spacecraft to stream of AO at energy of approximately 5eV. Space flight experiments have demonstrated that many polymers, organic films, and composite materials undergo significant mass erosion and changes in the surface properties during the exposure to AO. These changes in surface properties of materials include the properties related to spacecraft charging, and make the prediction of spacecraft charging throughout the orbital life of a spacecraft very difficult.

For the reduction of the surface charging, the motion of the conducting electron and holes present in the insulator should be good enough to avoid the development of very large electric field on insulators[(13)]. Insulator discharge pulse begins to occur when the field strength in insulator is more than 1×10^5V/cm. Hence for reliable prevention of spacecraft charging problem, there should be sufficient conduction below a given limit. This conduction of hole and electron will take place on the surface of the insulator or on the bulk side dissipating charge on insulator. This distribution of charge will cause change in IPG or NPG condition. However, with the aging of the insulator surface and change in surface characteristics due to AO exposure on the surface materials will modify the behaviour of charge propagation on the surface and bulk of insulator. Thus AO exposure will readjust the potential condition of insulator and hence the whole system, as it will affect the triple junction charge balance also.

Thus some basic requirements are,

- Realisation of the facility that generates LEO atomic oxygen environment.
- Exposure of sample with atomic AO for same amount of fluence as satellite orbit in consideration.

- Measurement of resistivity of AO exposed sample as per space requirement.

1.2 Outline of the dissertation

This thesis deals with the effect of atomic oxygen exposure on spacecraft surface material polyimide in terms of the surface charging properties, in specific resistivity. In this thesis, we discuss the development of in-lab facility for simulating the atomic oxygen (AO) environment of lower earth orbit (LEO). We also discuss the development of measurement methods of the bulk and surface resistivities. Using the developed measurement method, this thesis discusses the effect of AO exposure equivalent to 10years in orbit at 800km on the resistivity properties of polyimide. We found that surface resistivity of polyimide increases by a factor of two after atomic oxygen exposure, and the volume resistivity remains the same. The result established in this thesis about the change of surface resistivity value of polyimide due to atomic oxygen exposure will be incorporated in a spacecraft charging analysis tool, named Multi-Utility Spacecraft Charging Analysis Tools (MUSCAT) developed by KIT and JAXA and is being used for designing Japanese spacecraft. The thesis consists of five chapters. They are briefly abstracted as follows:

Chapter 1: Introduction

This chapter first makes the statement of problem, what problem the author tries to solve and its impact. The author makes a thorough review on the previous work in the related field. The literature were reviewed about the effect of atomic oxygen on the surface materials, the simulation method of AO exposure on the ground, measurement method of charging properties, previous work on charging property change due to material degradation and concerning ideas. At the end, this chapter discusses the research motivation, the purpose of the study in brief.

Chapter 2: AO exposure facility and atomic oxygen characterization

This chapter describes the development of AO exposure facility based on the laser supported detonation (LSD) of a molecular oxygen flow. The facility was designed to generate higher atomic oxygen flux comparable to orbital condition, so that the desired exposure of 10years AO fluence can be carried out. The characterization of AO beam was done using a spectrometer which detected fluorescence dominated by 777.6nm, produced due to O(P)→O(S) transition. This chapter discusses the method to characterize the generated atomic oxygen energy and velocity based on Time Of Flight (TOF) technique. This chapter also discusses the measurement of atomic oxygen fluence using silver coated QCM and polyimide coated QCM. An equipment was developed to coat polyimide on QCM crystal which in turn is used for measuring fluence.

Chapter 3: Resistivity measurement of insulator and mathematical formulation

Measurement method of resistivity for space application is quite different from measuring resistivity for general application and it is still an evolving technique. In this chapter, we discuss the method to measure resistivity for the space application purpose. We introduce a new experimental method for the measurement of surface and volume resistivity based on surface charge decay principle. This method exposes one side of the insulator in vacuum to a charge source, with the metal electrode attached to both back and front sides of the insulator for measuring surface and volume resistivity. These charges deposited on the surface of the insulator diffuse on the surface and migrate downward. Surface potential drop data is obtained by capacitive coupling using a surface potentiometer. We also discuss the mathematical formulation for the development of the resistivity.

Chapter 4: Results and Discussion

In this chapter, we discuss the effect of AO beam on the silver and polyimide using the SEM imaging. The drop of the surface potential was analyzed in one-dimension and in two-dimensions using the surface potentiometer which scanned the surface at a regular interval of time. The potential drop pattern was analyzed and found to be consisting of two parts: the first part due to surface polarization of dielectric materials and the later part due to the flow of charge through the bulk and the charge diffusing on the surface of dielectric materials. The chapter also deals with the effect of AO exposure on the surface and bulk resistivity of the polyimide. Atomic oxygen exposure does not affect the value of volume resistivity. The value of surface resistivity is changed by a factor of 2 or more. This change in the surface resistivity is supposed to be due to the change in surface morphology which enhances the net length for the flow of charge on the surface due to increase in the roughness of the surface.

Chapter 5: Summary

This concluding chapter gives the conclusion of this thesis and future issues of this field. In the end of the dissertation, we include the appendix.

1.3 Literature Reviews

Space is often incorrectly thought of as a vast, empty vacuum that begins at the outer reaches of the Earth's atmosphere and extends throughout the universe[14:1,15,16]. In reality, space is a dynamic place that is filled with energetic particles, radiation, and trillions of objects, both very large and very small. Compared to what we experience on the Earth, it is a place of extremes, having large distance, and very high to low velocities, with large temperature difference for small distance. Charged particles, solar storms, photon and many outer space generated species continually move in space among which some have so much energy that they pass completely through an object in space. Magnetic fields can be intense which may govern the life of satellite and human existence on the Earth too. Above all,

environment in space is constantly changing. All of these factors influence the design and operation of the space systems. For this thesis, the literature are reviewed about the space environment, effect of atomic oxygen on the surface materials, the simulation of AO exposure environment on the ground, measurement method of charging properties, previous work on charging property change due to material degradation and others related aspects.

1.3.1 Space environment

Spacecraft operates and interacts with the atmosphere of space. This environment generates a limiting condition on the operation of the spacecraft, and under the extreme circumstances may cause the loss of spacecraft/satellite. The environment around the satellite can be grouped into orbits. In this dissertation, the major concern is with the space environment of Low Earth Orbit (LEO), Polar Earth Orbit (PEO), Highly Elliptical Orbit (HEO), and other satellites/spacecrafts passing through atomic oxygen environment of space.

Low earth orbit (LEO):

The Low Earth Orbit (LEO) satellites are those having orbits of an apogee of more than 100km and not more than approximately 1000km with inclination value below 65^{o} (Hasting). Most LEOs are nearly circular with eccentricity very close to zero. Considerable amounts of space debris are present in the higher altitudes of LEO above 700km. LEO also has residual atmosphere dominated by the atomic oxygen generated due to dissociation of molecular oxygen by Ultra Violet (UV) radiation present in solar spectrum. The plasma environment of LEO is cold with dense ionospheric plasma.

Polar earth orbit (PEO):

The polar Earth orbit satellites are those which pass near or on the top of the two poles having altitude of more than 100km and inclination of above 65^{o}. PEO therefore has an inclination of around 90 degrees to the equator. It also has residual atmosphere of earth

like LEO. The plasma environment of this region is different from the LEO due to presence of high energy particle.

Highly elliptical orbit (HEO):

Perigee of the HEO orbit also passes through the Earth residual atmosphere which has higher presence of atomic oxygen.

1.3. 2 Classification of space environments

The environment to which a spacecraft is subjected consists of the combination of the ambient (typically a function of the orbit) that generated by the spacecraft itself[(14:1)]. The combination of these environments may not be their simple sum but a more complex environment brought about by a synergistic, nonlinear interaction. The self-generated environment of a spacecraft will be substantially different from the ambient environment of the orbit, hence not always the primary orbital environment in consideration is characterizing the in-situ spacecraft environment, it is the generated environment which is also important and this varies with the design, fabrication materials of spacecraft and its interaction with the space environment for a certain period.

It is useful to characterize the environment in terms of four physical components[(14:1)]:

- The neutral environment,
- The plasma environment,
- The radiation environment, and
- The particulate environment.

The neutral environment includes the residual atmospheric gas and it is released by the spacecraft surface materials through outgassing or decomposition, deliberately vented from the spacecraft, or emitted during thruster firings.

The plasma environment includes the ambient plasma or that created by hyper velocity impact with the spacecraft surfaces.

The radiation environment has two components electromagnetic and corpuscular. The electromagnetic radiation environment includes the ambient solar photon flux that is reflected (and emitted) from the Earth, and the electromagnetic interference (EMI) is generated by the operation of spacecraft systems or arcing. It also includes electromagnetic waves generated by the plasma environment and photons emitted from spacecraft nuclear sources. The corpuscular radiation environment consists of the ambient flux of particles (Electrons, photons, heavy ions, and neutrons) and any high-energy particles emitted by nuclear sources or reactors.

The particulate environments consist of ambient meteoroids, orbital debris, and particulates released by the spacecraft. These are from a number of sources ranging from dust on the surfaces to materials decomposition under thermal cycling and exposure to ultraviolet radiation.

Interaction between the environments and a spacecraft: Each of the four environmental components can affect the design and operation of space vehicles or its systems. The effect may not be constant over time and will often change as the vehicle ages. Even on very short time scale (a fraction of orbital period), the effects of an environmental interaction may vary substantially.

1.3.3 Atomic oxygen in LEO

1.3.3.1 Formation and presence of atomic oxygen in LEO

AO is formed by the photo-dissociation of molecular oxygen O_2[17], as shown in Figure 1.2, initiated by the absorption of near solar ultraviolet (UV) radiation dissociating oxygen molecules (O_2) into free oxygen atoms (O) in the outer ionosphere for altitudes greater than

80km as shown in Figure 1.3. The orbits having atomic oxygen are LEO, PEO and HEO as shown in Figure 1.4. AO is the predominant species in LEO (below ≈ 1,000km) as shown in Figure 1.5. These neutral oxygen atoms have mean free paths of the order of 10^4 m at 400km, resulting in extremely low probabilities of re-association.

The density of the atomic oxygen in LEO varies with the altitude. Atomic oxygen density is highest in the range of 100 – 200km. This values goes on decreasing; however, atomic oxygen remains the dominant component as shown in Figure 1.6. Figure 1.7 shows the AO flux against the altitude for the City of Kitakyushu. This data is based on the AO density data downloaded from the MSIS model provided by NASA for March 2010 (Appendix 1). The density data needs to be converted in flux data with the necessary consideration on orbital velocity of satellite. In this data the x-axis represents the altitude and the y-axis represents the atomic oxygen flux in atoms$cm^{-2}s^{-1}$. This data is used for the calculation of total fluence a spacecraft surface will interact in its life time. AO's concentration changes as sunspot activity varies during the 11-years solar cycle. This effect must be accounted for if long-lived operation of the spacecraft system is to be expected.

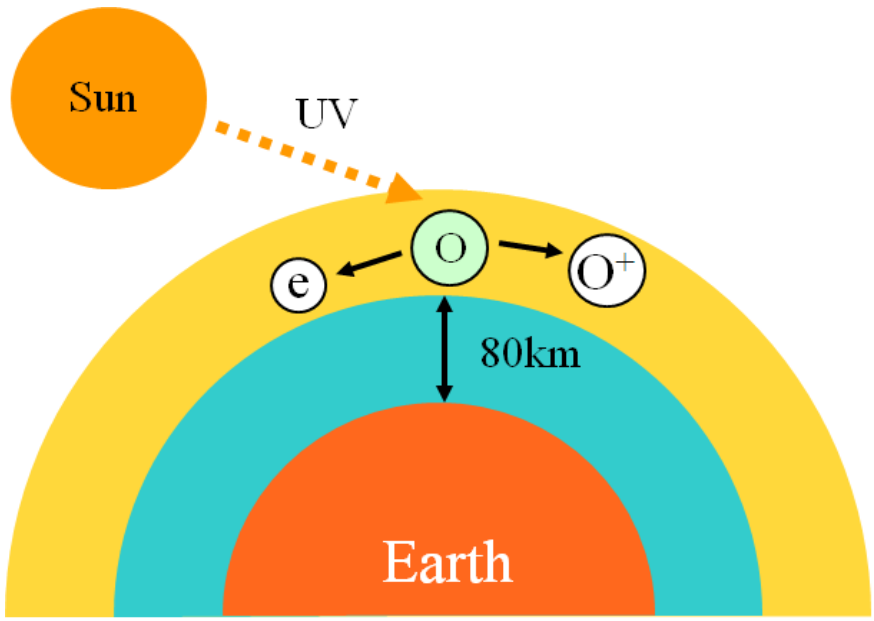

Figure 1.2 Formation of atomic oxygen in Lower Earth Orbit (LEO).

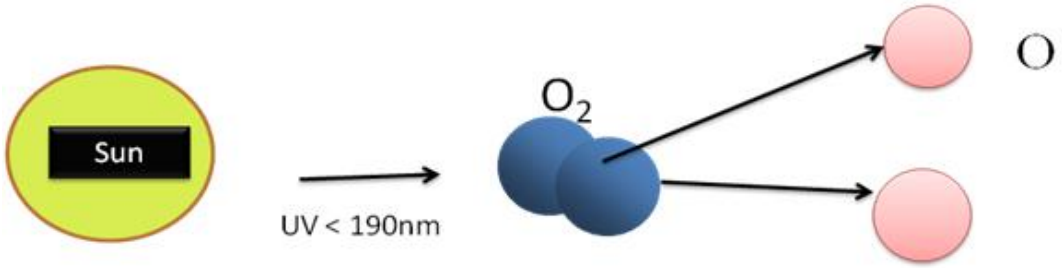

Figure 1.3: Dissociation of molecular oxygen into atomic oxygen by solar UV radiation.

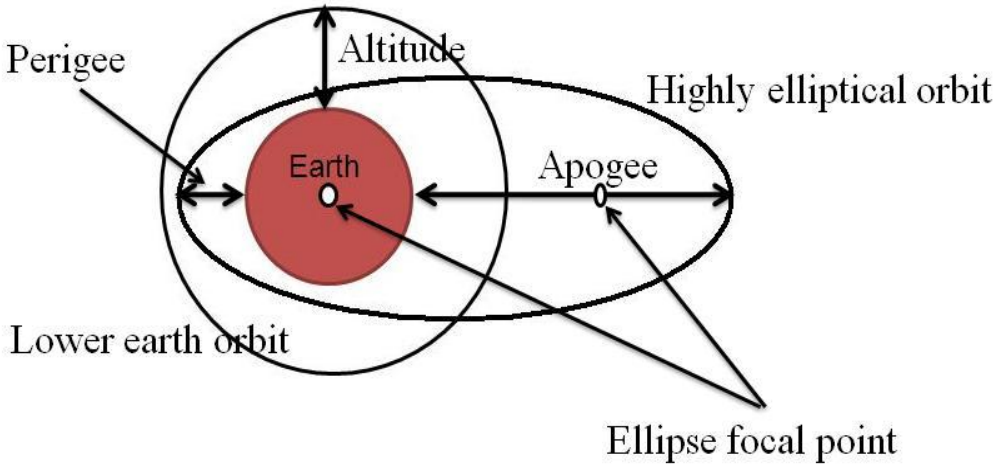

Figure 1.4: Orbits having atomic oxygen presence.

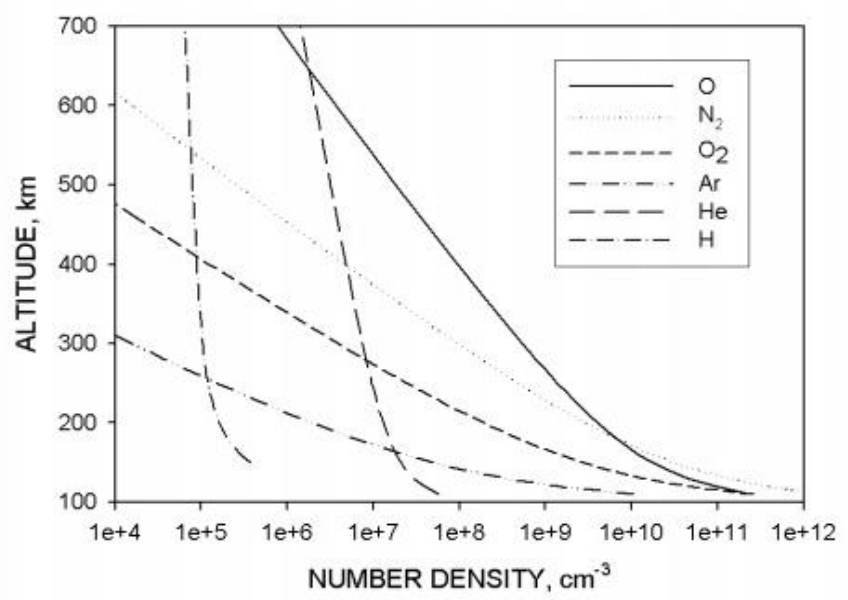

Figure 1.5: Density of atmospheric constituents as a function of altitude

(http://gltrs.grc.nasa.gov/reports/2004/TM-2004-213400.pdf)[18]

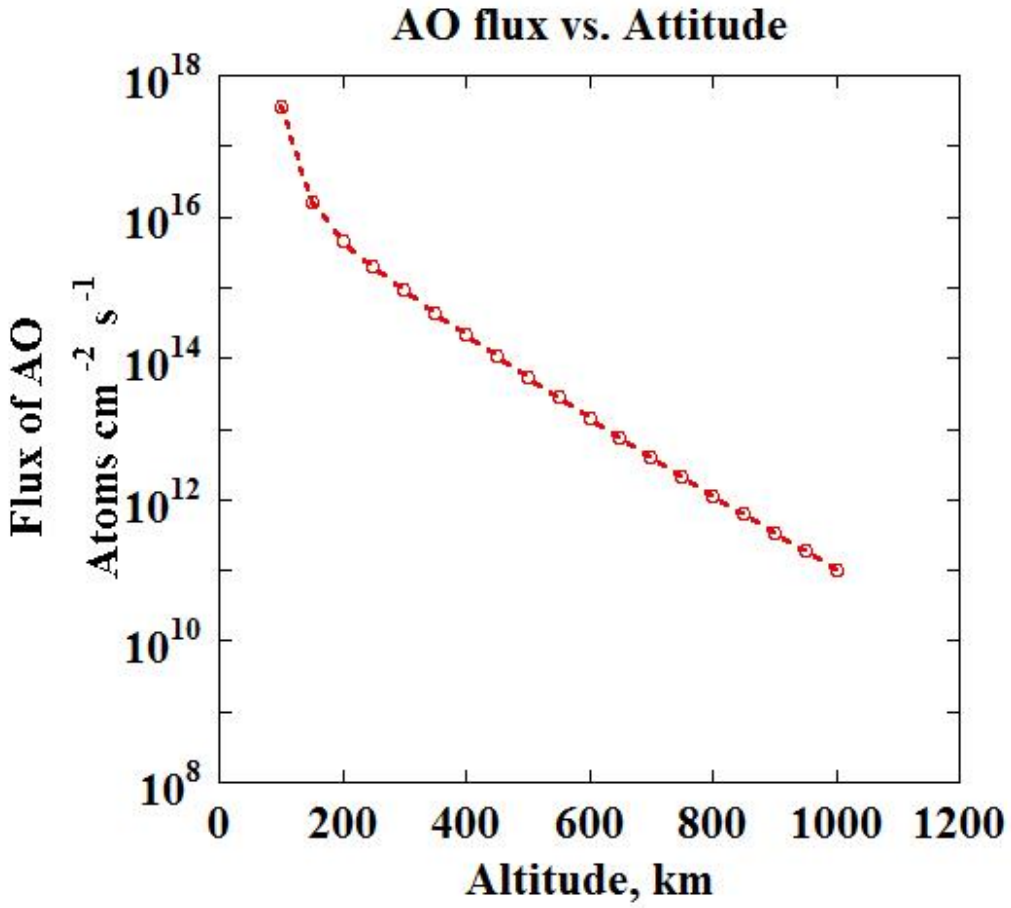

Figure 1.6: Flux of atomic oxygen against altitude for lower earth orbit satellites.

1.5.2 Principal of Interaction of AO with materials

Oxygen atoms are highly corrosive, combining with most materials they encounter. Recent space flight experiments have demonstrated that many polymers, organic films, and composite materials undergo significant mass erosion and changes in surface properties during exposure to AO[18]. In addition, a spacecraft's orbital velocity of 8km/sec has the effect of exposing a spacecraft to a stream of AO at the energy of approximately 5eV. The mass is lost and the surface properties change as the spacecraft collides at orbital speed (7.8km/sec) with AO within the Earth's upper atmosphere. The degree of surface degradation is directly proportional to AO fluence (total integrated flux). Fluence, in turn, is determined by several factors[19], including:

Spacecraft altitude: Oxygen populations decrease with greater altitude, although the density at different altitudes will vary with the solar cycle or radiation exposure.

Attitude: Surfaces in the ram or windward direction will be exposed the most, while the exposure decreasing by the cosine of the angle of incidence on surfaces away from the ram direction.

Orbital inclination: High inclination orbits expose spacecraft to greater cosmic radiation (near the geomagnetic poles and in the South Atlantic anomaly), which can have a synergistic effect with AO and possibly to longer periods of solar UV.

Mission duration: Longer missions mean longer exposure and the greater risk of failure due to AO or AO+UV erosion.

Solar activity: The Sun emits more UV and X-ray during solar maximum (sunspots are associated with magnetically active areas) which directly affect spacecraft surfaces and also expand the upper atmosphere, thus increasing AO populations at altitude.

Models are available on the internet through the NASA space Environments and effects program to estimate AO fluence. MSIS-E-90 is one such model which was used for the estimation of atomic oxygen fluence in orbits of interest in this thesis. From these, we estimate surface erosion.

AO by itself is extremely damaging, however, the other elements of the near-Earth space environment should not be ignored. The readers of this thesis should also keep in mind that the total, combined space environment may affect materials in a variety of ways. Optical properties (solar absorptivity and thermal emissivity) may change due to AO bleaching or UV radiation darkening. Polymeric films may peel due to thermal cycling. In turn, this opens new surfaces that can be attacked by AO or AO+UV[19]. The electrical conductivity of a material gets affected by AO which is the main investigation of this research hence resulting

in spacecraft charging[20]. The strength of the composite structures may degrade due to the AO erosion of resin binders. The AO effect can reduce the thermal capacity of thermal blanket.

1.3.3.3 Effect of atomic oxygen on materials in space flights

Polymers, such as Polyimide KAPTON® and Teflon FEP (fluorinated ethylene propylene) are commonly used spacecraft materials due to their desirable properties such as flexibility, low density, electrical properties, and in the case of FEP, a very low solar absorptance and high thermal emittance[21]. Polyimide has space environmental durability, low solar absorptivity (α), and sufficient electrical conductivity to mitigate static charge build-up. Examples of the use of polymers on the exterior of spacecraft include metallized FEP thermal control materials covering, Kapton solar array blankets and Teflon ePTFE (expanded polytetrafluorethylene) cable insulation on the International Space Station (ISS).

These polymers on the exterior of spacecraft are exposed to atomic oxygen (AO) in the low earth orbit (LEO) environment. The average energy of an oxygen atom impacting spacecraft at ram velocities is 5eV. Recent research has shown the scattering of atomic oxygen on the ram surface happen and one needs to be careful to calculate net fluence considering the scattered atomic oxygen for a particular geometry of spacecraft[22].

With the energy of 5eV, number of processes can take place when an atomic oxygen strikes spacecraft polymeric or metallic surface. These include chemical reaction with surface atoms or adsorbed molecules, elastic scattering, scattering with partial or full thermal accommodation, recombination, or excitation of ram species[18]. Because the oxidation product for most polymers is a gas, AO erosion of polymers in LEO is a serious threat to spacecraft durability[21]. For example, more than 0.0127cm (0.005″) thickness of Kapton and Mylar sheets were eroded away after 5.8years in LEO on the leading edge, or ram AO

surface, of the Long Duration Exposure Facility (LDEF). The AO fluence for the leading edge of LDEF was 8.99x 10^{21}atoms/cm^2. A cone-like or carpet-type morphology is developed, which is the characteristic of directed AO erosion for materials with gaseous oxidation products, as shown in Figure 1.7. The atomic oxygen erosion for fixed direction arrival with all materials that have volatile oxides is such that it causes the surfaces to erode to produce left-standing cones which represent a small fraction of the erosion depth[18]. Protective coatings can be effective in preventing AO erosion, yet oxidation erosion of the underlying polymer can occur at pinhole and can scratch defects through AO undercutting erosion.

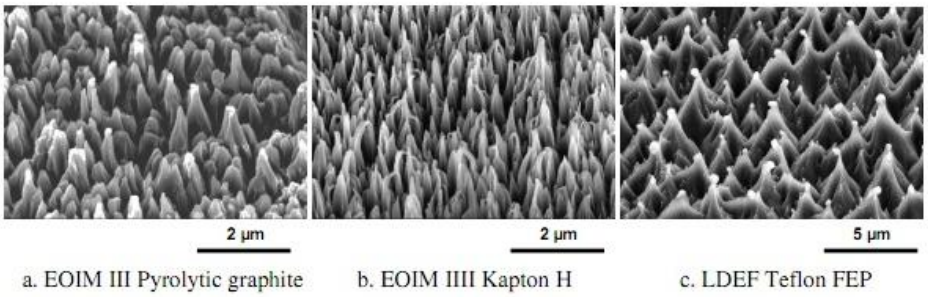

Figure 1.7: Scanning electron microscope images of pyrolytic graphite, polyimide Kapton and Teflon FEP exposed to directed LEO atomic oxygen on EOIM III or the LDEF. (http://gltrs.grc.nasa.gov/reports/2004/TM-2004-213400.pdf)[18]

Apart from the physical degradation to the structural ability of the polymers, such as for the support of photovoltaic cells on solar array, AO is a threat to other materials' properties. The polymer used for the thermal control due to their thermal emittance characteristics can lose its efficiency due to the change in the thickness of the polymer. Thus erosion of the polymer by AO can result in a reduced thermal emittance capability, which would give rise to increases in spacecraft temperature. It is, therefore, essential to understand the AO erosion

yield (E, the volume loss per incident oxygen atom) of polymers being considered in spacecraft design.

In addition to change in these physical properties, atomic oxygen can also modify the electrical properties as well as chemical properties of the surface. The change in electrical properties will be discussed in different sections of this thesis.

Different methods have been established for simulating the laboratory-based AO environment to carry out interaction evaluation of materials for space applications. Although ground laboratory procedures have been established and are used for erosion yield determination, actual in-space data is more reliable, and therefore, more desirable than results of ground tests. The National Aeronautics and Space Administration (NASA) of US, Japanese Space Agency (JAXA) and Russian space agency (ROSCOSMOS) have been exposing different polymers to the LEO environment on the exterior of the ISS. MISSE is a passive materials flight experiment sponsored by NASA, as shown in Figure 1.8 and 1.9. Most of the data related to the behaviour of materials in the AO environment are obtained from experiments aboard, the U.S space shuttle, LDEF, Russian Mir station and currently from the International Space Station.

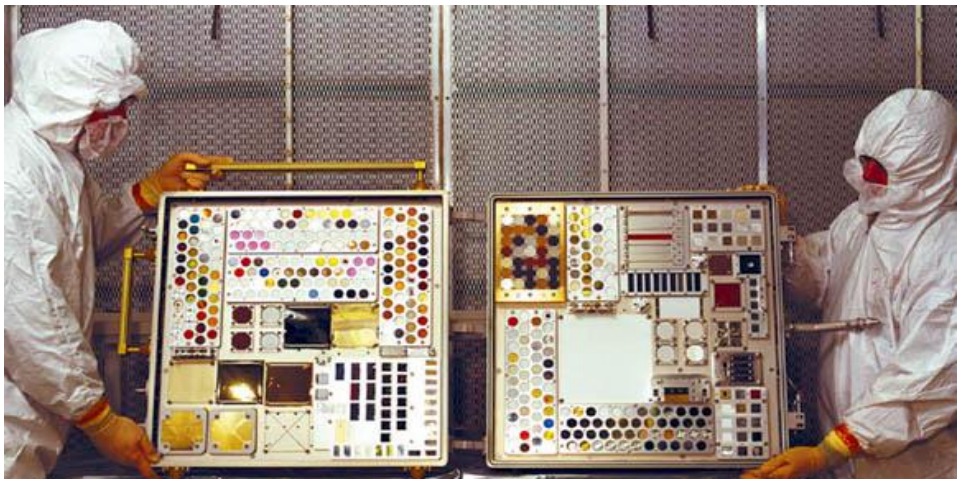

Figure 1.8: MISSE project specimens are placed onto trays and inserted into Passive Experiment Containers (PECs). www.nasa.gov/centers/langley/news/factsheets/MISSE.html

Figure 1.9: MISSE experiments being carried out at ISS in space

(www.nasa.gov/centers/langley/news/factsheets/MISSE.html)

1.3.4 Ground-based atomic oxygen facility

It is quite difficult to make facilities for generating atomic oxygen which produce same effect as the space atomic oxygen. However, there are a few famous methods for producing atomic oxygen source. Some of these are listed below:

- Atomic oxygen source with compact ECR plasma[24].
- Atomic oxygen source based on chemical reaction between nitrogen atoms with nitric oxide to produce, beside atomic oxygen, molecular nitrogen[25].
- Atomic oxygen flux by extracting atomic oxygen ions from Hall Effect ion source thrusters and then de-ionizing[26].
- Atomic oxygen source based on cold cathode ion source[27].
- Atomic oxygen source based on laser supported detonation (LSD) of molecular oxygen flow [28, 29].

Most of the facilities used across the world such as, like NASA, ESA, JAXA and Kobe University are based on the laser induced dissociation. Some of the facilities, especially the Beijing Institute of Satellite Environmental Engineering (BISEE) is based on the Electron Cyclotron Ion Source (ECR). The other facilities are scattered around the world.

The facility built at KIT is based on Laser Supported Detonation (LSD). The conceptual theory of this method was developed by Physical Science Incorporation (PSI), USA and was realised by Caledonia *et al.* at PSI.

It has been experimentally proved that the atomic oxygen effects in a ground-based facility are sometimes very different from those exposed in low Earth orbit (LEO). This difference has often been attributed to a synergistic reaction between atomic oxygen and vacuum ultraviolet radiation present in many ground-based atomic oxygen facilities[30,31]. Tagawa *et al.* have shown enhanced erosion rate for Fluorocarbon Polymers; however, they have shown that enhancement is relatively small. Energy and presence of charged species also play a role in this observed difference in erosion yield. It was found that each polymer appears to have atomic oxygen synergistic effects with different components of the environment[32,33]. Ground testing using the expected space environment components, and the development of correlation factors to relate the ground test to a particular mission environment, are important for space material durability and charging requirement.

1.3.5 Spacecraft charging and its analysis

For a satellite, the electrical conductive nature of the surrounding plasma results in the charging of the surface. The plasma component of the environment represents a current flow to the spacecraft skin and the exposed parts. Charging of the surface happens mainly due to the difference between the ambient electron and ion fluxes from the plasma. Electrons move faster than ions because of their mass difference, and therefore, the ambient electron flux is

often much greater than the ambient ion flux. Intrinsic imbalances in this current flow result in the build-up of charge on all surfaces exposed to the plasma. For typical surface areas, charging takes a few milliseconds to come to equilibrium. The time is longer for differential charging[5]. At LEO altitudes, charging is at low level, tens of volts, only unless high voltage solar array is not used[4]. This happens as the ambient plasma in this region is dense and not energetic. If the surface potential tries to increase, the opposite charges would be attracted in abundance to prevent any high potential formation[4]. Since the ions in LEO are slower than a spacecraft, there is a void of ions in the spacecraft wake, where the potential tends to be negative. The only significant natural charging region in the LEO environment is the auroral zone where the electrons are often directional and energetic.

Since different surface materials have different properties, such as secondary and backscattered emissions, photoelectron and resistivity characteristics, a spacecraft covered with different pieces of surface materials may suffer from differential charging.

For LEO Spacecraft, which has strong magnetic field, charging may be induced by the motion of the spacecraft across the geomagnetic field which introduces anisotropies. The anisotropy induced by the magnetic field means that the spacecraft can easily collect electrons from the direction of **-V** and from the direction of **B** but not from the **V X B**[14:2].

The current flow to the spacecraft also may be significantly modified by the electric fields generated by a high-voltage power system exposed to the space environment, electron and ion beam, exposed high potential junction, highly biased electrode and plasma contractors.

The differential charging can produce potential gradient between electrically isolated surface of the spacecraft and relative to the spacecraft ground and space plasma. The build-up of differential potentials on the surface of the spacecraft or on the power system can give rise to destructive arc discharges or micro-arcs which generate electromagnetic noise and

erode surfaces. Surface erosion from the surface of satellite contributes to the gas and dust environments near the spacecraft which generate new current balance.

For highly biased solar arrays in LEO plasma, the arcing for conventionally designed solar cells is so severe that it destroys the array. The space station solar arrays were chosen to operate at 160volts to stay comfortably below an empirically determined arcing threshold of 200volts.

The passive way of charge mitigation are sharp spike, conducting grid, semi-conducting paints, high secondary electron yield; whereas the active way to mitigate the effects of surface charging is hot filament, electron beam, ion beam, plasma emission, evaporation, and metal based dielectric on the spacecraft[(5)]. The dense plasma supplies the charge required to neutralize the differential charge build-up on the surface and to balance the currents due to the ambient plasma while maintaining a desired frame potential. Thus the central theme of spacecraft charging is how spacecraft interacts with the plasma environment to cause charging. Spacecraft accumulates charge and adopts potential in response to the interaction with plasma environment.

Material properties are significant area of difficulty for spacecraft charging because of the uncertain or no-standardized properties. Even simulation tools for spacecraft charging, like MUSCAT, are not certain because of the sensitive nature of the material properties and their electrical characteristics. The key parameters in modelling spacecraft charging are the electron emission properties of insulating materials such as,

- Surface and bulk resistivity of metal and insulating materials
- Secondary electron emission (SEE) coefficient, and
- Photoemission (PE)
- Backscattered electrons

These parameters determine how much charge will accumulate in key spacecraft components in response to incident electron, ion, and photon fluxes. We will discuss each one in some details.

1.3.6 Surface and bulk resistivity for space application and LEO atomic oxygen effect

American Standard for Testing of Materials (ASTM) method of resistivity measurement does not provide the resistivity values of very high resistant materials correctly. Further the duration of the data collection is quite short and hence the primary current used to determine the resistivity are caused by the polarization of the molecules by the electric field. NASA handbook 4002, NASA technical paper 2361, and other documents for spacecraft design advice the use of slightly conductive insulator is preferred to mitigate spacecraft charging. However, it is difficult to find valid measurements for the conductivity of the insulating materials during service in the space environment. Ohm's law provides a common perspective for predicting particle currents in spacecraft insulator, but it is not sufficient[(35)]. Instead, one must consider the generation of mobile electrons and holes, their trapping, thermal de-trapping, mobility, and recombination. J. R. Denssion *et al.* have done some great work in the field of resistivity measurement for space application. They gave a plot of decay time as a function of resistivity based on $V(t) = V_0 e^{-t/\tau}$ or , $\sigma(t) = \sigma 0\ e^{-t/\tau}$ with $\tau = R\ .\ C$, where, V_0 and σ_0 are the initial voltage or charge density respectively for parallel-plate capacitor model. This plot (in Figure 1.10) gives idea about the safety in designing the satellite. Based on the above concept, plot of resistivity against the decay time for the charging safety condition is shown in Figure 1.10.

Considering these results, marginally dangerous conditions begin to occur for materials with resistivity in excess of ~ $10^{16}\Omega$cm with $2 < \varepsilon_r < 4$, when τ exceeds ~1hours. More severe

charging condition occur for $\rho \cdot \varepsilon_r \geq 10^{18}\Omega$cm, when decay time exceeds ~1 days[35]. The method of resistivity measurement can be classified into two categories:

A. Classical Methods: Classical methods measure thin-film insulator resistivity based on parallel-plate capacitor method. This method determines the conductivity of insulators by applying a constant E-field. The presence of two conducting surfaces, the charge and E-field profile, and the charge injection method differ from typical spacecraft scenarios. Hence this method cannot be accepted as the true case of the space. Also, the classical methods ignore the fact that resistivity continues to change over long time periods as the material responds to the applied electric field and the accumulated charge distribution. The durations of standard test are short enough when primary currents used to determine resistivity are often caused by the polarization of molecules by the applied electric field rather than by charge transport through the bulk of dielectric. In order to reduce the influence of the polarization condition on the resistivity values, testing should be done for much longer periods of time under well-controlled vacuum environment, so that accurate observation of the more relevant charged particle transport through a dielectric material is possible.

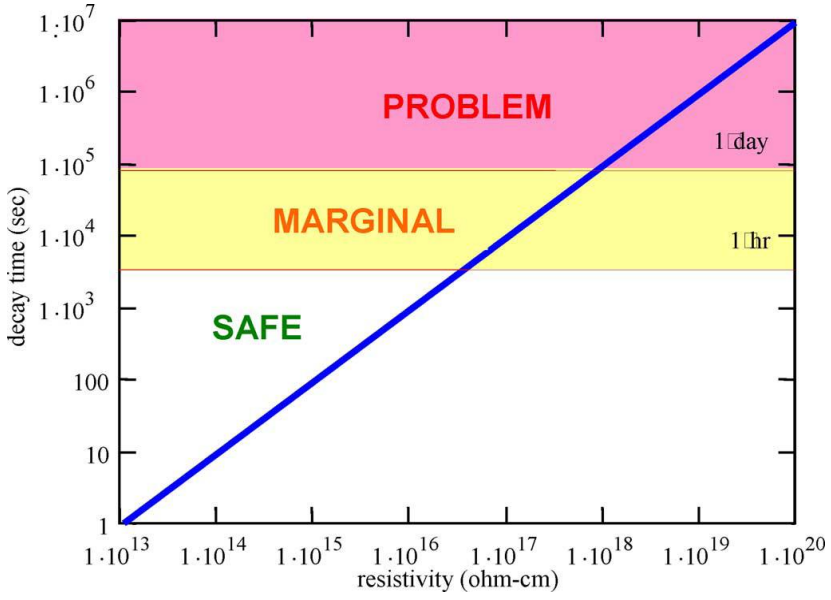

Figure 1.10: Decay time as a function of resistivity based on a simple capacitor model[35].

B. Charge Storage Method:

The charge storage method was developed by Frederickson *et al.* and others to measure the resistivity in a more applicable configuration[35]-[37]. In this method, charge is deposited near the surface of an insulator and allowed to migrate through the dielectric to a grounded electrode; with this configuration one can measure volume resistivity. The charge on the surface can decay by the following mechanism; neutralization by gaseous ions generated in pair by natural background radiationr, surface conduction (which is highly dependent on condition of surface and surrounding environment), charge injection into the bulk and charge trapping and de-trapping process, volume conduction[36]. The microscopic details of this method can be found in the works of Denision *et al.* and M. Debska[38].

We introduce further modification to measure surface and volume resistivity together by allowing the diffusion of charge on dielectric surface as well as its migration through the materials. This thesis focuses on the change in resistivity properties of polyimide which is predominantly used on satellite surface for thermal control purpose.

The interaction of the LEO atomic oxygen with the outer surfaces of a satellite can result in materials degradation by modifying their chemical, electrical, thermal, optical, mechanical and charging properties. Thus atomic oxygen influences on how charge will accumulate and redistribute across the spacecraft's AO-modified surface, as well as the timescale for charge transport and its dissipation.

1.3.7 Secondary electron emission (SE) coefficient measurement

The energy of the electron beam in space varies from several electron volts to several kilo electron volts. The satellite will interact with these electrons depending on the orbits in which they are placed. Secondary electrons (SEs) are those electrons, which were initially part of

the valence or core levels of the material and have been excited to escape the materials under the primary electron (PE) beam from the space plasma (Electrons).

The Secondary Electron Yield (SEY) δ (E) of a surface material is not only a function of primary energy and incident angle but also on the surface condition such as physical features, the chemical composition, the lattice structures, the dose of electrons or ions deposited, the surface temperature, the thickness of layers, surface smoothness or coarseness[(34)]. Here δ(E) depends on the incidence angle of the primary electrons. For a coarse surface, the incident angle varies from one point to another on the surface. For surfaces with grooves, the groove walls can partially re-absorb the secondary electrons emitted from by the depth of the grooves. If the material is very thin, secondary electrons can come out not only from the front side but also from the back side[(34)]. In the case, where very thin materials are used on the surface, the primary electrons can penetrate the top layer and influence underneath layer which may have different material properties. The effect of the temperature of the surface will also affect on SEY.

Long time bombardment by atomic oxygen, other gas species, energetic ambient electrons and ions will affects the surface morphology, surface chemical composition, and lattice structure near the surface. Atomic oxygen can cause the surface erosion as well as chemical reaction, whereas protons and ions can cause sputtering by knocking out neutral atoms. The knocked out materials from one part can settle in another parts. Energetic electron penetration into dielectrics can cause build up of significant internal electric fields, depending on the dose and fluence. All these will affect the value of secondary electron emission with time. Hence the SEE emission yield of the satellite surface materials will be a time dependent function.

1.3.8 Photoemission measurement

The presence of solar radiation of all wavelengths can also have strong influence on the surface charging of satellite. The three primary interaction of photon with the materials are photoelectric effect, Compton scattering and pair production. In photoelectric effect, photons of sufficiently low wavelength present in solar spectrum eject electron from the surface of materials. Photoelectrons are emitted when a single photon of energy '$h\nu$' is absorbed by the solid. Photoelectron coefficient varies according to the nature of materials. The energy of the photon must be larger than the energy separation between the top of the valence band and the vacuum level. For metal, this energy is the work function. In the case of insulators where the Fermi level is not defined, photoelectron threshold is just the energy between the most weakly bound electron state and the vacuum level.

The phenomenon of photoemission is one of the method by which satellite can have charging of its surface depending on the photoemission coefficient of materials surface. The change in surface morphology will affect the photoemission coefficient of the materials. Hence the effect of atomic oxygen on the surface may modify the photoemission coefficient of materials, while changing the charge balance of the surface with space plasma, which can cause generation of differential charging condition also.

Photoemission from surfaces depends not only on the surface material but also on the surface condition[34]. The photoelectron yield $Y_{ph}(R)$ per incoming photon decreases as the reflectance R increases.[34]

$$Y_{ph} = (1- R(\omega))Y_{ph}(0, \omega)$$

R is a function of the photon frequency ω. If there is no reflectance, every incoming photon is absorbed. With a finite R, some photons are reflected, resulting in less energy

transfer from the incident light to the surface material. The photoelectron flux $J(R)$ generated from a surface is given by

$$J(R,\omega) = J(0,\omega)(1-R(\omega)) = I(\omega)\, Y_{ph}\, R(\omega)$$

Where, $$J(0,\omega) = I(\omega)\, Y_{ph}(0,\omega)$$

Here, $I(\omega)$ is the incident light intensity. Varying the photoelectron current I_{ph}, the spacecraft charging calculations would be affected. Surfaces with deep grooves emit less photoelectron than smooth surfaces. Though the incident photons may be well absorbed by the material, the photoelectrons generated from the deep grooves may be re-absorbed by the walls of the grooves. A highly reflective surface generates little or no photoemission.

If a highly reflective surface is located next to a non-reflective one, the difference in their photoemissions renders differential charging between the surfaces in sunlight. In turn, differential charging may cause a sudden discharge, which may cause satellite anomalies or failures. Further, difference in SEY and photoelectron yield will cause differential charging between two different insulators and even for same insulator with different surface condition. For spacecraft charging simulation tools, such as MUSCAT, it is insufficient to use a value of the photoelectron yield and secondary electron yield of virgin materials for entire time of satellite in orbit. The knowledge of surface condition with the progress of time is essential-hence the modified values of SEY and photoelectron yields are required.

1.3.9 Backscattered electrons

When the electron beam strikes the material surface, some of the electrons will reverse the direction and will backscatter from the materials, much in the same way as space craft interact with the gravity of a planet. Electron are attracted to the positive nucleus but if the angle is just right instead of being captured it will circle the nucleus and come back out of the

materials without slowing down. These electrons are called backscattered electrons because they come back out of the materials.

The effects on backscattering due to surface coarseness and contamination need to be understood [34].

1.3.10 Spacecraft charging property database

Figure 1.11 depicts the ratio and origin of satellite losses. From the figure, ESD accounted for more than 50% of all satellite accidents.

Some spacecraft charging analysis tools were developed to analyse the pre-launch feasibility of spacecraft/satellite in orbits. They are designed to analyse the space environment with given structural and material properties of satellite/spacecraft in question. One such spacecraft charging analysis tools is NASCAP for NASA. Japanese Space Agency (JAXA) in collaboration with KIT developed Multi-Utility Spacecraft Charging Analysis Tools (MUSCAT) that provides charging analysis for Japanese spacecraft/satellites. This MUSCAT needs materials parameters of virgin as well as aged materials. So, the need for the database of materials property is felt.

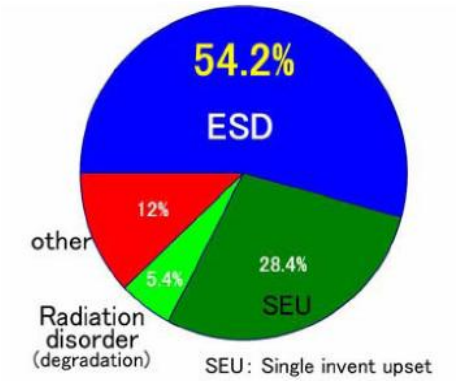

Figure 1.11: Satellite obstructions due to space environment. This statistics had been researched by Koons et al. (during the period form1973 to 1997)[39].

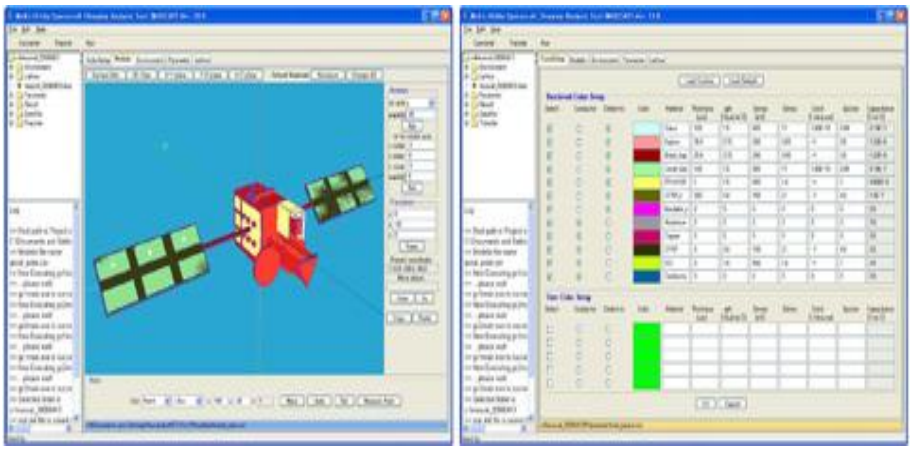

Figure 1.12: Spacecraft charging tools MUSCAT; inputting the values of materials' parameters for simulating spacecraft charging condition.

Resistivity is a key material parameter input for analytic spacecraft charging model, such as MUSCAT, developed by KIT/JAXA, shown in Figure 1.12. Especially, we focus on how to measure the resistivity for space application.

1.4 Research Motivation

Since the late 1990s, the size of telecommunication satellites has increased drastically as a demand of more communication capacitance and increase of satellite TV channels. To save the launch cost by keeping the number of launches low, the number of transponders per satellite was increased. Satellite power level has been also increased. Now-a-days, major commercial telecommunication satellites consume power larger than 10kW. To manage the large power efficiently, photovoltaic generation and transmission voltage were also increased. Satellite bus voltage has increased to 100V from 50V that was used commonly for previous satellites in 90s or before.

As the satellite voltage was increased, accidents on solar array occurred very frequently. The accidents were mostly due to arcing and subsequent short circuit of array circuit. The accidents were also not limited to GEO (Geosynchronous Earth Orbit). Polar Earth Orbit

(PEO) satellites also suffered the accident; one example was the total loss of Japanese satellite ADEOS- 2 in 2003.

The central theme of spacecraft charging is how spacecraft interacts with the plasma environment to cause charging. Spacecraft accumulates charge and adopts potential in response to interaction with the plasma environment. The key parameters in modelling spacecraft charging are the electron emission properties of insulating materials, such as Secondary Electron Emission (SEE) coefficient, Photo Emission (PE), and surface and bulk conductivity of metal, and insulating materials used on the surface of satellites/spacecrafts. These parameters determine how much charge will accumulate in key spacecraft components in response to incident electron, ion, and photon fluxes. It has been recognized that atomic oxygen present in LEO is one of the most important hazards to the spacecraft polymeric material resulting in modifying the surface properties of the materials. Thus the interaction of the LEO's atomic oxygen with the outer surfaces of a satellite may result in material's degradation, modifying their chemical, electrical, thermal, optical and/or mechanical properties. This influences how charge will accumulate and redistribute across the spacecraft atomic oxygen modified surface as well as the time-scale for charge transport and dissipation.

1.5 Purpose of Study

This thesis focuses on the change in resistivity properties of polyimide, predominantly used on satellite surface due to lower earth atomic oxygen exposure. Resistivity is a key material parameter input for analytic spacecraft charging model, such as MUSCAT, developed by KIT/JAXA. Special focus is on how to measure resistivity for space application. To measure the resistivity of spacecraft insulator materials, the charge storage method developed by Frederickson *et al.* is the most suitable configuration in space type environment. In this method, charge is deposited on the surface of an insulator and is allowed

to migrate through the dielectric. With this configuration, one can measure volume resistivity. This dissertation introduces further modification to measure the surface and volume resistivity together by allowing the diffusion of charge on dielectric surface as well as its migration through the materials. In the present work, we discuss a laser detonation source which produces LEO-type atomic oxygen environment having less than 10eV similar to LEO. After the degradation of spacecraft surface materials due to exposure, surface properties like bulk and surface resistivity are measured. A comparative study between the exposed and virgin materials will give more accurate prediction of charging and arcing process on spacecraft.

1.6 Scope of study

We will use these data for the spacecraft charging and arcing simulation tool MUSCAT, developed at our laboratory. This will make more accurate and precise prediction of charging and arcing condition for spacecraft throughout its lifetime.

Previous researchers faced obstacles in exploring the charging characteristics of atomic oxygen modified materials because of the lack of a reliable reference and scarcity of research work done in the field of charging characteristics of surface modified by atomic oxygen and space environment. The development was further handicapped by the high cost and difficulty in simulating atomic oxygen environment in laboratory and other charging characterisation facilities.

Both of these obstacles are successfully solved in this research in term of the experimental achievement.

In this research, we first discuss the development of atomic oxygen facility, and then we present the technique for measuring the surface and bulk resistivity of atomic oxygen

exposed sample, along with the necessary mathematical formulation used for calculating resistivity which can be further improved to measure secondary electron characteristics.

1.7 References

1. Cho M.: Failure Mechanism and Protection Method of Spacecraft Power System, Proceedings of International symposium on Electrical Insulating Materials, Jan 5-9, 2005, Kitakyushu, Japan, pp. 45-48.

2. Maejima H., Kawakita S, Kusawake H, Takahashi M., Goka T, Kurosaki T., Nakamura M., Toyoda K., and Cho M: Investigating the Power System Failure of a LEO Satellite, 2nd international Energy Conversion Engineering Conference, 16-19 Aug, 2005. AIAA 2004-5657

3. Hatta, S., Muranaka, T., Kim, J., Hosoda, S., Ikeda, K.., Kurhara, N., Cho, M., Ueda, H., Koga, K. and Goka, T.: Accomplishment of Multi-utility Spacecraft Charging Analysis Tool (MUSCAT) and its Future Evolution, Acta Astronautica, Vol. 64, No. 5-6, 2009, pp. 495-500.

4. Shu T Lai: A Survey of Spacecraft Charging Events, AIAA-98-1042, 36th Aersospace Science Meeting & Exhibit, US, 1998.

5. Shu T. Lai, A Critical Overview on Spacecraft Charging Mitigation Method, IEEE Transaction on Plasma Science, Vol. 31, No. 6, 2003, pp. 1118-1124.

6. Linkar J. J., and Bogorad A.: Solar Array Plasma Interaction: Influence of Inter Connector Shape on Primary Arac Parameters, Journal of Spacecraft and Rockets, Vol. 45, No. 5, Sep-Oct 2008, pp 928-934.

7. (1: 2) Vincent L. P.: The Space Environment and its Effects on Space System, AIAA Education series, ISBN 978-1-56347-926-7. Chapter 8, pp (1) 207-208: pp (2) 227-239.

8. Cho M.: Surface Discharge on Spacecraft, AIAA report- to be published.

9. Hirokazu Masui, Tomoki Kitamura, Teppei Okumura, Kazuhiro Toyoda and Mengu Cho: Laboratory Test Campaign for ISO Standardization of Solar Array ESD Test Methods, 45th AIAAA Aerospace Sciences Meeting and Exhibit, 8-11 January 2007, Nevada, AIAA 2007-277.

10. I L Harris, A R Chambers and G T Roberts: Preliminary Results of an Atomic Oxygen Spaceflight Experiment, Materials letter 31, June 1997, pp. 321-328.

11. Reddy, M. R.: Review Effect of Low Earth orbit Atomic Oxygen on Spacecraft Materials, Journal of Materials Science, Vol. 30, 1995, pp. 281- 307.

12. Chambers A. R., Harris I. L., and Roberts G. T.: Reaction of Spacecraft Materials with Fast Atomic Oxygen, Materials Letter, Vol. 26, 1996, pp. 121-131.

13. Frederickson, A. R. and Dennison, J. R.: Measurement of Conductivity and Charge Storage in Insulators Related to Spacecraft Charging, IEEE transactions on Nuclear Science, Vol.50, No. 6, 2003, pp. 2284-2291.

14:1. Daniel Hasting and Henery Garrett, Spacecraft Environment Interaction, Published by Cambridge University press ISBN 0-521-60756-6. Chapter 1, pp. 1-11.

14:2. Daniel Hasting and Henery Garrett, Spacecraft Environment Interaction, Published by Cambridge University press ISBN 0-521-60756-6. Chapter 5, pp. 152-154.

15. Lucy Rogers, It's ONLY Rocket Science, Springer, ISBN 978-0-387-75377-5., 2007, chapter 1, pp. 1-17.

16. Michael D. Griffin and James R. French, Space Vehicle Design, AIAA education series, ISBN 1-56347-539-1, 2004, Chapter 3, pp. 49-99.

17. Harris I. L., Chambers A. R., and Roberts G. T.: Results from the Space Technology Research Vehicle 1a Atomic Oxygen Experiment, Journal of Spacecraft and Rockets, Vol. 35, No 5, 1998, pp. 647-652.

18. Bank B. B., Groah K. K. de. And Miller S. K.: Low Earth Orbital Atomic Oxygen Interaction with Spacecraft Materials, NASA/TM- 2004-213400, Nov. 2004.

19. Dooling D., and Finckenor M. M.: Material Selection Guidelines to Limit Atomic Oxygen Effects on Spacecraft Surface, NASA/TP- 1999- 209260, June 1999.

20. Mundari N. D. A., Khan A. R., Chiga M., Okumura T., Masui H., Iwata M., Toyoda K., and Cho M.: Effect of atomic oxygen exposure on surface resistivity change of spacecraft insulator material,Trans. JSASS Aerospace Tech. Japan Vol. 9, 2011, pp. 1-8.

21. Gorah K. K. de., Banks B. A., Clark J. W., Hammerstrong A. M., Youngstrom E. E., Kaminski C., Fine E. S., and Max L. M.: A Sensitive Technique using Atomic Force Microscopy to Measure the Low Earth Orbit Atomic Oxygen Erossion of Polymer, NASA/TM – 2001-211346.

22. Banks B. A., Groh K. K. de., Millers S. K., and Waters D. L.: Lesson Learned from Atomic Oxygen Interaction with Spacecraft Materials Interaction in Low Earth Orbit, NASA/TM – 2008-215264.

23. Noor Danish Ahrar Mundari, Arifur Khan, Minoru Iwata, Kazuhiro Toyoda, Mengu Cho: Understanding the Effect of Atomic Oxygen Exposure on Surface and Volume Resistivity Change in LEO. Proceedings of the 60th International Astronautical Congress, IAC-10.D5.3.9, Czech Republic, Oct 2010, pp. 1-9.

24. Zhao-xing R., Ke-ming S., and Qing-ao L.: Atomic- Oxygen Beam Source with Compact ECR Plasma, , Plasma Science & Technology, Vol. 4, No. 6, 2002, pp.1545-1550.

25. Azmi B. Z, Moksin M. M., Yunus W. M. M., Talib Z. A., Wahab Z. A., Senin H. B., and Williams A. W.: An Atomic Oxygen Source for Simulation of Lower-Earth Orbit Environment, J. Solid St. Sci. Tech. Lett. Vol. 1, No. 2, 1994, pp. 5-10.

26. Hohman K. W., Olson L. B., Brogan T. R., Prebola Jr J. L., and Studkey J. A.: Development of an Atomic Oxygen Source for Space Simulation Applications, AIAA 2008-461, 46th AIAA Aerospace Science Meeting and Exhibit, 7-10 Jan 2008.

27. Bitetti G., Marchetti M., Mileti S., Valente F., and Scaglione S.: Degradation of the surfaces exposed to the space environment, Acta Astronautica, Vol. 60, 2007, pp. 166-174.

28. Caledonia, G. E., Krech, R. H. and Green, B. D.: A high Flux Source of Energetic Oxygen Atoms for Material Degradation Studies, AIAA journal, Vol. 25, No. 1, 1987, pp. 59-63.

29. Caledonia, G. E., Krech, R. H., Green, B.D., Pirri, A. N.: Source of High Flux Energetic Atoms, United states patent, Patent number: 4,894,511, Jan 16, 1990.

30. Tagawa, M., Yokota, K., Kishida, K., Okamoto, A., Minton, T. K.: Energy Dependence of Hyperthermal Oxygen Atom Erosion of a Fluorocarbon Polymer: Relevance to Space Environmental Effects, ACE Appl. Mater. Interface, Vol. 2, No. 7, 2010, pp. 1866-1871.

31. Tagawa M. and Yokota K.: Atomic Oxygen-induced Polymer Degradation Phenomena in Simulated LEO Space Environments: How do Polymers React in a Complicated Space Environment, Acta Astronautica, Vol. 62, 2008, pp. 203-211.

32. Miller S. K. R., Banks B. A., and Waters D. L.: Investigation Into Difference Between Atomic Oxygen Erossion Yields of Materials in Ground- Based Facilities and LEO, SAGE Journal- High Performance Polymer, Vol. 22, No 4-5, 2008, pp. 523-534.

33. Miller S. K. R., Banks B. A., and Waters D. L.: Investigation into the Difference in Atomic Oxygen Erosion Yields of Materials in Ground Based Facilities Compared to those in LEO, Proc. of the 10th ISMSE & ICPMSE, Collioure, France, 19-23 June.

34. Shu T Lai.: Importance of Surface Conditions for Spacecraft Charging, Journal of Spacecraft and Rockets, Vol. 47, 2010, pp. 634-638.

35. Dennison, J. R., Bruson, J., Swaminathan, P., Wesley, N. and Frederickson, A. R.: Method of High Resistivity Measurement Related to Spacecraft Charging; IEEE transaction on plasma society, Vol. 34, 2006, pp. 2204-2218.

36. Lutz, B. and Kinddersberger, J.: Determination of Volume Resistivity of Polymeric Insulators by Surface Charge Decay, proceeding of 16th International symposium on high voltage engineering. ISBN 978-0-620-44584-9

37. Green N. W., Frederickson A. B., and Denison J. R.: Experimentally derived resistivity for dielectric samples from the CRRES internal Discharge Monitor, IEEE Transaction on Plasma Science, Vol. 34, No. 5, 2006, pp. 1973-1978.

38. Debska M.: surface potential decay on triglycine sulfate crystal, Journal of Electrostatics, 63, 2005, pp. 1017-1023.

39. Miyake H., Nitta K., Michizono S. and Saito Y.: Secondary Electron Emission Measurement of Insulator Materials for Spacecraft, XXIInd Int. Sump. On Discharges and Electrical Insulation in Vacuum, 2006, pp. 770-773.

Chapter 2: AO exposure facility and atomic oxygen characterization

It is quite difficult to make facilities which generate atomic oxygen producing the same effect as the space atomic oxygen. However, there are few known methods for producing atomic oxygen source. Some of those here:

- Atomic oxygen source with compact ECR plasma[(1)].
- Atomic oxygen source based on chemical reaction between nitrogen atoms with nitric oxide to produce, beside atomic oxygen, molecular nitrogen[(2)].
- Atomic oxygen flux by extracting atomic oxygen ions from Hall Effect ion source thrusters and then de-ionizing[(3).]
- Atomic oxygen source based on cold cathode ion source[(4)].
- Atomic oxygen source based on laser supported detonation (LSD) of molecular oxygen flow[(5,6)].

Most of the facilities used across the world, such as at NASA, ESA, JAXA, Kobe University, are based on the laser induced dissociation. Some of the facilities, especially the Beijing Institute of Satellite Environmental Engineering (BISEE) is based on the Electron Cyclotron Ion Source (ECR). The other facilities are scattered around the world.

The facility built at KIT is based on laser supported detonation (LSD). The conceptual theory of this method was developed by Physical Science Incorporation (PSI), USA and was realised by Caledonia *et al.* at PSI[(5,6)].

2.1 Designing of AO generation facility

AO generation technique used in this study is based on the dissociation of molecular oxygen into atomic oxygen, originally developed by Caledonia *et al*. The molecular oxygen is introduced into a previously evacuated expansion nozzle by a fast acting pulse valve whose pulse opening time is chosen to just fill the nozzle with oxygen gas. A pulsed CO_2 laser of 5.5

joule is then used to break down the gas with the subsequent laser supported detonation (LSD) wave creating high temperature plasma near the throat region of the nozzle. Hence it causes high velocity of atomic oxygen in an evacuated hypersonic nozzle. The plasma expands down the nozzle as a blast wave, ingesting and dissociating the gas in front of it, with ultimate conversion of thermal energy to directed velocity. The expansion is so tailored as to allow for electron-ion recombination without atomic recombination. Thus each laser pulse produces a temporally narrow high flux pulse of oxygen atom at the nozzle exhaust.

This atomic oxygen flux interacts with materials kept inside chamber for exposure testing. This accelerated exposure test will produce almost the same effect on the materials surface as if it is exposed to the actual atomic oxygen environment of LEO. The exposed material will be tested for the charging properties, like bulk conductivity and surface conductivity. A schematic diagram of AO chamber showing different component location for AO generation, exposure, detection is shown in Figure 2.1.

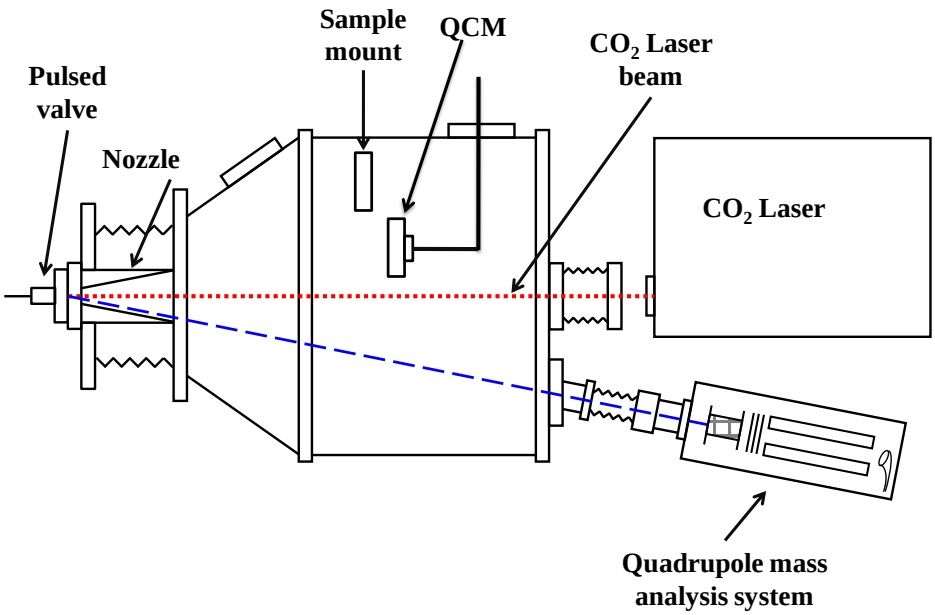

Figure 2.1: Schematic of atomic oxygen formation facility.

The most important requirement of this research was to make an AO-facility which generates atomic oxygen with higher flux compared to space so that the materials can be exposed for equivalent amount of atomic oxygen fluence of 10years orbital life time. This means that system should have higher flux and should be able to be used at higher frequency. The combination of higher flux and higher frequency operation will make the exposure of satellite surface materials to AO environment fast as needed. Frequency of operation is calculated using the following formula keeping the restriction of 10^{-3}Pa pressure before shooting of laser for fast operation. The restriction of 10^{-3}Pa comes from the condition to make collision free atomic oxygen. A pressure of above this value will cause the recombination of generated atomic oxygen and hence reducing the AO flux. The second part of the limitation comes from the operation of turbomolecular pump for this facility whose pumping rate is 2300l/s. The frequency of operation is calculated by using the following formula:

$T = V/S \ \mathrm{Ln}\ (P_2/P_1)$,

In term of frequency, above equation becomes,

$f = 1/T = S/V \ ln\ (P_1/P_2)$

Where T = time taken to come back to original pressure (10^{-3} Pa);

V= volume of the chamber;

S= pumping speed of the pump:

P_2= pressure after AO generation;

P_1 = minimum required pressure of 10^{-3}Pa.

Using the above mathematical calculation, we calculate the frequency of operation, as shown in Figure 2.2, which can be carried with certain size of chamber with given pumping system. Figure 2.2 shows that, for the given TMP pump of 2300liter/s capacity, frequency of

about 4Hz for the chamber of 100liters and a frequency of about 8Hz for the volume of about 50liters are possible. The carbon dioxide laser "ALL MARK APS from Altec" has a maximum operation frequency of 10Hz. The expected local fluence of AO per pulse is calculated by considering the dissociation of molecular oxygen in AO and its distribution in the area of 0.1256m^2 (radius of the chamber 0.20m) with 0.1SCC particle entering into the chamber with each shot. The number of atomic oxygen will be in the range of 10^{18}atoms/m^2 at a distance of 0.40m from the nozzle.

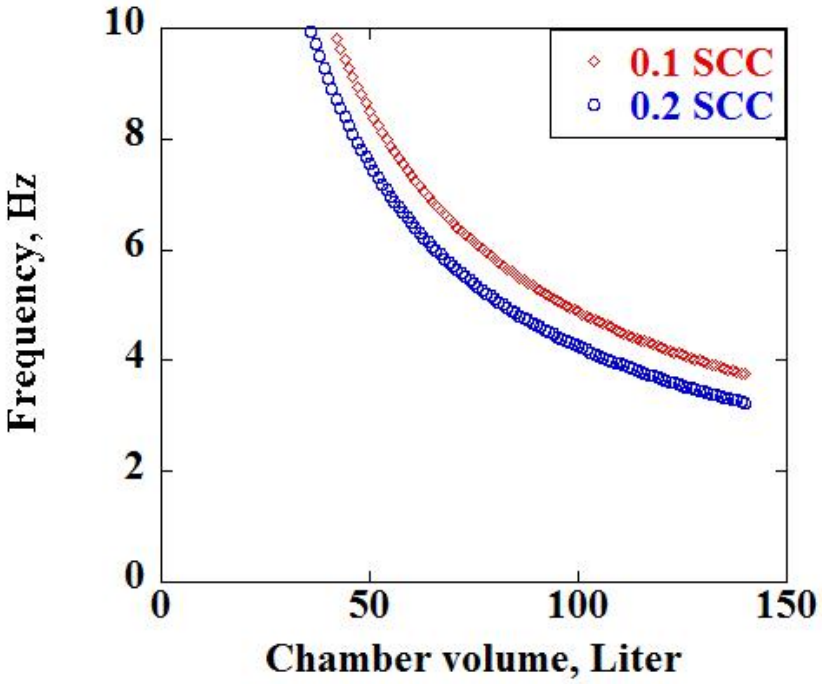

Figure 2.2: Volume vs. frequency graph for 0.1 SCC and 0.2 SCC operations to keep the pressure below 10^{-3}Pa.

The AO exposure facility has the following main sections:

Vacuum Chamber:

The chamber, as shown below in Figure 2.3, is designed in two parts with the first part being conical and the second part being cylindrical. The total volume of the chamber is around 100liters. It has detachable conical part having a volume of about 45liters, which can

be used separately for operation of about 8Hz. The cylindrical part is having a volume of 55liters. With its total volume of 100liter, the system can be used for 4Hz operation for the exposure experiment. The chamber is equipped with a few viewports and is feed through ports for the insertion of various detection and analysis instruments.

Vacuum system:

The operating background pressure of 10^{-5}Pa, sufficiently low to ensure collision-less passage of the energetic oxygen atom beam is achieved by using a turbomolecular pump (TMP) of 2230l/sec in conjunction with a rotary pump. With this pumping system we can use up to 8Hz operation of the system by using only the conical part of 45liters. For the full AO-exposure facility, operating frequency of 3Hz is used with safety margin for the full length of chamber is to be used. The current exposure experiments are carried out with the full chamber configuration.

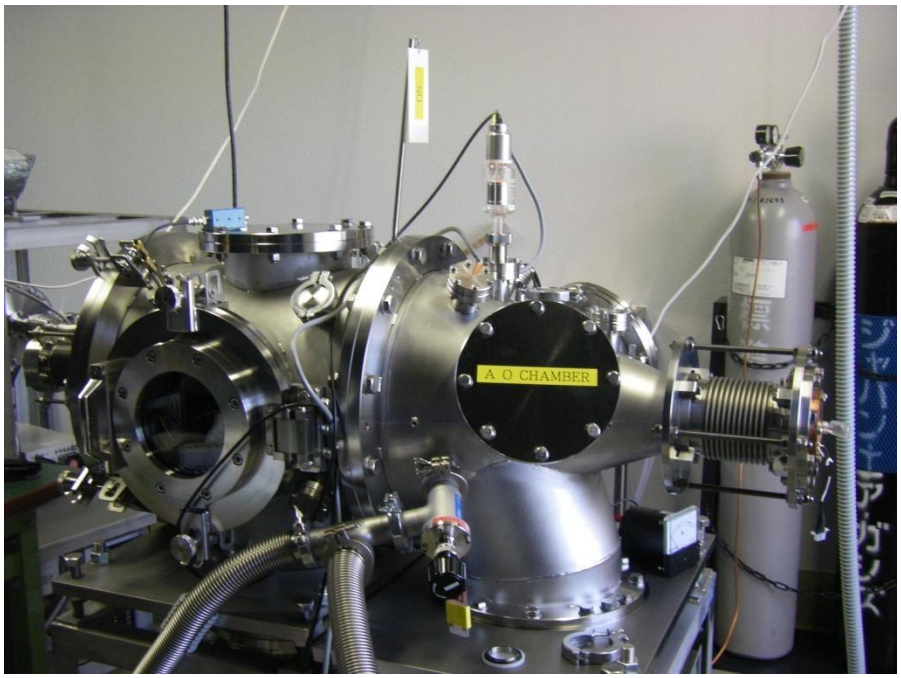

Figure 2.3: The vacuum chamber in which atomic oxygen is generated

Laser System:

A CO_2 pulsed laser provides 5.5J of energy per pulse at 10.6μm of wavelength for dissociating molecular oxygen is employed in this research. The laser system works at 30kV discharge voltage. This laser application voltage can be controlled to modify the energy of the beam. The laser frequency at which we operate is 3Hz for exposure analysis. The laser beam power distribution is 27x 27mm. Laser pulse is focused on the nozzle tip using ZnSe lens, as shown in Figure 2.4, where the dissociation of molecular oxygen into atomic oxygen occur. A laser alignment system using the diode laser is used for the proper alignment of CO_2 laser pulse at pulse valve.

Pulse valve:

Pulse valve, as shown in Figure 2.5, injects oxygen into nozzle in pulse form. The gas released from cylinder is injected into the chamber in pulses using a pulse valve, whose opening time allows the control of the amount of gas to be injected into nozzle for the dissociation.

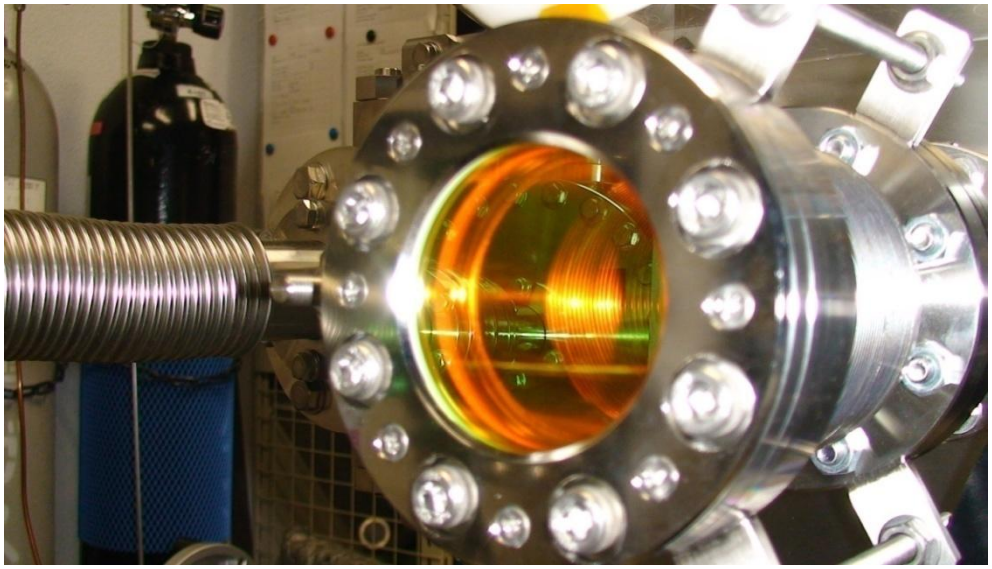

Figure 2.4: Lens used for focusing CO_2 laser beam at nozzle.

Figure 2.5: Pulse valve used for injecting molecular oxygen into nozzle.

Nozzle:

The pulse valve injects oxygen gas in the nozzle, connected as shown in Figure 2.6, where it interacts with laser beam. This causes the dissociation of oxygen to atomic oxygen from where the atomic oxygen moves towards the chamber at high energy. The nozzle is made of oxygen free copper material in order to dissipate heat energy quickly. The nozzle also does the function of focusing of laser beam by multiple reflections from its wall.

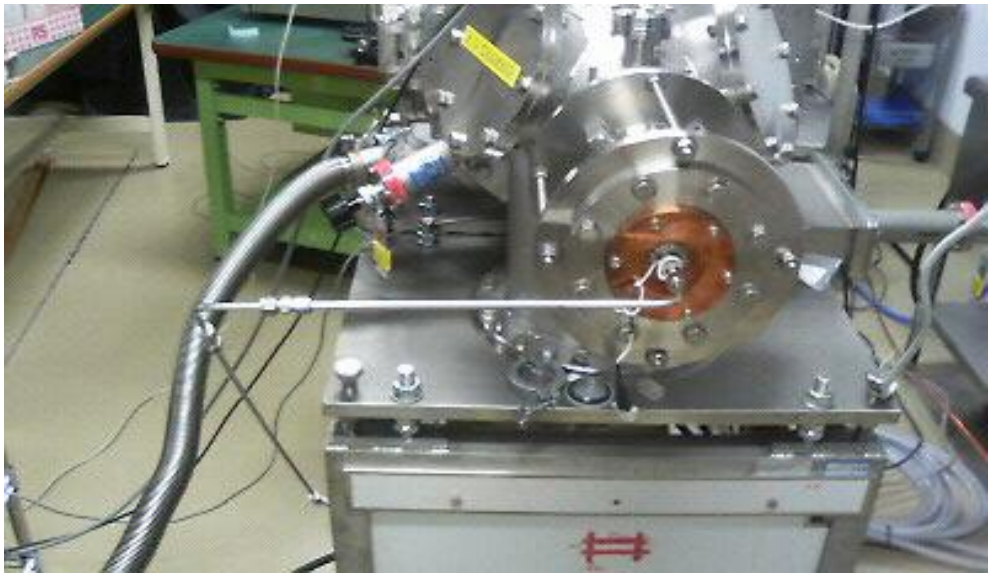

Figure 2.6: Pulse valve connected to the nozzle head.

Mass flow controller:

The molecular oxygen gas released from the cylinder is injected into the nozzle using a pulse valve in controlled and measured amount by using a mass flow controller. Block diagram showing position of MFC is shown in Figure 2.7.

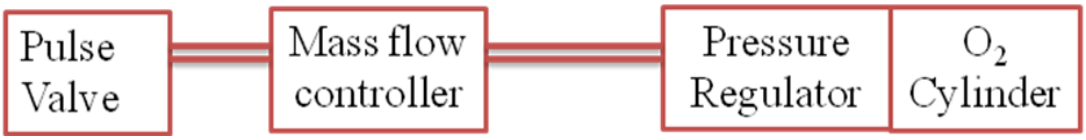

Figure 2.7 location of Mass Flow Controller (MFC) in the gas supply line

System for separating AO chamber with Quadrupole Mass Analysis System (QMAS) Chamber:

It is very important to maintain low pressure in QMAS chamber as the instrument can function only below 10^{-4}Pa. So we separated the two chambers using an orifice (shown in Figure 2.8) and gate valve. Diameter of the hole in the orifices is 0.1mm. The block diagram shown in Figure 2.9 shows the location of orifice and gate valve in the facility separating QMAS chamber with the AO-exposure chamber.

Figure 2.8: Orifice with 1mm hole diameter for allowing passage of generated AO.

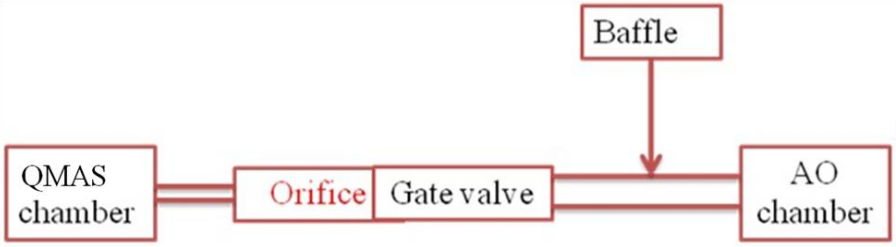

Figure 2.9: Position of orifice in facility.

In order to understand, how much gas will pass through the orifice, conductance of a free molecular flow from circular orifice is calculated. Conductance is given by

$$U \text{ (orifices)} = 62.5\, A / M^{1/2} \text{ liter/sec at } 20^0\text{C}$$

Where,

A = area of the orifice in cm^2

M = gram molecular weight (concerned gas)

Hence, Conductance can be measured as,

$U = 62.5 \times 3.14 \times 0.1 \times 0.1 / (4 \times 32^{1/2}) = 0.0867$ liter/sec $= 86.7 cm^3/s$

Throughput can be given by,

$$Q = U\,(P_2 - P_1)$$

If we consider the pressure of the main chamber, $P_2 = 10^{-5}$Pa and QMAS chamber's pressure $= 10^{-7}$Pa, we get,

$Q = 86.7 \times 10^{-6}\ (10^{-5} - 10^{-7}) = 86.7 \times 10^{-6} \times 9.9 \times 10^{-6} Pam^3/sec = 858.33 \times 10^{-12} Pam^3/sec$

Control unit (Delay Pulse Generator, DPG):

DPG controls the time delay between the pulse valve opening and laser triggering. It acts as the heart of the system, which sends signals to different units for synchronised operation. Figure 2.10 shows the functioning of the DPG. In this Figure, the red lines show the signal sent by DPG. DPG is used to send spike signals to the pulse valve and the laser system. The first spike signal is sent to the pulse valve to control the opening of the PV. The pulse valve,

opening time is controlled by the pulse valve controller unit, which allows fixed amount of gas injection into the nozzle. This time-period, for which the pulse valve remains open, is called “opening time of PV”.

DPG generates the second spike signal for the laser system. This second signal for the laser ignition is generated with certain time delay after the first signal for the pulse valve controller for PV opening. The time delay between the two signals is called Laser Delay (LD). The time delay allows the passage of gas from the PV input to the nozzle input in a pulse. Figure 2.11 shows the two signals PV and LD.

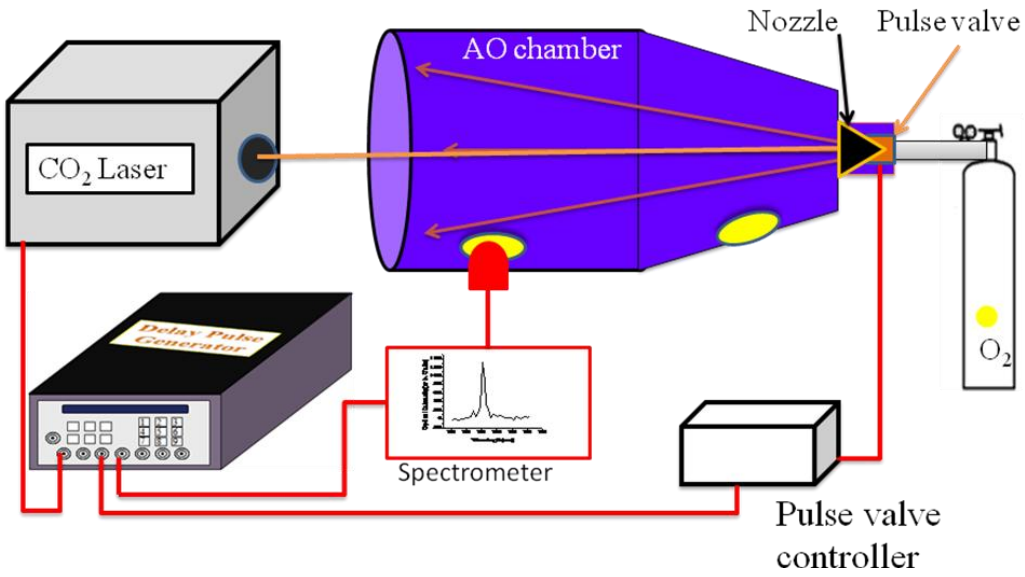

Figure 2.10: Functioning of the DPG; the red line shows the signal send by DPG.

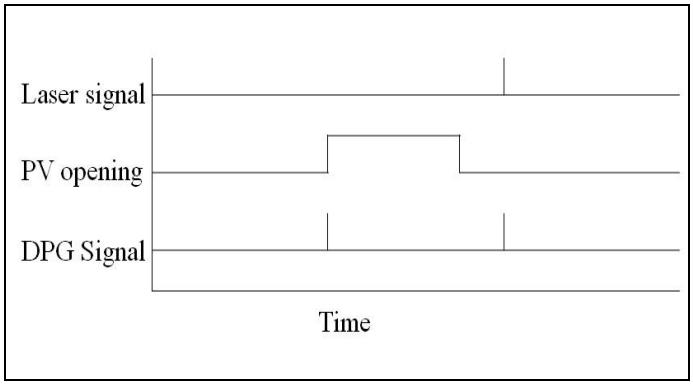

Figure 2.11: Signal sent by DPG control pulse valve opening and Laser triggering.

The block diagram of the complete AO facility is shown in Figure 2.12. Figure 2.13 shows the facility at operation at KIT. This facility is used for the exposure of materials.

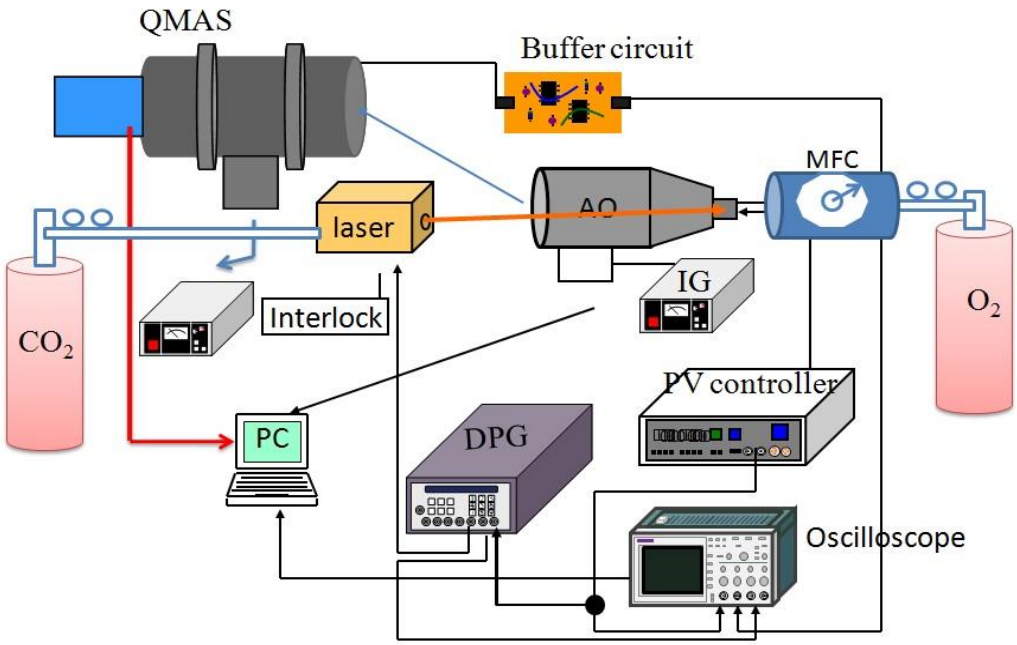

Figure 2.12: Block diagram of full AO facility.

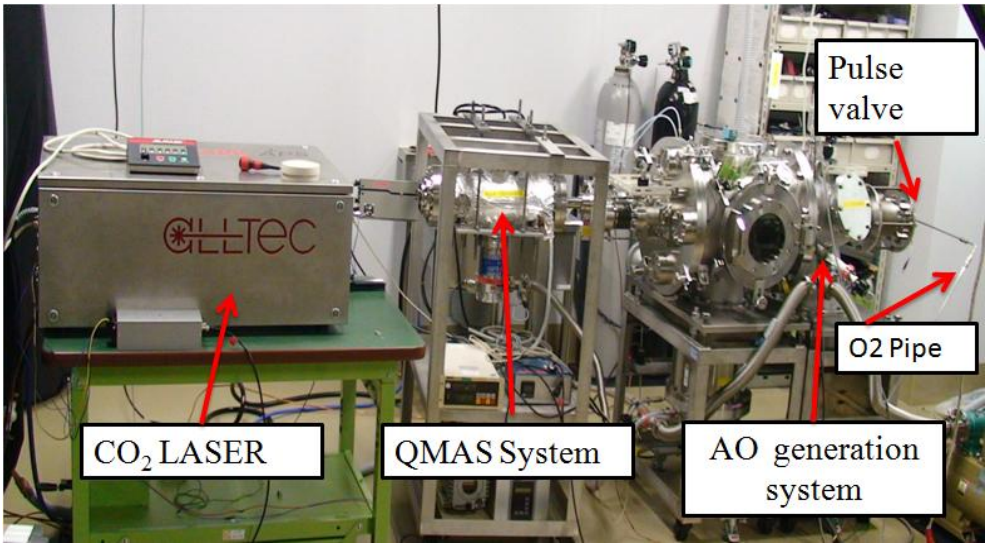

Figure 2.13: AO exposure facility built at KIT.

2.2 Spin coating equipment for measuring the mass response

Polyimide-coated QCM is used for the measurement of AO-Fluence[7]. Polyimide-coated QCM crystals are not available commercially for sale. An equipment, which can make

polyimide coated QCM was developed. Polyimide gel was bought from the Toray, Japan, and was coated in laboratory on gold-coated QCM crystal with the lab-built spin coating system. The QCM head is shown in Figure 2.14. The lab-built facility to coat polyimide on QCM crystal is shown in Figure 2.15 and Figure 2.16.

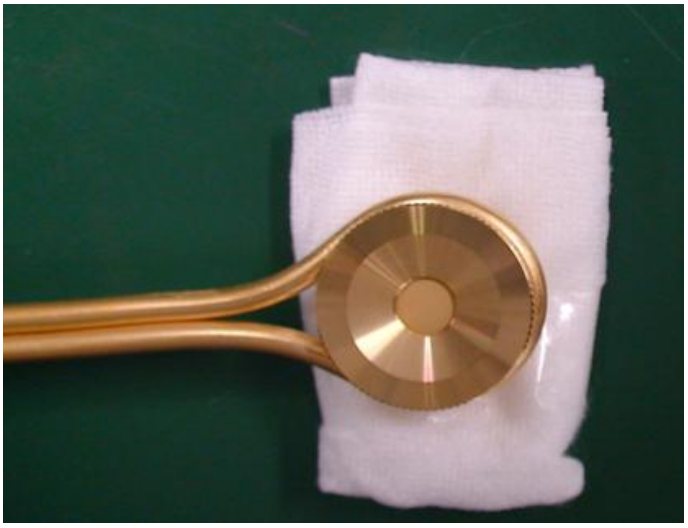

Figure 2.14: QCM head showing the position of crystal.

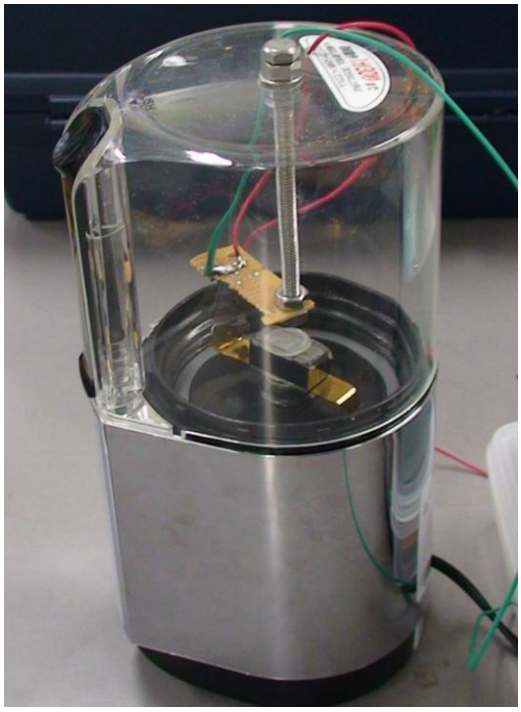

Figure 2.15: Lab-built spin coating facility for coating polyimide on gold-coated quartz crystal.

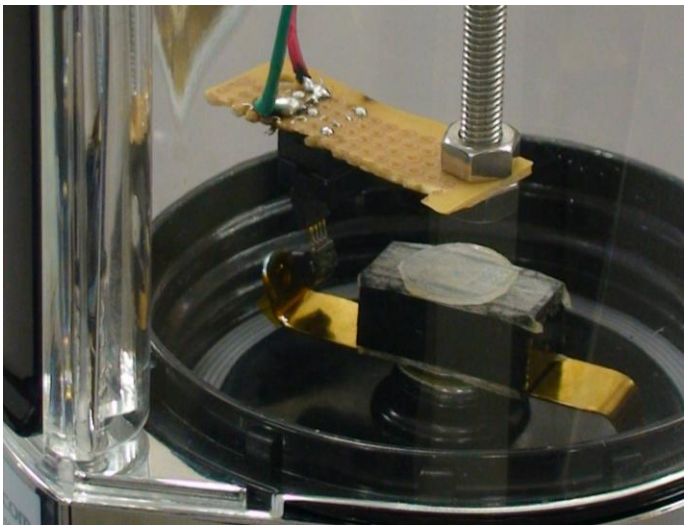

Figure 2.16: Spin coating head unit for fixing crystal.

After coating the polyimide gel on gold-coated QCM, the crystal is annealing at high temperature in vacuum, to make the coating permanent with good adhesion, as per the instruction of the company.

Quality testing of the polyimide-coating on QCM crystal is done by taking the optical microscopic and roughness measurements of the surface. The roughness measurement of polyimide-coated QCM crystal is shown in Figure 2.17. The roughness measurement is carried out using SURFOCOM 1400D-12, as shown in Figure 2.18. This instrument has the resolution in the range of 0.2μm to 0.0004μm with different settings; this was enough for polyimide coating on QCM. In this graph, x-axis is the length of the QCM crystal and y-axis is the roughness value. It shows that the coating was quite uniform and good in quality. This polyimide-coated QCM crystal is used for the measurement of AO-fluence. Figure 2.19 shows the gold-coated QCM crystal and polyimide-coated QCM crystal. For polyimide coating on gold-coated QCM crystal is used as the base crystal in order to prevent the reaction of AO with the gold. AO is almost inert against gold.

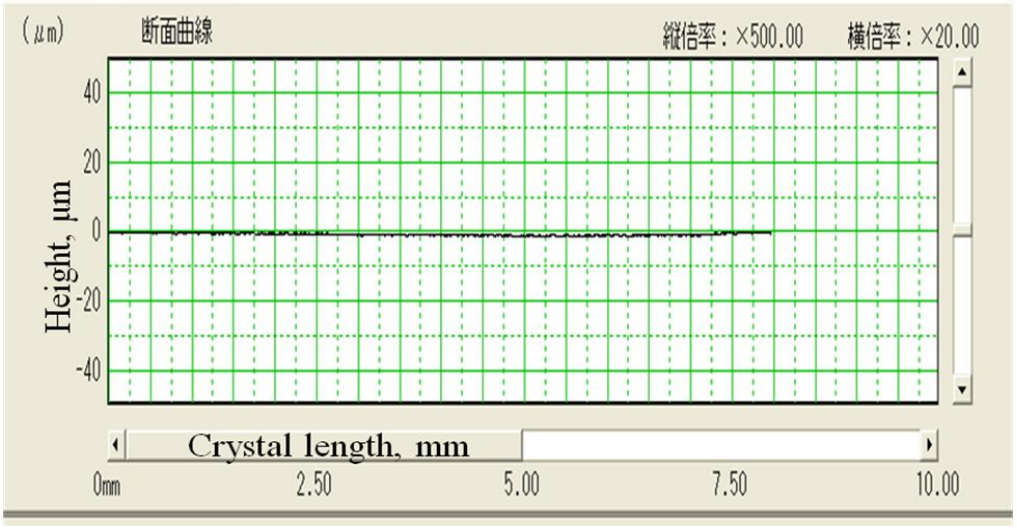

Figure 2.17: Roughness measurement of polyimide coated QCM crystal.

Figure 2.18: Surface roughness measurement instrument SURFCOM1400D-12

http://www.accretech.jp/english/pdf/measuring/sfcm14de.pdf

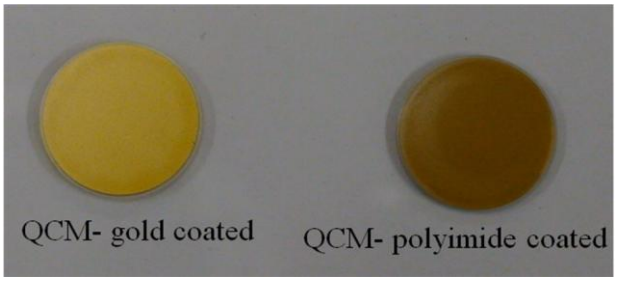

Figure 2.19: QCM crystals before and after polyimide coating, gold coated QCM is used as base crystal.

2.3 Calculation of number of particle injected into the chamber:

The number of particles injected into the chamber is calculated using the rise of the chamber pressure for different primary cylinder pressures and PV opening times. This was accomplished on the basis of the change in pressure observed by the ionisation gauge response. The limitation for this method was the ionization gauge response time and efficiency. The calculation is based on ideal gas dynamics.

We know, $p = n\ k\ T$

Hence, $n = p/\ kT$

Where, n= Number of particles, m^{-3}

k= Boltzman`s constant ($1.38 \times 10^{-23} m^2 kgs^{-2} K^{-1}$) and

T= Temp (295K)

p= Chamber pressure, Pa

Hence, $n = p/\ 1.38 \times 10^{-23} \times 295 = (p / 407.1) \times 10^{-23}\ m^{-3}$

Based on this method, the number of particles entering in the chamber for each PV opening time was calculated by multiplying "n" with the volume of the chamber $0.1 m^{-3}$. Figures 2.20 and 2.21 show the number of particle entering for different primary cylinder pressure and PV opening time for 1 Hz operation of PV, respectively. Figures 2.20 and 2.21 show the number of particle entering for different primary cylinder pressure and PV opening time for 10Hz operation of PV respectively.

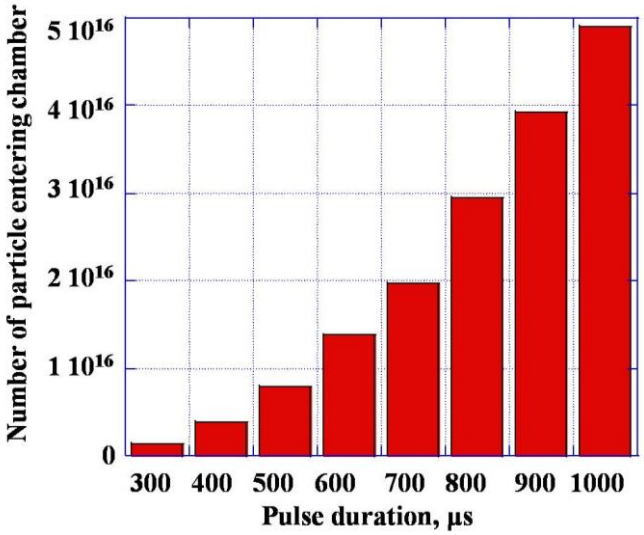

Figure 2.20: Number of particles entering the chamber for one Hz operation of pulse valve for different pulse valve opening time when the primary pressure of O_2 is 0.3MPa.

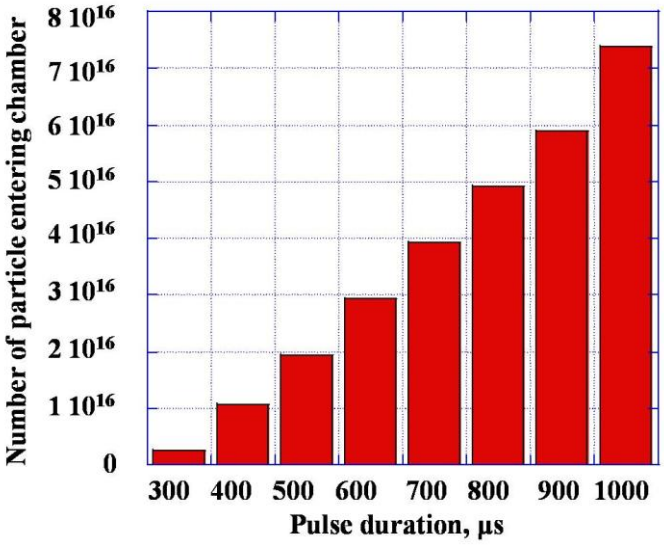

Figure 2.21: Number of particles entering the chamber for one Hz operation of pulse valve for different pulse valve opening time when the primary pressure of O_2 is 0.5MPa.

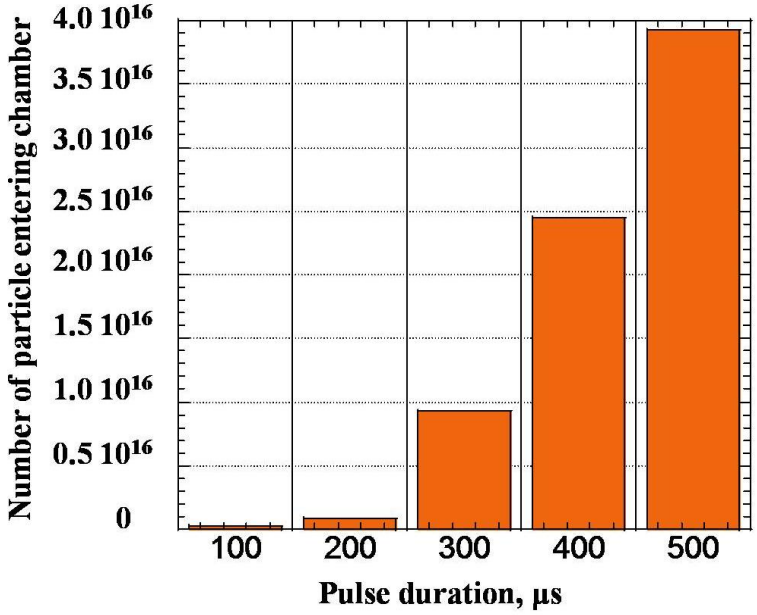

Figure 2.22: Number of particles entering the chamber for ten Hz operation of pulse valve for different pulse valve opening time when the primary pressure of O_2 is 0.6MPa.

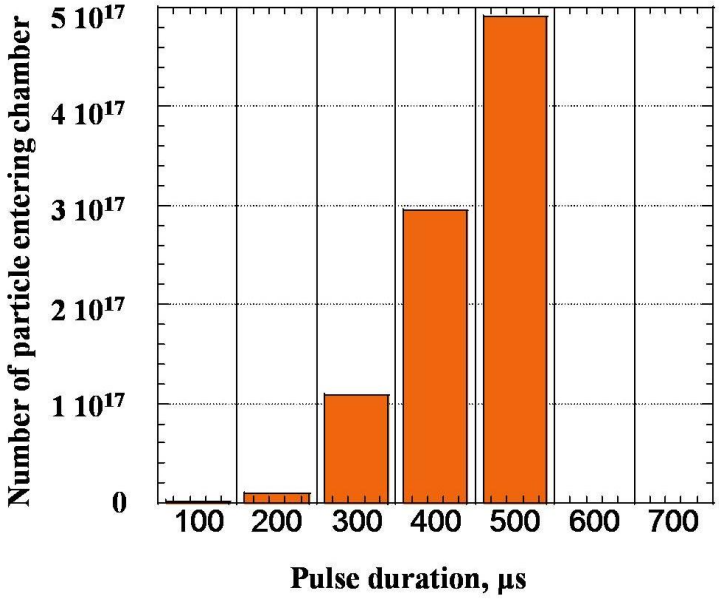

Figure 2.23: Number of particles entering the chamber for ten Hz operation of pulse valve for different pulse valve opening time when the primary pressure of O_2 is 0.7MPa.

Figure 2.20 and 2.21, we observe that the increase in pulse valve opening time increase the amount of O_2 gas entering into the chamber per pulse. We also notice that for the same PV

opening time, the increase in the primary pressure of the O_2 cylinder increases the amount of gas injected into the chamber. Experiments are also carried out for the 10Hz frequency operation of the PV. In this case, the chamber pressure gets stabilized to a constant value for higher frequency operation and that constant value was used for the calculation of number of particles. Figure 2.22 and 2.23 show that the number of particles entering into the chamber increases with the increase in pressure of primary cylinder. The number of entering particles also increases with the increase in the PV opening time. So PV opening time and primary cylinder pressure are controlling the number of particles entering into the chamber.

2.4 Atomic Oxygen Diagnosis

2.4.1 Detection of atomic oxygen generation

Ultra-high purity molecular oxygen (99.9999%) is the feed gas for the AO beam. No carrier gas is required to generate the atomic oxygen beam. The primary species in the beam is atomic oxygen. AO beam diagnosis is done by using a quadrupole mass analysis system (QMAS) in single mass mode and spectroscopic analysis of AO generation beam.

The fast oxygen atom pulse exhibits some fluorescence, dominantly from the 777.6nm $O(P) \rightarrow O(S)$ transition. This excited state is produced by electron ion recombination of residual O^+ in the beam, i.e.,

$$O^+ + e + e \rightarrow O + e$$

The AO generation is confirmed through the use of spectrometer monitoring the 777.6nm neutral oxygen atom transition produced through de-excitation. Figure 2.24 shows the principle of detection of AO using spectrometer. Figure 2.25 shows the spectrometer output.

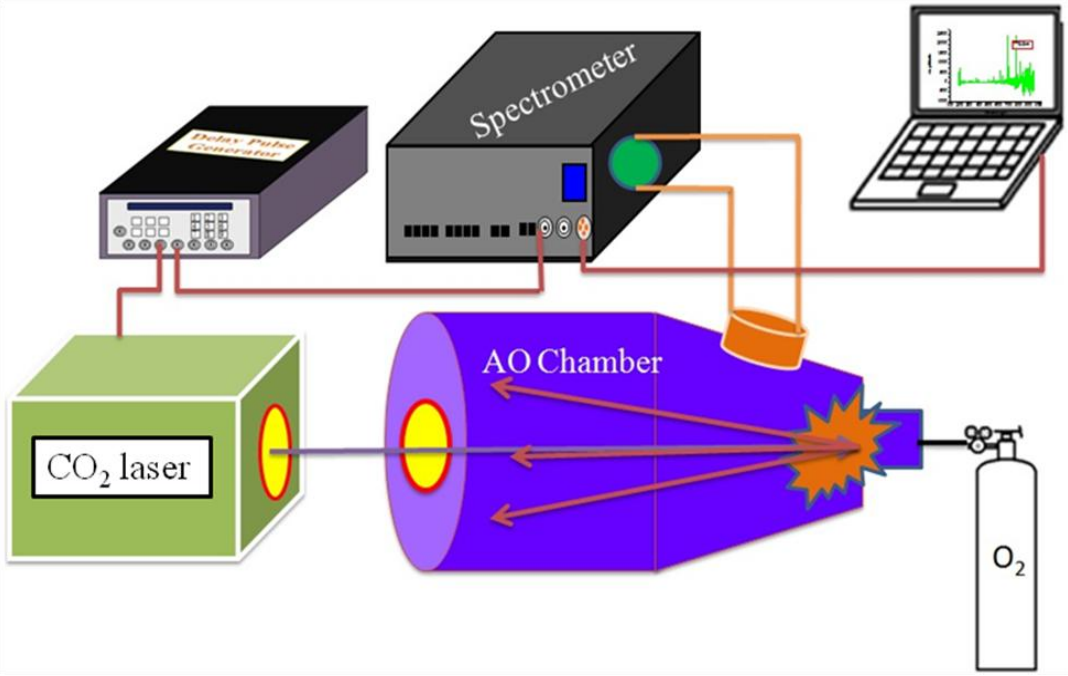

Figure 2.24: Principle of detection of AO beam using spectrometer.

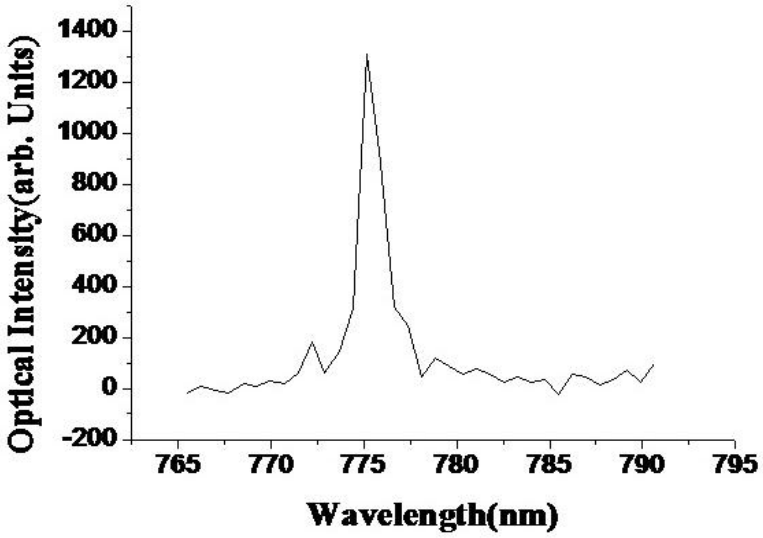

Figure 2.25: Emission spectrum of atomic oxygen.

The shift in the wavelength is analysed and it is found that this shift is due to non-standardizing of the spectrometer. The spectrometer needs to be calibrated by using some calibration source; e.g., it can be He-lamp or could be some laser system, which produce a known calibration wavelength.

The Figure 2.26 shows the spectrometer spectrum for different PV opening time, after the mandatory standardization of the spectrometer. It shows that the emission intensity increases with increase in Pulse Valve (PV) opening time initially and then again decreases. This gives us an idea about the PV opening time for which system gives higher percentage of AO. It also gives idea about the ionization of the oxygen.

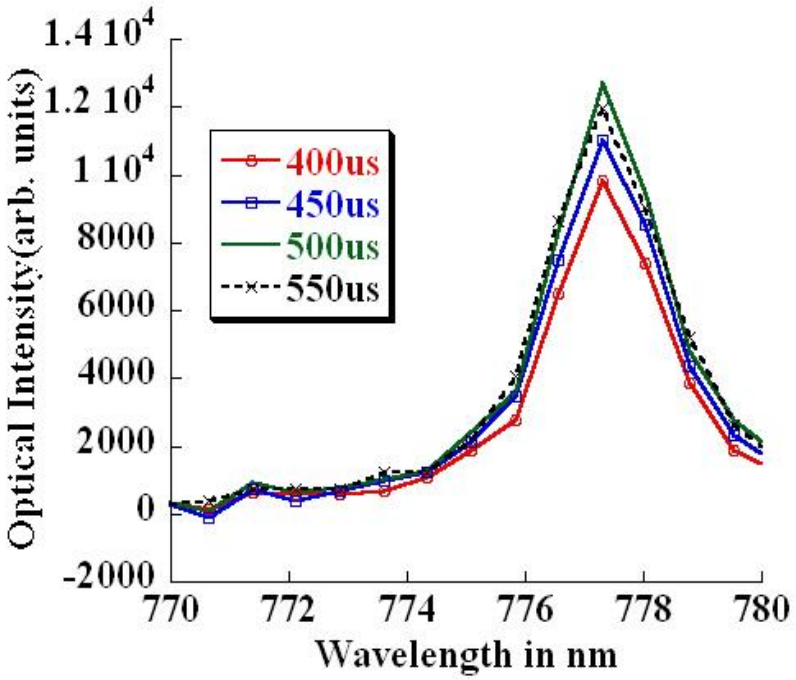

Figure 2.26: Emission spectrum of oxygen plasma for four different Pulse Valve (PV) opening times.

The second confirmation of the AO-formation is done by using the QMAS in single mass mode. The QMAS is a mass analyzer used in mass spectrometry, consisting of 4 circular rods which are set parallel to each other, for filtering sample ions, based on their mass-to-charge ratio (m/q). QMAS can be fixed for the desired value of q/m. This value for the atomic oxygen is 16. So, if some signal on QMAS output, with q/m= 16, is detected, it confirms the production of the AO by LSD of molecular oxygen. Figure 2.27 shows the principle of detection of atomic oxygen signal by QMAS, whose output is shown on the oscilloscope.

Figure 2.28 shows the output of the QMAS; it also shows the detection of optical light beam detected by photodiode, produced due to LSD and O(P) → O(S) transition, as discussed before. The Figure 2.28 implies that after the LSD, the atomic oxygen moves toward that QMAS and is detected after certain time.

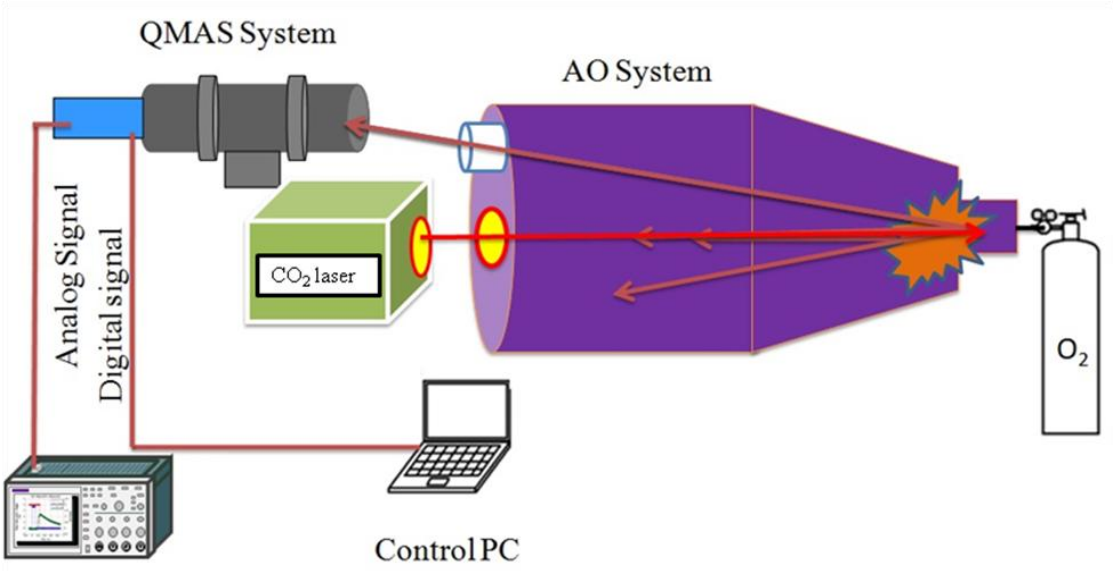

Figure 2.27: Principle of detection of AO beam using QMAS system in single mass mode for q/m=16.

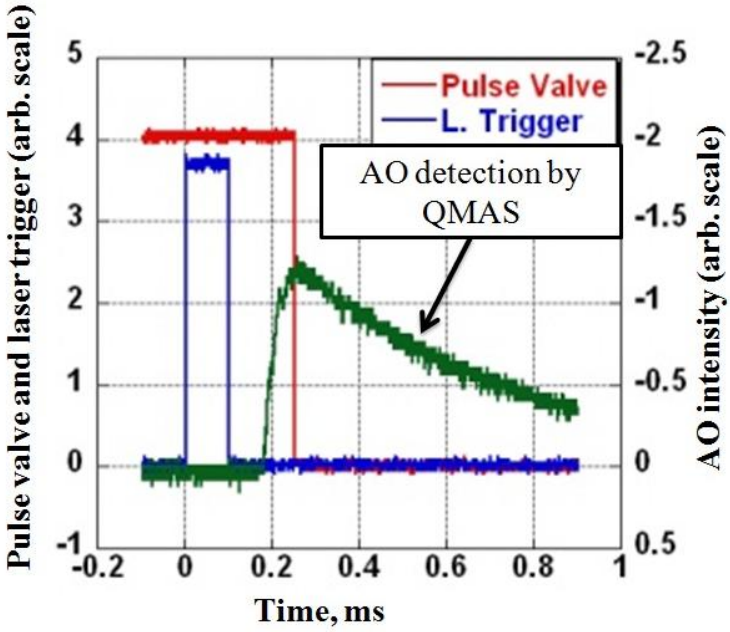

Figure 2.28: Detection of AO in single mass mode along with the photodiode signal.

2.4.2 Measurement of energy of atomic oxygen

Translational energy and hence velocity of AO species in the beam are calculated using TOF distribution. The QMAS is a mass spectrometer of small physical dimension which is enclosed in a separate chamber, pumped separately using a TMP of 150l/sec in conjunction with a rotary pump connected with the main chamber with a baffle using gate valve and orifices. The energy of AO beam is measured by calculating the time taken by AO to reach the quadrupole head from the nozzle which is about 1.9 meters. Figure 2.29 shows the QMAS system and Figure 2.30 shows the principle of measuring velocity and distribution. Figure 2.31 shows the Time of flight (TOF). The time zero is defined as the time when the LSD happens on the Nozzle-Pulse valve conjunction. Usually, it is observed that there is a time delay of 40μs between the laser shooting and the LSD observed using the photodiode or spectrometer looking for 777.6nm, as shown in figure 2.31. Figure 2.33 shows velocity distribution profile of atomic oxygen at the QMAS head. The generated atomic oxygen moves at the peak velocity of about 10-12km/sec. Later improvement in velocity measurement technique showed that the velocity measurement was affected by QMAS setting, it was found that the actual AO velocity was lower than 10-12km/sec and was indeed in the range of 8-9km/sec.

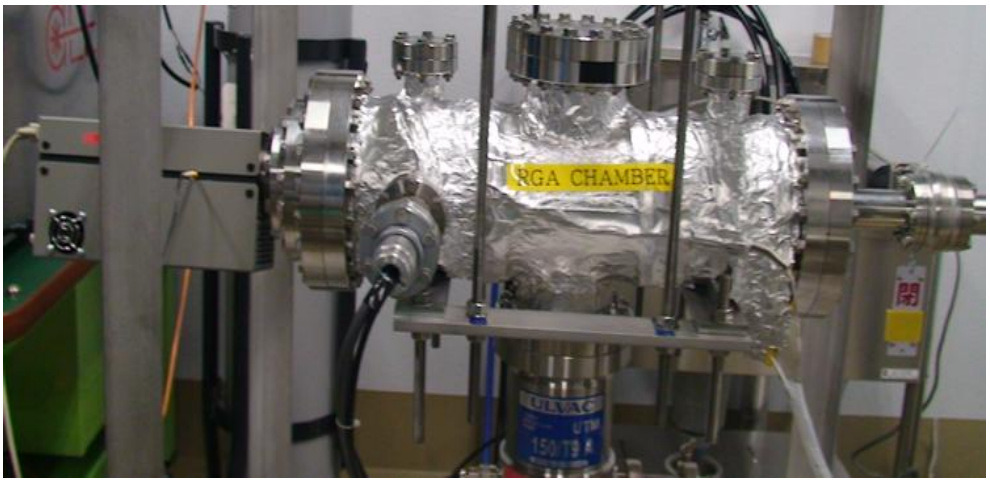

Figure 2.29: Quadrupole mass analysis system used for measuring the TOF of AO.

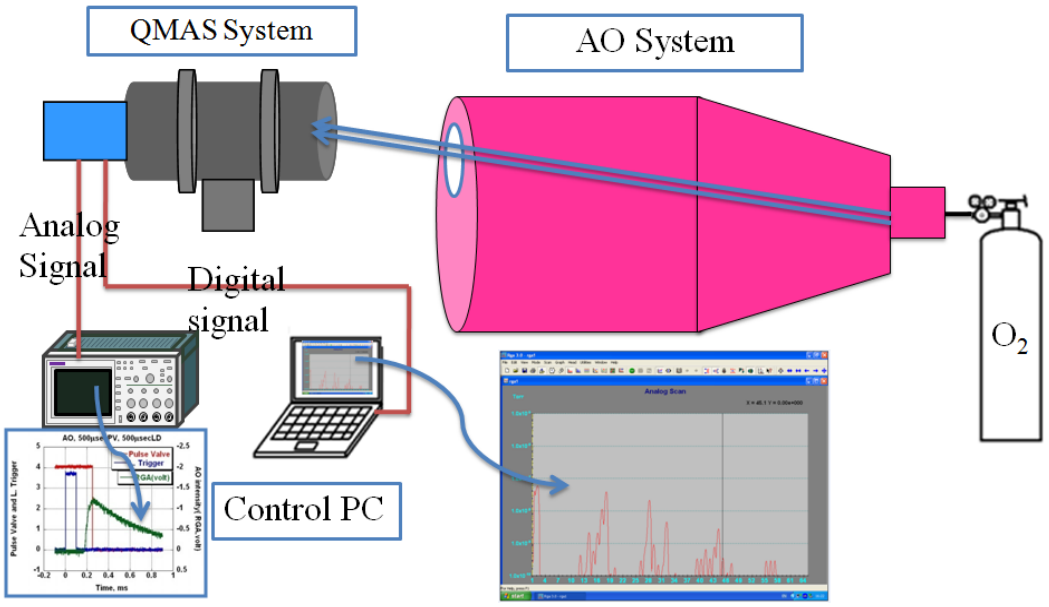

Figure 2.30: QMAS system for detection of atomic oxygen and its velocity measurement.

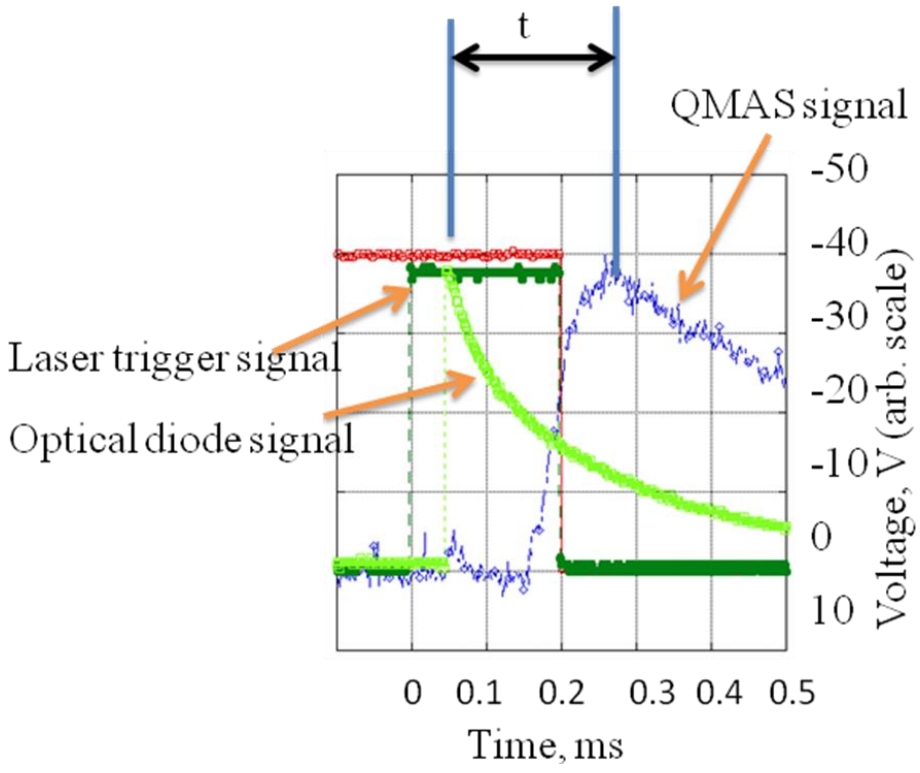

Figure 2.31: Different signal used for the velocity measurement of generated AO.

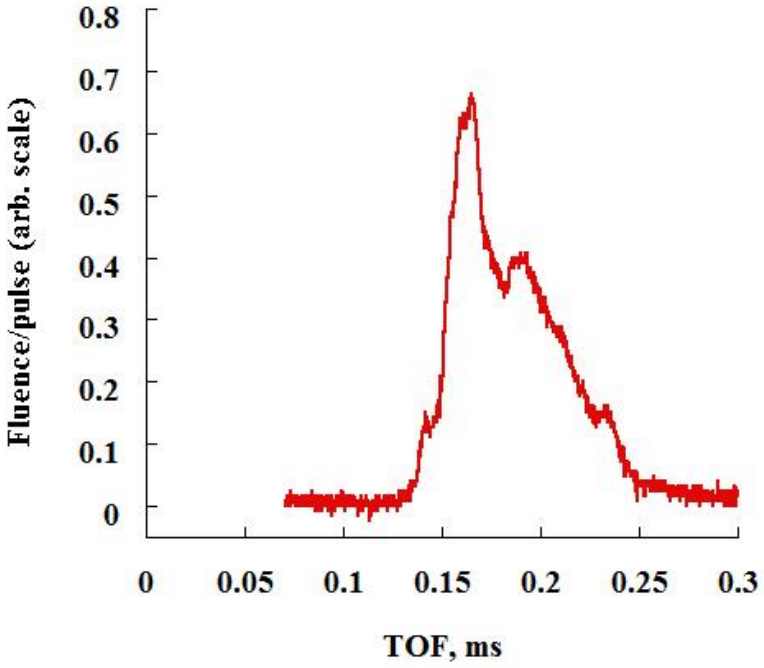

Figure 2.32: TOF distribution of AO at quadrupole mass analysis head.

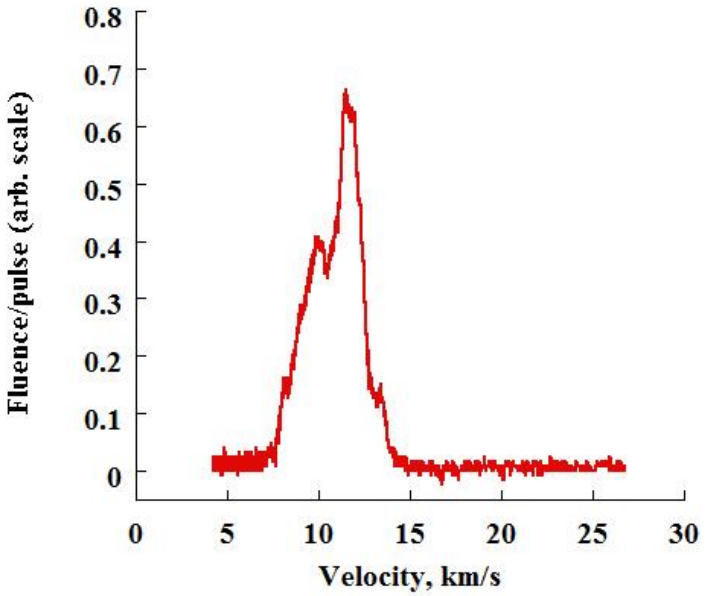

Figure 2.33: Velocity distribution of AO at quadrupole mass analysis system head.

2.4.3 Measurement of the flux and fluence of AO beam

The fluence of AO-generated inside the chamber can be measured using two techniques, namely, silver-coated Quartz Crystal Microbalance (QCM) and polyimide-coated QCM. Both

methods get application in space systems across the world. Both of them have their advantages and some disadvantages depending on the reaction mechanism and application limitation. We have used both of the methods for the measurement of the fluence and our results give same value of fluence.

2.4.3.1 Mass response of the silver coated QCM crystal

Silver mass change is one of the methods to calculate the fluence of atomic oxygen in AO chamber. Since silver reacts with atomic oxygen to form silver oxide, the mass of the silver coated QCM changes with the fluence of AO. Thus silver-coated QCM provides good means to measure the fluence of atomic oxygen in a newly-built facility. Silver reaction with oxygen is an ionic reaction, where the silver gives electrons to oxygen, and as a result, being silver oxide (Ag_2O). In the temperature range of 273K to 358K interaction of silver surface with hyperthermal atomic oxygen results in the formation of silver peroxide AgO. Liner oxidation was observed initially which changes to parabolic rate law as thickness of oxide film exceeds certain value. Possible oxidation reaction between silver and oxygen is

$$2\ Ag + O_2 \rightarrow Ag_2\ O_2\ (= 2\ AgO)$$

Calculating the thermo-dynamical equilibrium at standard temperature pressure (STP), one finds that reaction cannot proceed to the right-hand side, which means that under the given conditions, AgO is not a stable oxide. The calculated free enthalpy change of reaction at a partial oxygen pressure of 0.2atm. is +7473cal/mol[(8)].

The situation drastically changes when O-atoms instead of O_2 molecules are involved in the oxidation reaction with silver. Both oxide types are now stable even at very low pressures and also AgO is more stable than Ag_2O. It is then thermodynamically possible to oxidise Ag_2O to AgO, which is impossible with O_2 molecules. This is the case with our facility where the reaction takes place at room temperature but at 10^{-5}Pa.

The reaction rate curve for the oxidation of silver-coated QCM is shown in Figure 2.34. Here the x- axis corresponds to the number of shot and the y- axis is the change of mass. Silver crystal shows initial mass loss due to removal of vapour and dust particle from the suface; then it shows mass gain due to formation of silver oxide on the surface.

With this graph, we calculated the flux of AO using the linear region of data. Since mass response of silver is linear for long range, it is easy to calculate fluence value from the silver data. The flux calculated using silver QCM is 4.5x 10^{13}atoms/shot (Appendix 2).

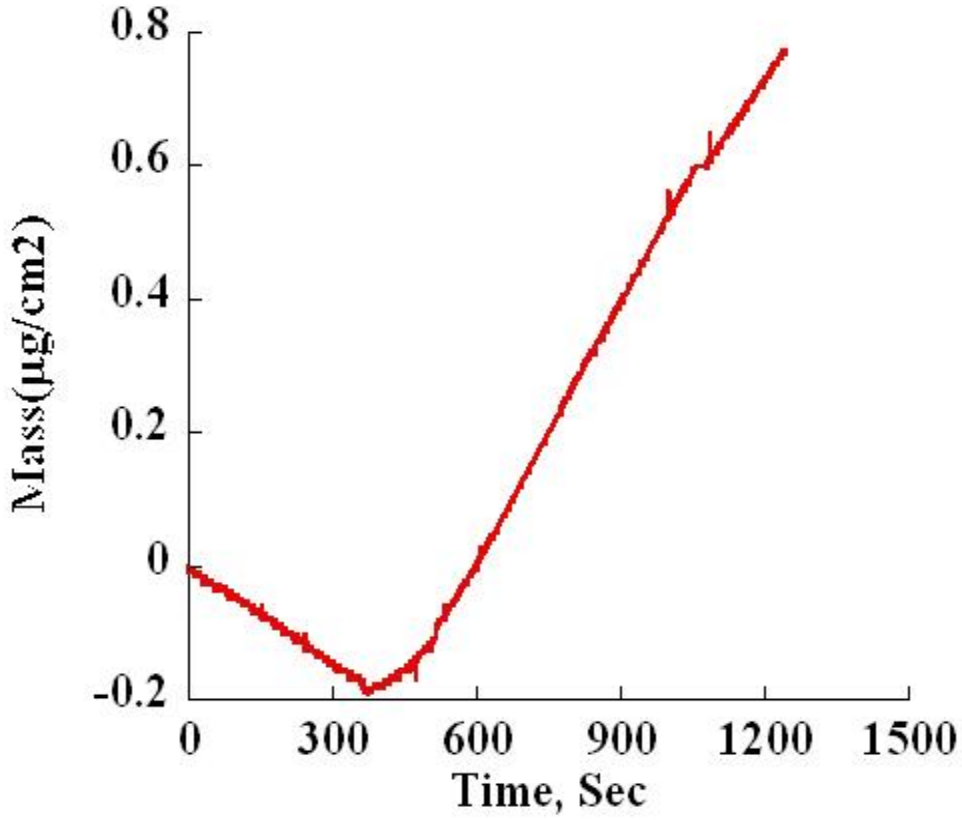

Figure 2.34: Response of silver coated QCM crystal against the atomic oxygen shot.

2.4.3.2 Mass response of the polyimide-coated QCM crystal

In-orbit exposure tests have been carried out regarding atomic oxygen effect on materials, and polyimide has been used for measuring the atomic oxygen fluence in such in-orbit tests. The fluence of atomic oxygen in LEO has been calculated from the polyimide erosion with

the established reaction efficiency of 3.0x $10^{24}cm^3$/atom (Kapton® equivalent fluence)[9]. As for the reference material to measure atomic oxygen fluence, the erosion yield of polyimide has to be stable against the other environmental factors such as temperature, ultraviolet, electron, ions, radiation, and so on. Erosion yield of polyimide in the temperature range between -30 to 100°C is constant and the activation energy is as low as 10^{-3}eV[9,10]. However, increase in the erosion yield of polyimide at the temperature above 120°C is reported. It is, therefore, important to maintain the temperature below 100°C when measuring atomic oxygen fluence with polyimide. On the other hand, the exposure condition to avoid synergistic effect with ultraviolet has not been established. In LEO, no synergistic effect was reported.

In this thesis, the flux and hence the fluence of the generated AO is measured using the polyimide mass loss. The quartz crystal having polyimide coating is used for AO flux measurement. The behaviour of the polyimide-coated QCM crystal against the atomic oxygen fluence is shown in Figure 2.35. The x-axis shows the number of laser shot. The y-axis shows the mass change of the crystal. After making the necessary calculation, the flux per shot comes about 4.2x 10^{13}atomscm^{-2}. AO-exposure facility is used at 2Hz for 132000 shots, for the current test sample; hence the total fluence was 5.4x 10^{18} atomscm^{-2} (Appendix 3). This fluence value is of about 10 years of AO exposure at 800km altitude of LEO, it is the region of 600-800km, where most of The Japanese satellites are placed and shows strong effect of discharge. Figure 2.36 shows the fluence of AO per year for different altitude of LEO.

Figure 2.37 shows the acceleration factor for the different altitude heights of LEO. This acceleration factor is shown for the case of AO generating flux of 10^{14}atoms/shot for 1Hz operation. For KIT AO-exposure facility, AO fluence is in the range of 3x 10^{13} to 1x 10^{14}

atoms/shot, observed depending on the case of PV, LD, laser beam energy and the range of velocity chosen for exposure.

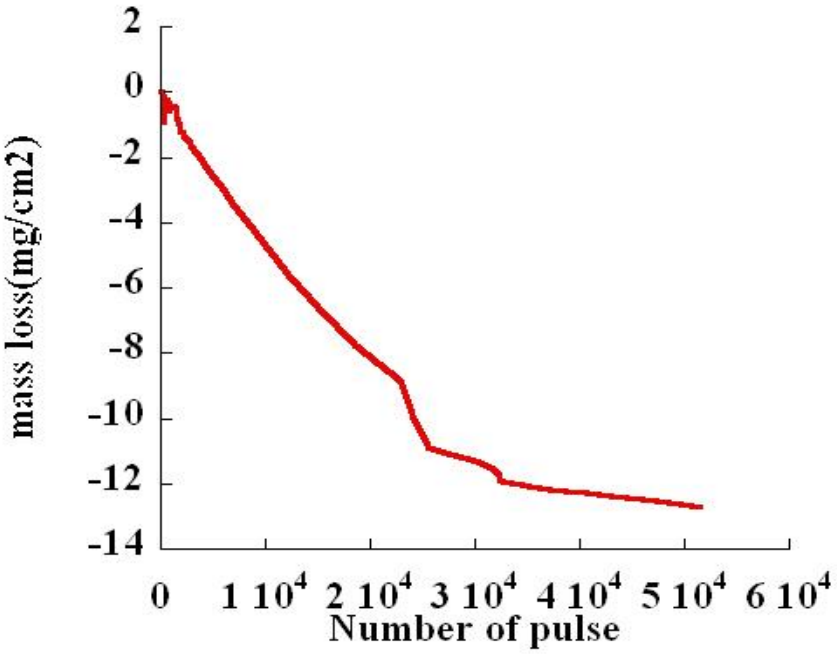

Figure 2.35: Response of the polyimide-coated QCM crystal against the atomic oxygen shot.

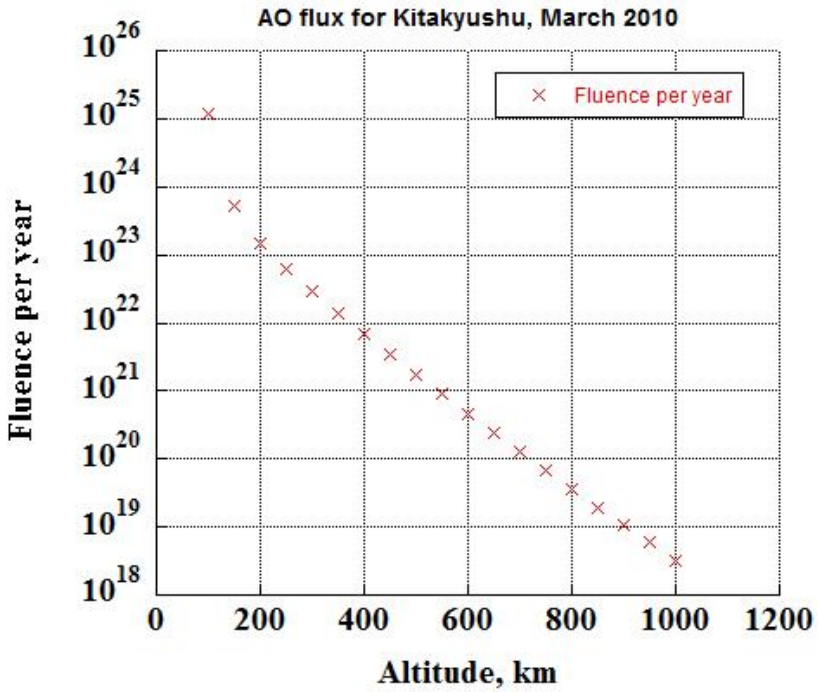

Figure 2.36: AO fluence of kitakyushu for one year at different altitude height.

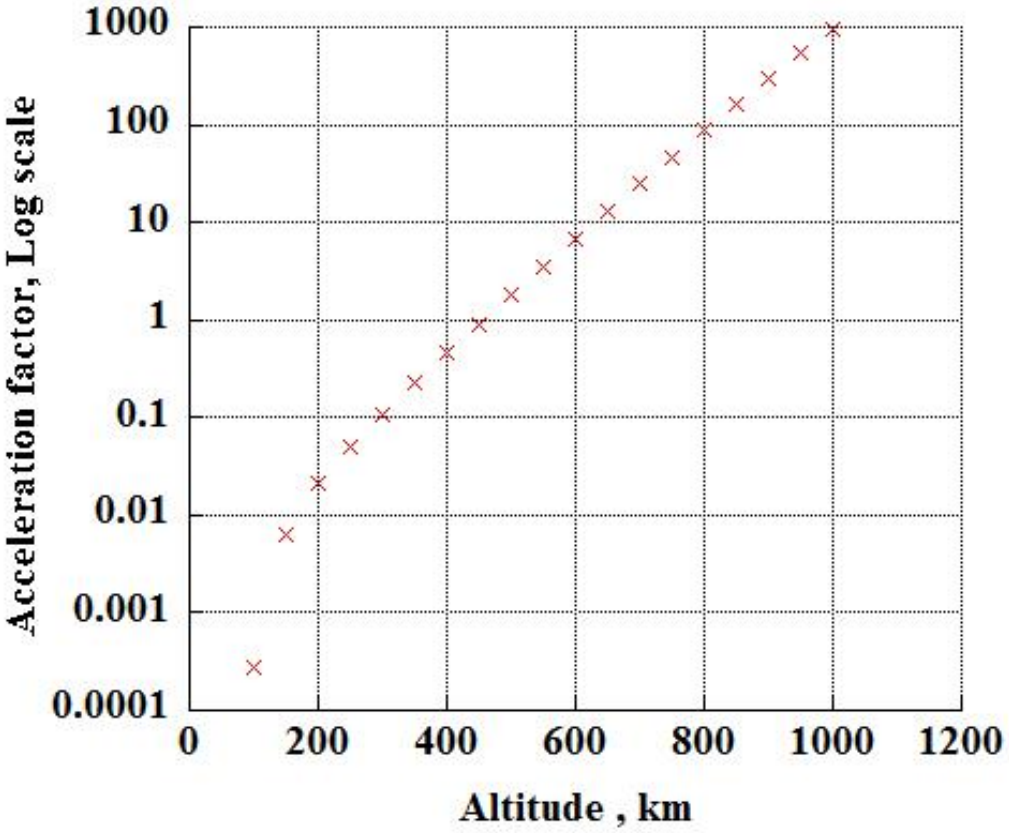

Figure 3.37: Acceleration factor calculated using 10^{14} atoms/shot at 1Hz.

2.5 Conclusion

- AO-exposure facility is built and the characterization of its velocity and energy is done.
- For measuring fluence, a spin coating facility is built for coating polyimide on QCM crystal.
- AO flux and fluence is measured using silver-coated QCM crystal and polyimide-coated QCM crystal.

2.6 References

1. Zhao-xing R., Ke-ming S., and Qing-ao L.: Atomic-Oxygen Beam Source with Compact ECR Plasma, , Plasma Science & Technology, Vol 4, No. 6, 2002, pp. 1545-1550.

2. Azmi B. Z., Moksin M. M., Yunus W. M. M., Talib Z. A., Wahab Z. A., Senin H. B., and Williams A. W.: An Atomic Oxygen Source for Simulation of Lower-Earth Orbit Environment, J. Solid St. Sci. Tech. Lett. Vol 1, No.2, 1994, pp. 5-10.

3. Hohman K. W., Olson L. B., Brogan T. R., Prebola Jr J. L., and Studkey J. A.: Development of an Atomic Oxygen Source for Space Simulation Applications, AIAA 2008-461, 46th AIAA Aerospace Science Meeting and Exhibit, 7-10 Jan 2008.

4. Bitetti G., Marchetti M., Mileti S., Valente F., and Scaglione S.: Degradation of the surfaces exposed to the space environment, Acta Astronautica, Vol. 60, No. 3, 2007, pp. 166-174.

5. Caledonia, G. E., Krech, R. H. and Green, B. D.: A high Flux Source of Energetic Oxygen Atoms for Material Degradation Studies, AIAA journal, Vol. 25, No. 1, 1987, pp. 59-63.

6. Caledonia, G. E., Krech, R. H., Green, B.D., Pirri, A. N.: Source of High Flux Energetic Atoms, United states patent, Patent number: 4,894,511, Jan 16, 1990.

7. Tagawa M., Yokota K., Kinoshita H., and Ohmae N.: Use of Quartz Crystal Microbalance on the Polymer Degradation Studies Regarding Atomic Oxygen Activities in Low Earth Orbit, Proceeding of the 9th International Symposium on Materials in a Space Environment, Noordwijk, The Netherlands, 16-20 June 2003. (ESA SP-540, September 2003).

8. Rooij A. D.: Exposure of silver to atomic oxygen, Product Assurance and Safety Department, ESTEC, Noordwijk, The Netherlands, ESA published document, http://esmat.esa.int/Publications/Published_papers/Exposure_of_Silver_to_Atomic_Oxygen.pdf

9. Yokota K., and Tagawa M.: Comparison of Polyethylene and Polyimide as a Fluence Monitor of Atomic Oxygen, Journal of spacecraft and rockets, Vol. 44, No. 2, 2007, pp. 434-438.

10 Yokota K., Tagawa M., and Ohmae N.: Temperature dependence in erosion rates of polyimide under hyperthermal atomic oxygen exposure, Journal of spacecraft and rockets, Vol. 40, No.1, 2003, pp. 143-144.

Chapter 3: Resistivity measurement facility for insulator and mathematical formulation

The central theme of spacecraft charging is how spacecraft interacts with the plasma environment to cause charging. Spacecraft accumulates charge and adopts potential in response to interaction with the plasma environment. The key parameters in modelling spacecraft charging are the electron emission properties of insulating materials, such as Secondary Electron Emission (SEE) coefficient, Photo Emission (PE), and surface and bulk conductivity of metal and insulating materials. These parameters determine how much charge will accumulate on the key spacecraft components in response to the incident electron, ion, and photon fluxes. It has been recognized that atomic oxygen present in LEO is one of the most important hazards to the spacecraft polymeric material resulting in modifying the surface properties of the materials. Thus the interaction of the LEO's atomic oxygen with the outer surfaces of a satellite may result in material's degradation, modifying their chemical, electrical, thermal, optical and/or mechanical properties. This influences how charge will accumulate and redistribute across the spacecraft atomic oxygen modified surface as well as the time-scale for charge transport and dissipation.

To measure the resistivity of a spacecraft insulator, the charge storage method, developed by Frederickson *et al.*[1,2] and others[3], is the most suitable configuration for space-type environment. In this method, charge is deposited on the surface of an insulator and is allowed to migrate through the dielectric. With this configuration, one can measure volume resistivity. We introduce further modification to measure the surface and volume resistivity together by allowing the diffusion of charge on dielectric surface as well as its migration through the materials. After the degradation of spacecraft surface materials due to atomic oxygen exposure, surface properties, like bulk and surface resistivity are measured. A comparative study between the exposed and virgin materials will give more accurate prediction of

charging and arcing process on spacecraft. We shall use these data for the spacecraft charging and arcing simulation tool MUSCAT, developed in our laboratory. This will enable more accurate and precise prediction of charging and arcing condition for spacecraft through its lifetime.

In this dissertation, we present the technique for measuring the surface and bulk resistivity of AO-exposed sample, along with the necessary mathematical formulation used for calculating resistivity.

3.1 Reisitivity measurment system

The resistivity of the sample is measured using the charge storage decay method. This method exposes one side of the insulator in vacuum to a charge source, with a metal electrode attached to both back and front side of the insulator for measuring surface and volume resistivity, respectively. The charges, deposited on the surface of the insulator, diffuse on the surface and migrate downward. Data are obtained by capacitive coupling to measure the resulting voltage (or, more correctly, the electric field) due to charge on the open surface. Measurements to determine resistance with this method requires the use of an external charge deposition source and a very good electrostatic field probe.

Figure 3.1 shows the experimental setup and circuitry of the system. This chamber is also equipped with an electron gun (OME-0050LL) that ensured electron shower with a maximum energy of 10KeV (Electron beam energy used in this dissertation is 2-3KeV), is showing a maximum current density of not more than $100mAm^{-2}$. The chamber is equipped with a non-contacting surface potential meter (Trek model 341B) which is used to monitor the surface charge distribution of sample with the help of stage motor and movers. These allow the scan of insulator surface along a serpentine-like course within an area of 50mm x 50mm (step size 1mm). A motor-driven shutter is located below the beam gun to expose the sample for a required time. All these experiment were performed in a vacuum chamber of a cylindrical

shape of 0.6m diameter and 0.9m length. This chamber is evacuated by a turbo-molecular pump (500l/s), which is backed by a rotary pump to achieve a pressure in the range of 5.0x 10^{-4}Pa.

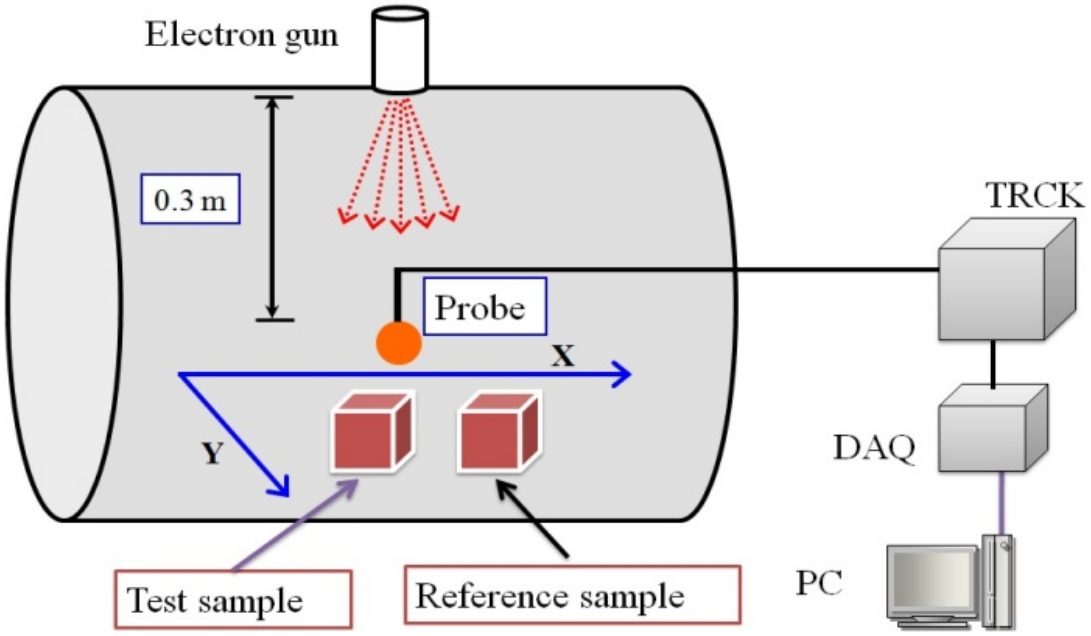

Figure 3.1: Schematic view of resistivity measurement facility.

3.2 Mathematics of surface charge decay for resistivity measurement

In order to measure resistivity by surface charge decay method, an insulator is assumed to be instantaneously charged at $t = 0$ by an electron beam, which produces certain surface potential and this surface potential is monitored afterward by the surface potential meter. The insulator of the thickness τ is attached with electrode in such a way that it allows charge diffusion on the surface and through material volume. The rate of change of the surface charge density when irradiated by an electron beam of current density j is given by the following expression,

$$\frac{\partial \sigma}{\partial t} = -j(1-\delta) + \frac{1}{R_s}\nabla^2\phi - \frac{1}{\rho\tau}\phi \quad (1)$$

Here, δ is the secondary electron coefficient, R_s is surface resistance (Ω/□"sq"), ρ is a volume resistivity (Ωm). If σ is electric charge density (Coulomb.meter^{-2}), ε is permittivity

(Coulomb.volt^{-1}.meter^{-1}), ϕ is surface potential and τ is thickness, then the relation between them is as follows:

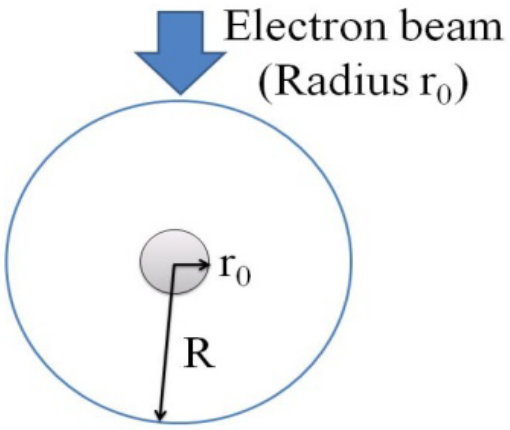

Figure 3.2: Sketch showing method of resistivity calculation.

$$\sigma = \frac{\varepsilon\phi}{\tau} \quad (2)$$

Therefore, it becomes a partial differential equation concerning the electrical potential distribution ϕ.

$$\frac{\partial\phi}{\partial t} = -\frac{j\tau}{\varepsilon}(1-\delta) + \frac{\tau}{\varepsilon R_s}\nabla^2\phi - \frac{1}{\rho\varepsilon}\phi \quad (3)$$

This equation is solved by using the cylindrical coordinates system. Thus,

$$\nabla^2\phi = \frac{1}{r}\frac{\partial}{\partial r}\left(r\frac{\partial\phi}{\partial r}\right) \quad (4)$$

Hence,

$$\frac{\partial\phi}{\partial t} = -\frac{j\tau}{\varepsilon}(1-\delta) + \frac{\tau}{\varepsilon R_s}\frac{1}{r}\frac{\partial}{\partial r}\left(r\frac{\partial\phi}{\partial r}\right) - \frac{1}{\rho\varepsilon}\phi \quad (5)$$

This equation is used for the fitting of potential decay curve to find the resistivity values. In Eq. [5], the radius r_o does not appear explicitly and the outer radius of R appears as the boundary condition. Therefore, the beam radius r_o, although defined in Figure 3.2 has little meaning in the following analysis.

3.3 Resistivity measurement sample layout and mesaurement methodology

Resistivity measurement is done with electrode configuration as shown in Figure 3.3. The top-view of the electrode configuration is shown in Figure 3.4. The electrode is made of copper tape having conductive adhesive. Adhesive provides very good electrical contact between polyimide and electrode. Test sample size was of 60x 60mm having thickness of 25µm was used. After irradiating electron beam on an area of r_0 = 5mm or r_0 = 2.5mm at the centre of test sample as shown in Figure 3.5, the charges are allowed to dissipate in Φ = 50mm, potential drop on the sample surface is scanned using surface potential meter. Surface potential meter scans the surface along a serpentine-like course with a distance resolution of 1mm. Surface potential meter to sample distance was about 2mm.

Figure 3.5 shows the experimental setup of the sample inside the chamber for resistivity measure. The electron beam enters vertically downward which was allowed to fall on the sample centre using two beam modifier plates. The hole size of 5mm and 10mm diameter in beam modifier plates are used to expose respective area of 5mm and 10mm diameter at the centre of test sample to electron beam directly.

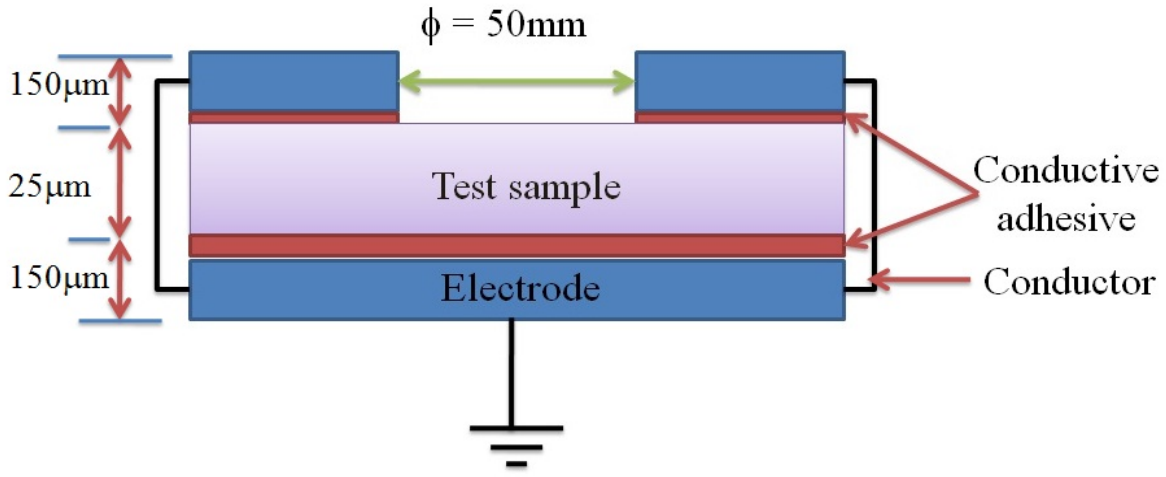

Figure 3.3: Electrode configuration for measuring surface and volume resistivity.

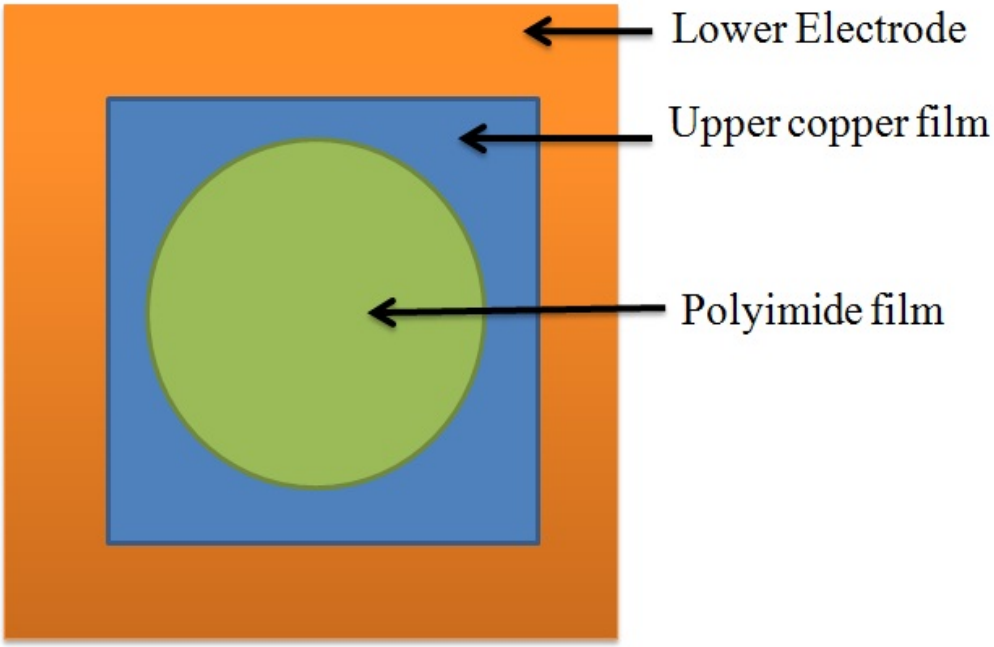

Figure 3.4: Top-view of the sample electrode arrangement used for resistivity measurement.

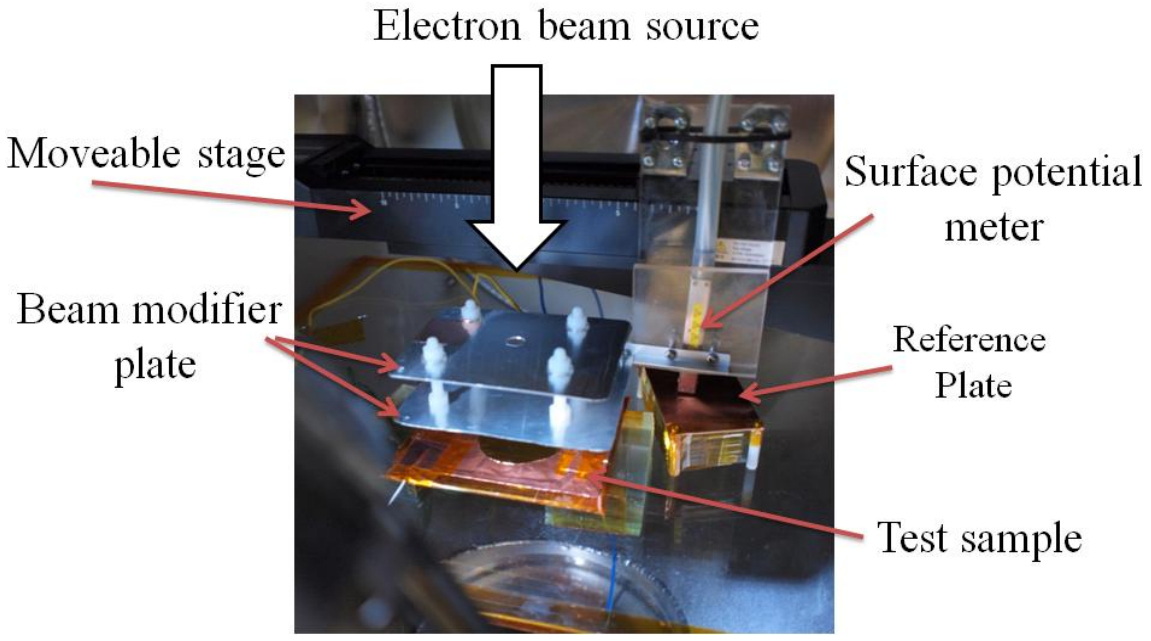

Figure 3.5: Inside chamber view of the setup for resistivity measurement.

Once the electron beam irradiates the sample centre of test sample for one minute, the electron beam exposure is stopped. Afterward, the surface potential meter scans the test sample surface at a regular interval using the moveable stage as shown in Figure 3.6 and the results look like as shown in Figure 3.7.

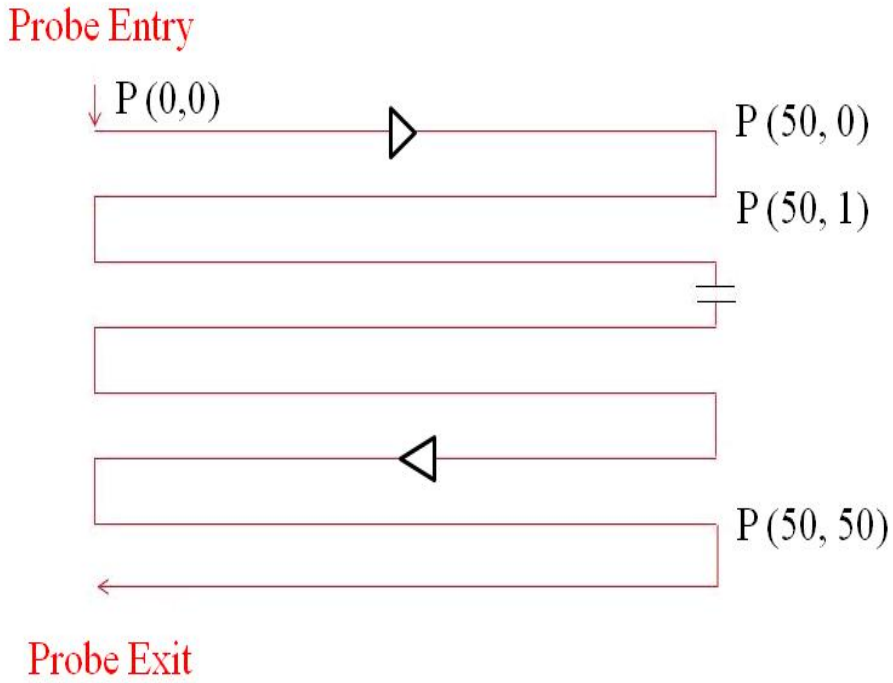

Figure 3.6: Surface potentiometer scans the surface in serpentine line fashion.

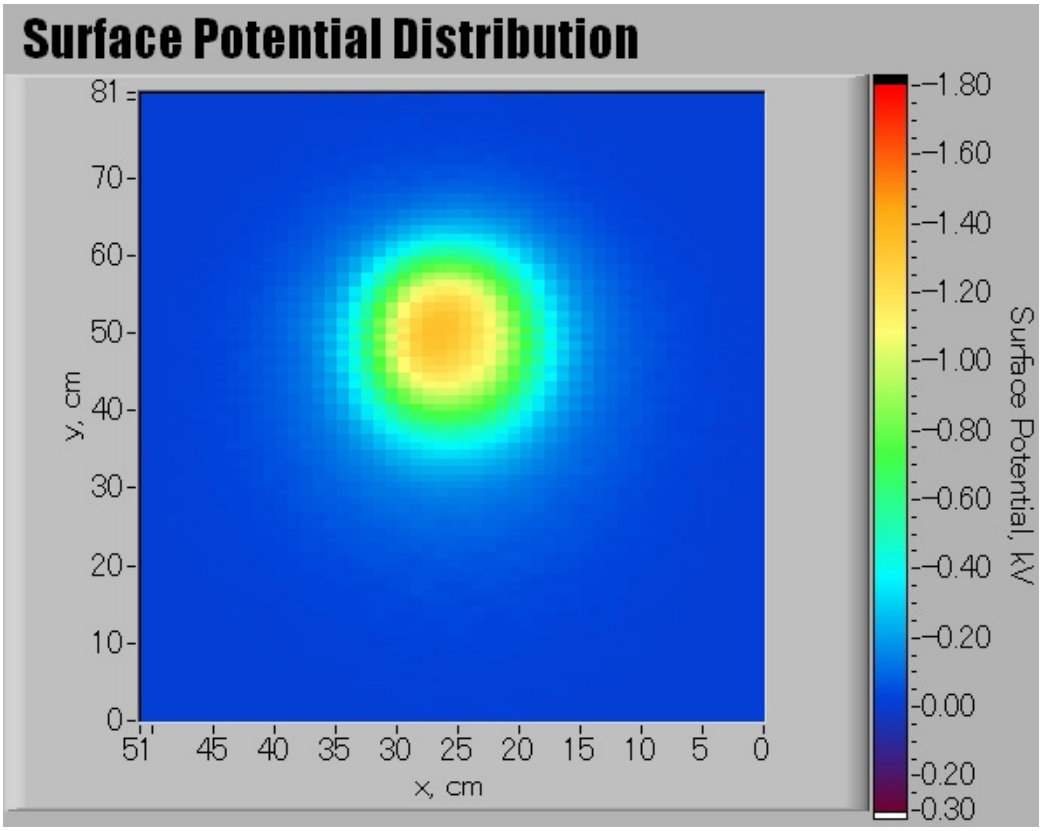

Figure 3.7: Recording of surface potential by potentiometer and display on PC screen.

3.4 Conclusion

- Experimental facility for measuring surface and bulk resistivity is realised.
- Mathematical formulation for the measurement of resistivity is done.
- Electrode configuration for the simultaneous measurement of surface and volume resistivity is done.

3.5 Reference

1. Dennison, J. R., Bruson, J., Swaminathan, P., Wesley, N. and Frederickson, A. R.: Method of High Resistivity Measurement Related to Spacecraft Charging; IEEE transaction on plasma society, Vol. 34, No. 5, 2006, pp. 2204-2218.

2. Frederickson, A. R. and Dennison, J. R.: Measurement of Conductivity and Charge Storage in Insulators Related to Spacecraft Charging, IEEE transactions on nuclear science, Vol. 50, No. 6, 2003, pp. 2284-2291.

3. Lutz, B. and Kinddersberger, J.: Determination of Volume Resistivity of Polymeric Insulators by Surface Charge Decay, proceeding of 16th International symposium on high voltage engineering. ISBN 978-0-620-44584-9

Chapter 4: Results and Discussion

In this chapter, the first section is about the study of AO-exposure on material's surface. The second section is about the effect of atomic oxygen exposure on resistivity characteristics of polyimide.

4.1 Effect of AO exposure on materials

AO-exposure changes the surface structure of materials. It influences surface properties very strongly. It may influence surface properties which might play an important role in spacecraft charging. Here we will study the change in surface properties of two materials namely silver and polyimide. Both of these materials were also used to measure the fluence of atomic oxygen in chamber.

4.1.1 Effect on silver

Scanning Electron Microscopic (SEM) analysis: SEM images of the non-exposed and AO-exposed silver are shown below in Figure 4.1 for two different magnifications. The AO-exposed surface shows clear difference from the virgin surface due to the formation of silver oxide formation on the surface. This phenomenon is called oxide growth, is also observed on silver in space experiment[1,2]. The silver oxide is formed after chemical reaction of AO with silver in high vacuum condition. The oxidation of silver in AO is essentially linear-parabolic as postulated by De Rooij[1] and experimentally confirmed by Chambers *et al*[3]. In present research, as the silver was exposed to fluence (4.24×10^{16} atoms/cm^2), growth in the boundary was observed. This is understandable by analysing the change in mass of the silver coated QCM crystal, as shown in Figure 2.34 (Chapter 2), which shows linear increase in mass due to oxidation process.

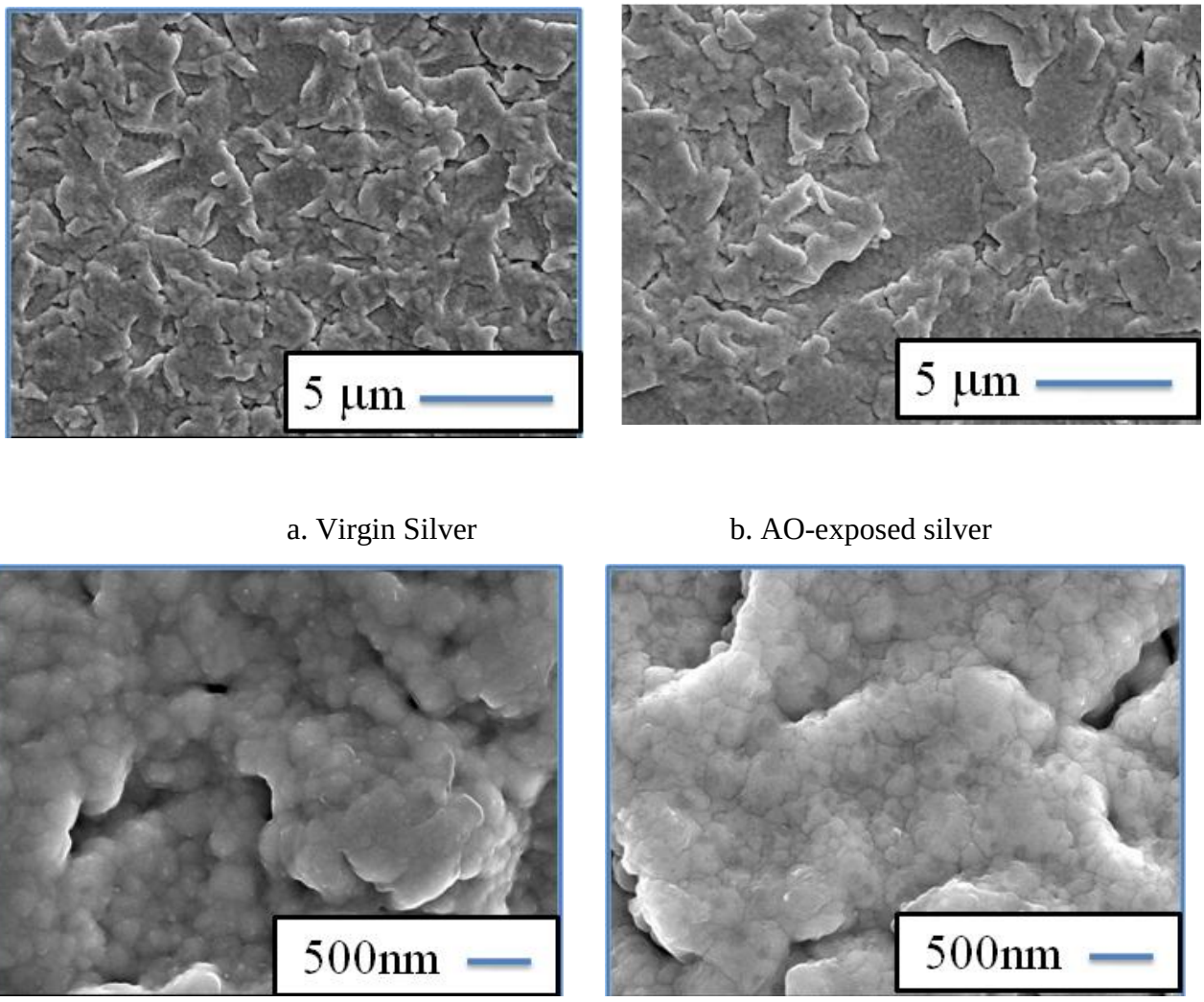

a. Virgin Silver b. AO-exposed silver

c. Virgin silver d. AOexposed silver

Figure 4.1: Scanning Electron Microscopy images of the virgin and AO-exposed silver with two different magnification.

EDS analysis of silver coated QCM: EDS analysis of the AO-exposed, having fluence 4.24x 10^{16}atoms/cm^2, and virgin silver-coated QCM crystal was done. The results are shown in Table 4.1. The EDS result shows that the atomic percentage (%) of oxygen increases with the AO-exposure. This is due to the formation of silver oxide on the surface.

Table 4.1: EDS analysis of AO-exposed and Virgin silver-coated QCM.

Elements ↓ condition→	Virgin (Atomic %)	AO exposed (Atomic %)
O (K)	6.79	8.68 ↑
Si (K)	21.51	15.44 ↓
Ag (K)	71.70	75.88 ↑

4.1.2 Effect on Polyimide

Polyimide is the most widely used dielectric materials on the surface of spacecraft. It finds it application as thermal control for spacecraft. However, this material is highly vulnerable to the atomic oxygen of LEO as observed in space flight experiment. Because of its extensive application and vulnerability, polyimide was chosen for the analysis of AO-exposure on its electrical properties.

SEM analysis: Change in surface morphology of polyimide using SEM was also studied. The SEM images prior to AO-exposure and after exposure are shown in Figure 4.2. The sample surface was smooth prior to the AO-exposure. However, surface morphology changed after the 5.4x 10^{18}atomscm^{-2} AO-exposure, which was equivalent to 10years at 800km AO-exposure having 10-12km/s velocity. This fluence values can be normalized for 8km/s condition in accordance with M. Tagawa *et al*[(4)]. It is obvious that, the surface morphology of polyimide sample became much rougher and significantly modified. This shows that AO surface erosion is much significant for the given AO fluence.

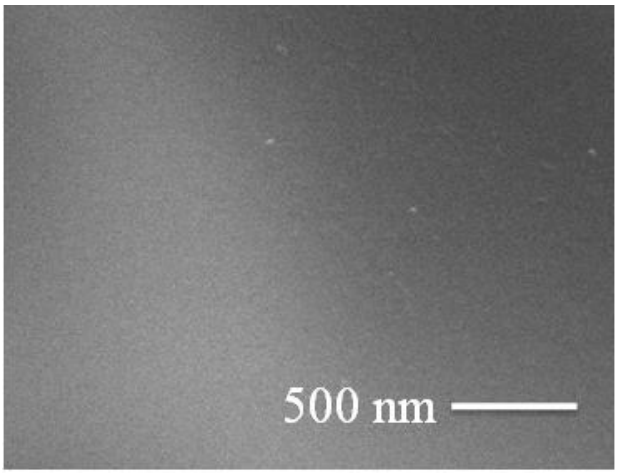

Virgin sample

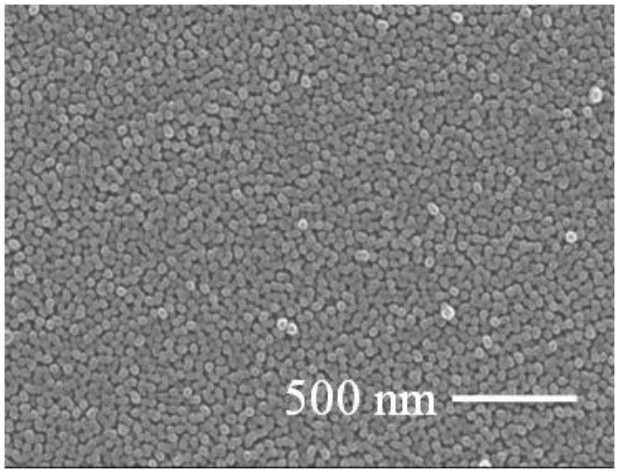

AO-exposed sample

Figure 4.2: Scanning Electron Microscopy of virgin and AO-exposed polyimide.

Laser beam imaging: The difference between the AO-exposed and virgin polyimide can be further understood by analysing the laser imaging of the surface. This is very easy to understand, if the visual images of the AO-exposed polyimide and virgin polyimide are studied, as shown in Figure 4.3. The first image is analysed using normal camera. It is observed that even with the camera, difference in reflectance of the AO-exposed and virgin polyimide coated on QCM crystal can be observed, the AO-exposed surface is encircled with blue which shows higher light reflectance. Then, this QCM surface is imaged using the laser scanning instrument. It is again observed that the AO-exposed and virgin sample show different reflectance.

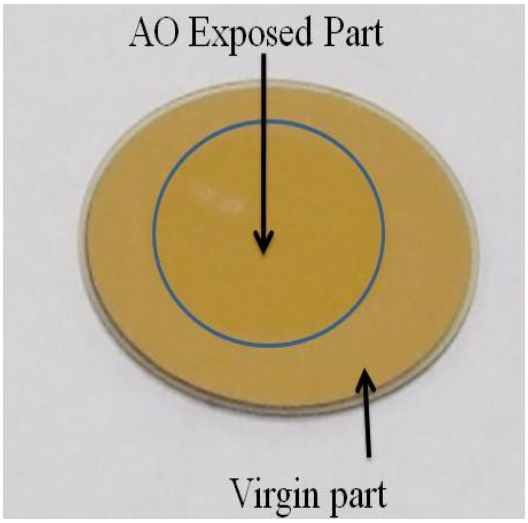

a. Camera-view showing the difference between AO-exposed and virgin area on QCM.

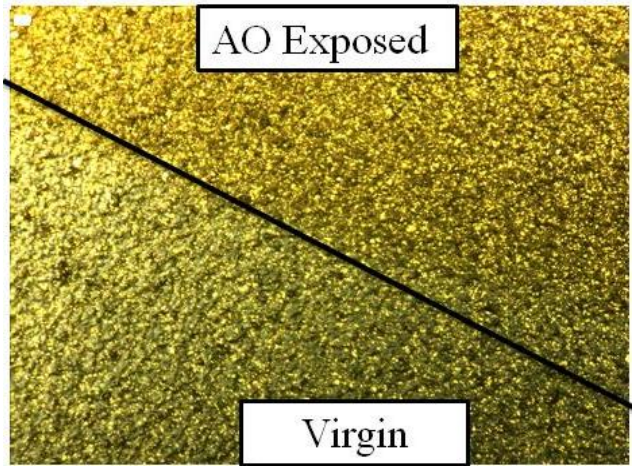

b. Laser imaging-view of QCM crystal having AO-exposure and virgin.

Figure 4.3: Difference in the two regions of the AO-exposed and virgin polyimide sample as observed by camera (a); and laser imaging (b).

Change in thickness of polyimide coated on QCM after AO-exposure: The change in the thickness of the polyimide coating on QCM due the AO-exposure was also studied. The results are shown in the Figure 4.4. The left side Figure 4.4 shows the AO-exposed and virgin parts separated by black line dividing two parts, the red line show the line of the scanning. The right side of the figure shows the scanner movement in magnified way to observe the change in thickness. It was observed that the exposure of AO reduced the thickness of the QCM crystal by 5.64μm for 5.4x 10^{18}atomscm^{-2} AO-exposure. For LDEF, the loss of

thickness was more than 127μm for the total AO exposure of 9x 10^{21}atoms/cm^2 [5,6]. This loss of thickness of 5.6μm, much higher than the case of LDEF for the given fluence, is explained on the basis of non linear mass loss response of the polyimide, as noted in the fluence measurement, as shown in figure 2.35.

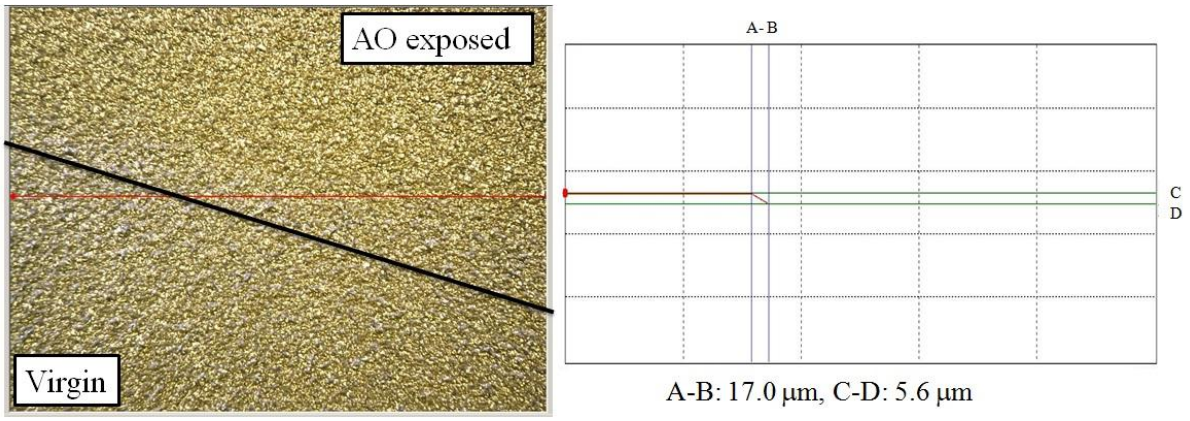

Figure 4.4: Measuring change in thickness of the polyimide coated QCM crystal using Laser spectroscopy.

EDS analysis:

EDS Analysis was done for the AO-exposed polyimide and virgin polyimide coated on the gold coated QCM. The gold coated QCM is used as base crystal for polyimide coating as AO do not react chemically with gold even if the AO erosion removes the polyimide layer. The EDS analysis was done on the location exposed to AO and on the location non-exposed on same crystal. Figure 4.5 shows the location where the EDS analysis was done on QCM crystal. The analysis result is shown in Table 4.2.

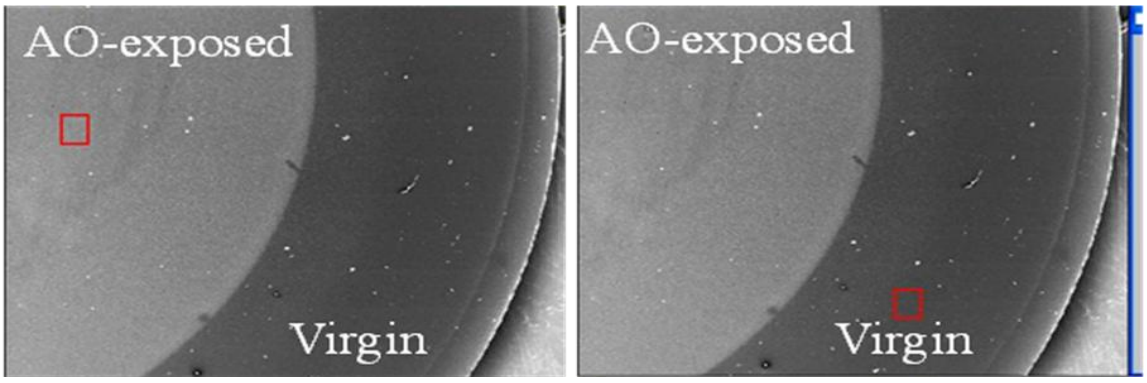

Figure 4.5: EDS of the AO-exposed polyimide on the gold-coated QCM

Table 4.2: EDS analysis of Polyimide coated gold QCM crystal.

Sample condition→ Composition↓	Virgin (Atomic %)	AO-exposed (Atomic %)
C+N+O	97.16	95.67↓
Si (K) (QCM has Si)	0.39	0.50↑
Au (M) (QCM coated with Au)	2.465	3.84↑

This table shows that the total concentration of C+N+O decreases on the surface and that of Au is increasing. This happens due to the removal of polyimide coating from the QCM surface, as it was shown that AO removed about 5.64μm thickness for 5.4×10^{18} atoms cm^{-2} AO-exposure.

XPS Analysis: The difference between AO-exposed and virgin polyimide was studied using the XPS[7,8]. The detailed XPS analysis showed the increase in the presence of oxygen on the surface. Figure 4.6 and 4.7 shows the XPS spectrum of the virgin and AO-polyimide. A shift of -3.5eV for all the peaks was observed, it happened due to the surface charging of the materials during the analysis, a well known phenomenon for the insulator surface. The analysis of the carbon peak 4.8 and 4.9 shows that the intensity of the carbon peak decreased after the AO-exposure indicating a decrease in carbon concentration. On analysing oxygen peaks of the virgin and AO-exposed polyimide, as shown in Figure 4.10 and 4.11, it was observed that the oxygen peak intensity increased indicating an increase of oxygen concentration on surface. The analysis of nitrogen peak, as shown in Figure 4.12 and 4.13, there is no change in the peak height due to AO-exposure. Thus from XPS analysis, it is concluded that the concentration of oxygen is increasing and that of carbon is decreasing due to AO-exposure, which is expected result. A peak of silicon was also observed; it indicates

that the given polyimide has silicon. The investigation of the peak height for C, O, N and Si is shown in Table 4.3. The investigation of C/O and C/N ration is shown in Table 4.4

Table 4.3: XPS analysis of Virgin and AO exposed polyimide

XPS signal	Carbon	Oxygen 1s	Nitrogen 1s	Silicon 2p
Biding energy (+ 3.15eV)	285.1	532.1	400.1	101.1
Peak Intensity (Virgin)	115950	128550	46100	9060
Peak intensity (AO-exposed)	106030↓	153630↑	4581	8510

Table 4.4: Effect of AO exposure expressed in term of C/O and C/N ratio.

Sample → Area ↓	Virgin polyimide	AO exposed polyimide
Area Carbon	1.01×10^6	8.61×10^5
Area Nitrogen	1.30×10^6	1.27×10^6
Area oxygen	1.77×10^6	2.10×10^6
C/O	0.56	0.41
C/N	0.78	0.68

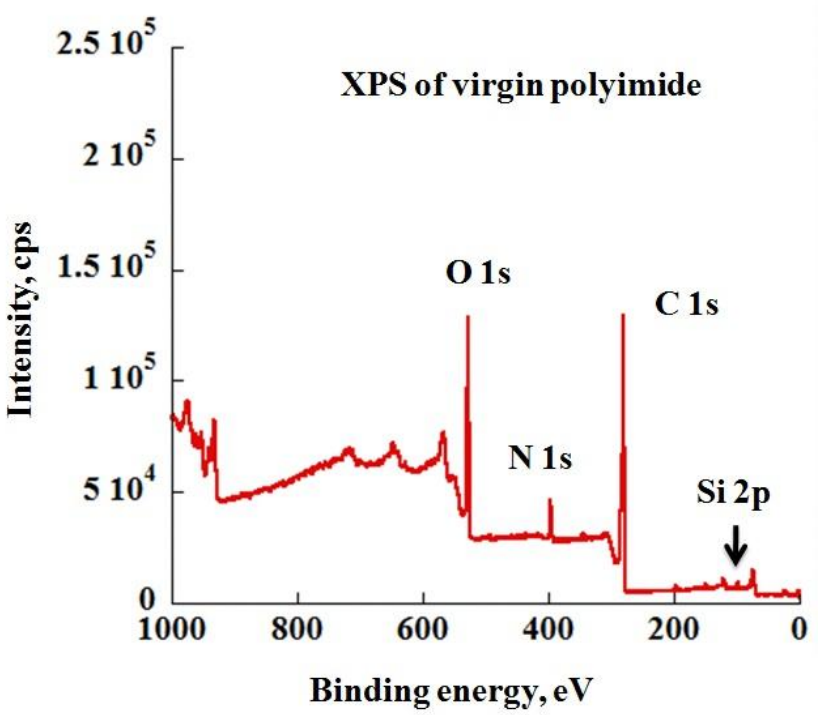

Figure 4.6: XPS of Virgin polyimide.

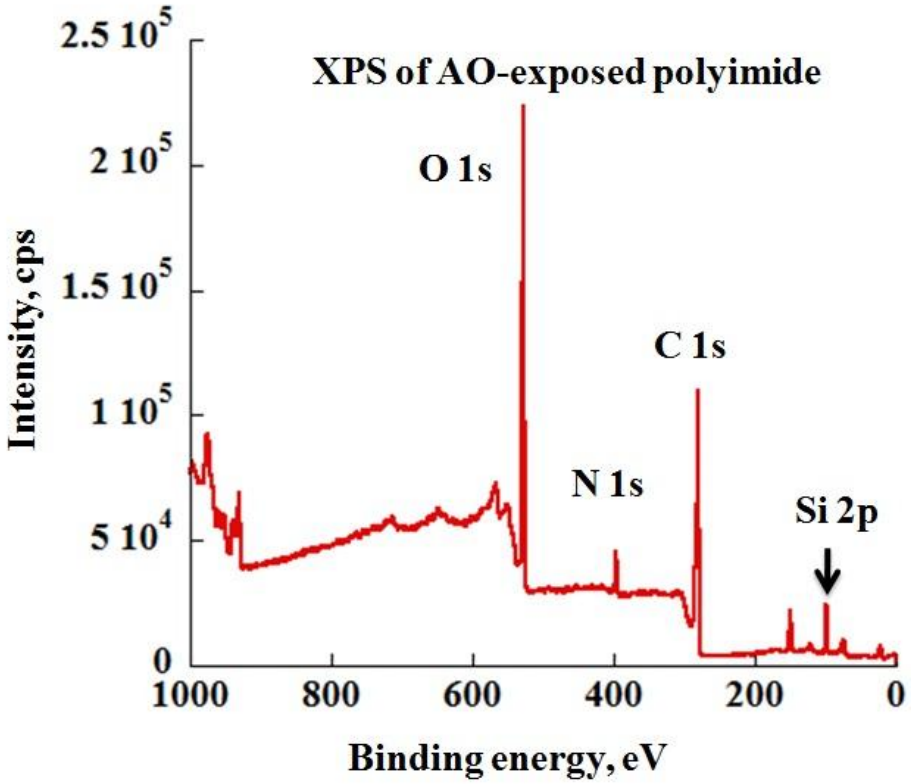

Figure 4.7: XPS of AO-exposed polyimide.

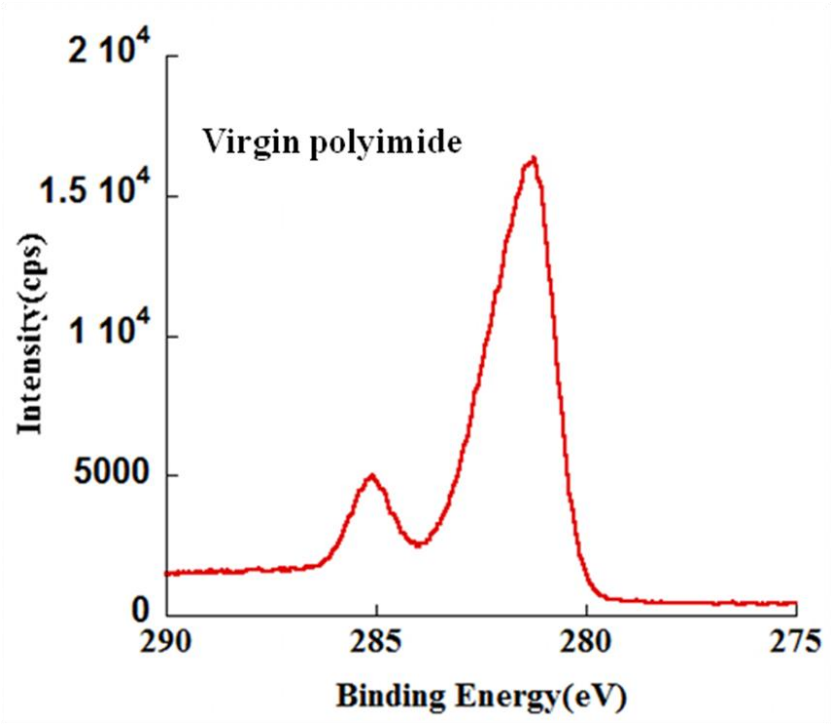

Figure 4.8: XPS of carbon for virgin polyimide.

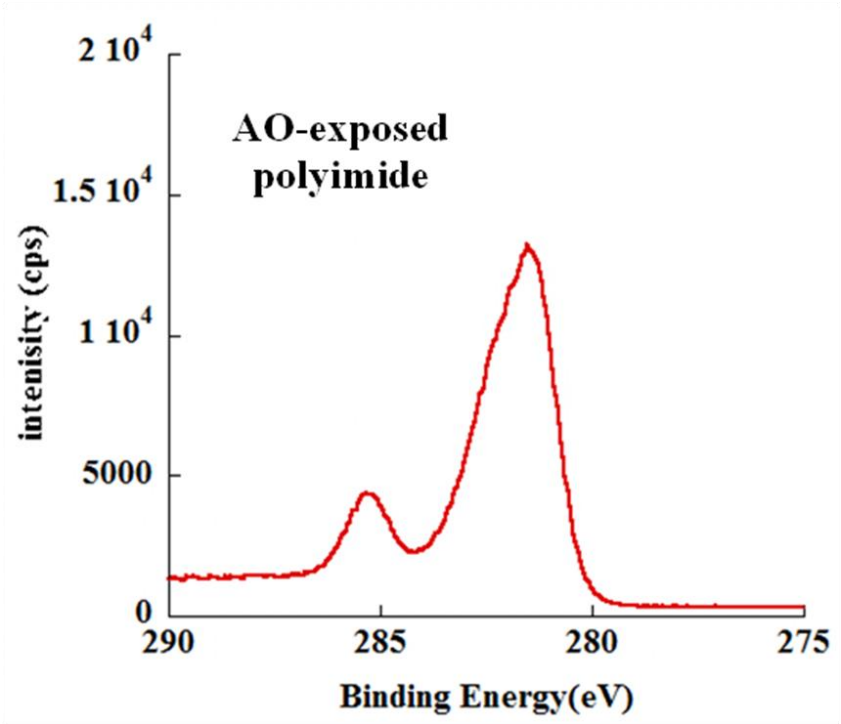

Figure 4.9: XPS of carbon peak for AO-exposed polyimide.

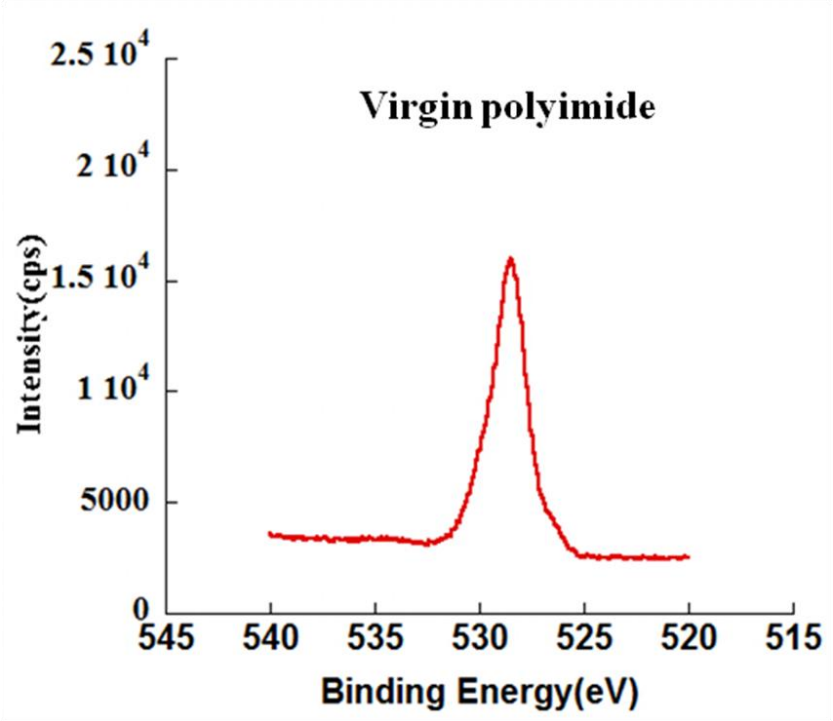

Figure 4.10: Oxygen peak of virgin polyimide.

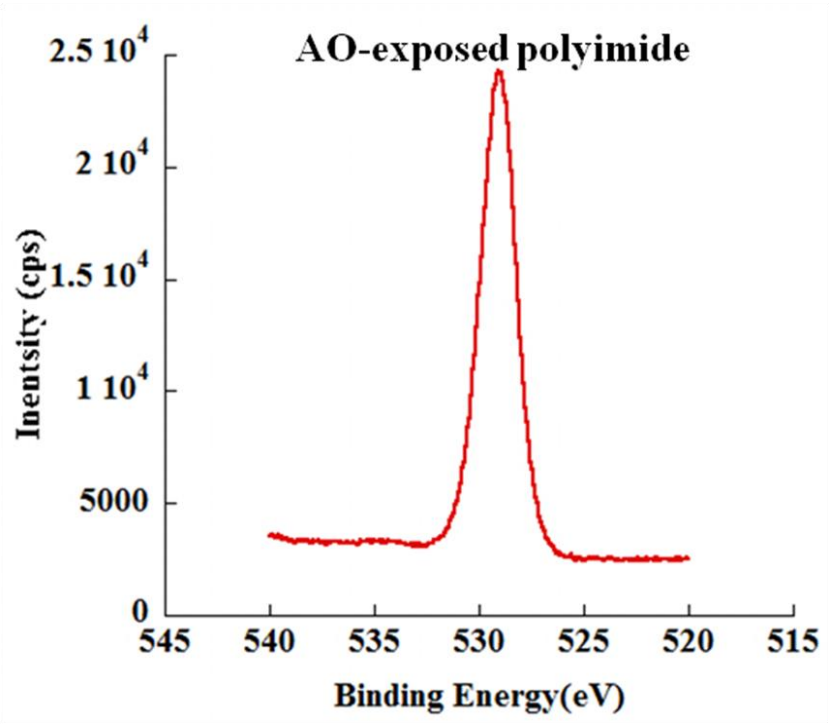

Figure 4.11: Oxygen peak of AO exposed polyimide.

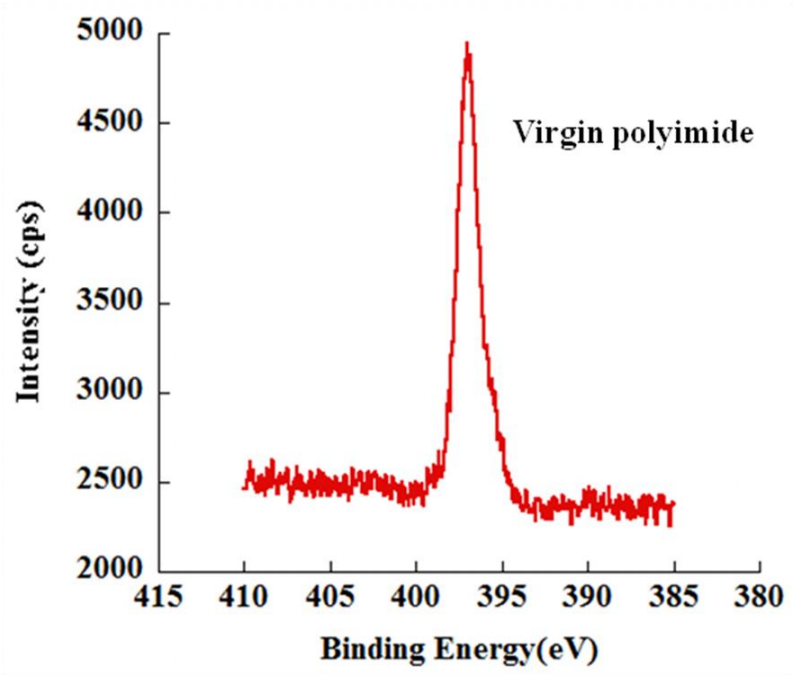

Figure 4.12: XPS of nitrogen peak in virgin polyimide.

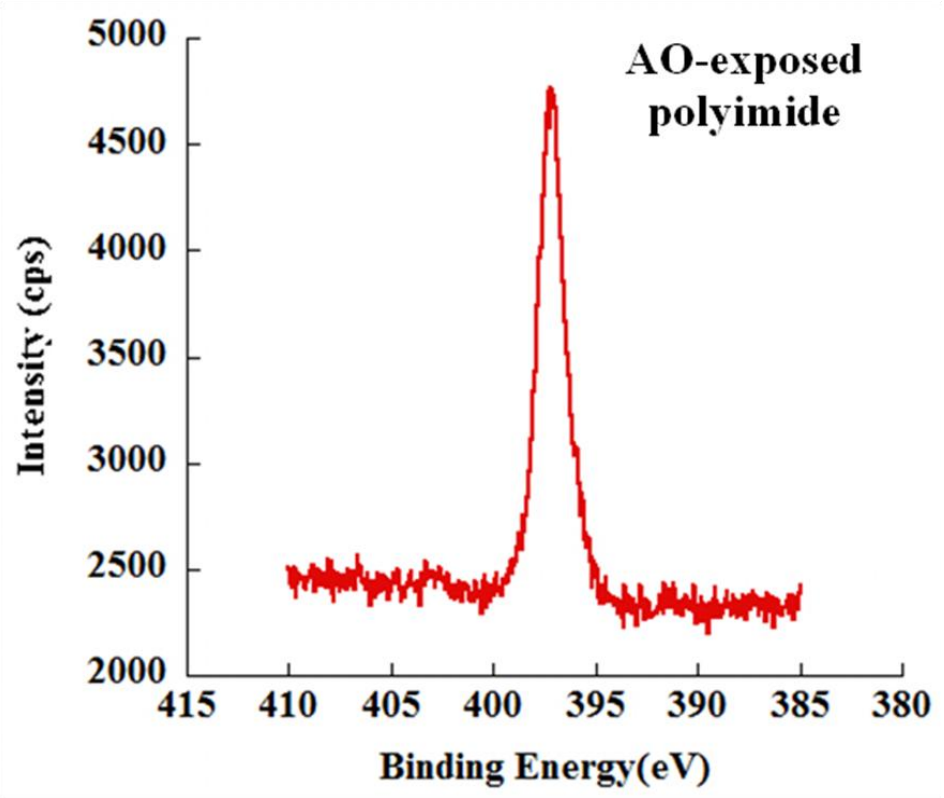

Figure 4.13: XPS of nitrogen peak in AO-exposed polyimide

4.2 Effect of AO exposure on resistivity

In order to measure the resistivity of sample, we first measured the decay of surface potential on the sample. The fall of surface potential gave an inlook into the resistivity values. Here, we first analysed the surface potential distribution and then the resistvity calculation from the fall of potential. All these resistivity experiments were performed at room temperature[9].

4.2.1 Surface potential distribution

Surface potential distribution was measured regularly for 96hours. Change of surface potential distribution was monitored and was displayed in a 2D-graph by assuming the rotation-symmetric shape. Figures 4.14 and 4.15 show the potential distribution view for virgin and AO-exposed sample along X-axis and Y-axis, for measuring surface and volume resistivity. They are shown for three times, 0hour (just after electron beam irradiation stopped), 24hours and 96hours time delay since the electron beam irradiation stopped. On analysing this figure, we observed that the rate of potential drop in two cases was different. This change in potential drop is considered to be due to the change in resistivity of sample caused by atomic oxygen exposure. The potential pattern was shown in such a way that the centre of the sample, where electron beam exposed sample, was chosen as centre of co-ordinate system and moving outward in two directions as Cartesian co-ordinate positive and negative axis. 2-D surface view of the potential drop for virgin and AO-exposed sample is shown in Figure 4.16.

3-D view showing the axis-symmetry nature of surface potential decay profile of the virgin and atomic oxygen exposed polyimide is shown in Figures 4.17. Figure 4.16 and 4.17 shows that the surface potential decay profile is axis-symmetric in pattern. The potential patterns are shown for just after electron beam irradiation, 10hours, 24hours and 96hours time delay since the electron beam irradiation stopped. From Figure 4.16 and 4.17, it is

observed that the potential shows centro-symmetric distribute along its centre. The potential drop with respect to time also shows symmetry in each case along its centre. The analysis of this potential drop gives the idea of resistivity values.

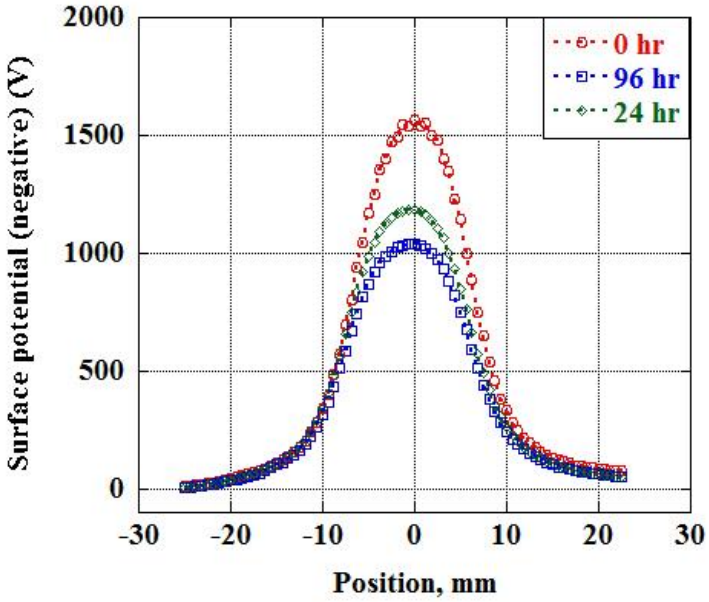

(a) Surface potential decay of virgin sample along X- axis

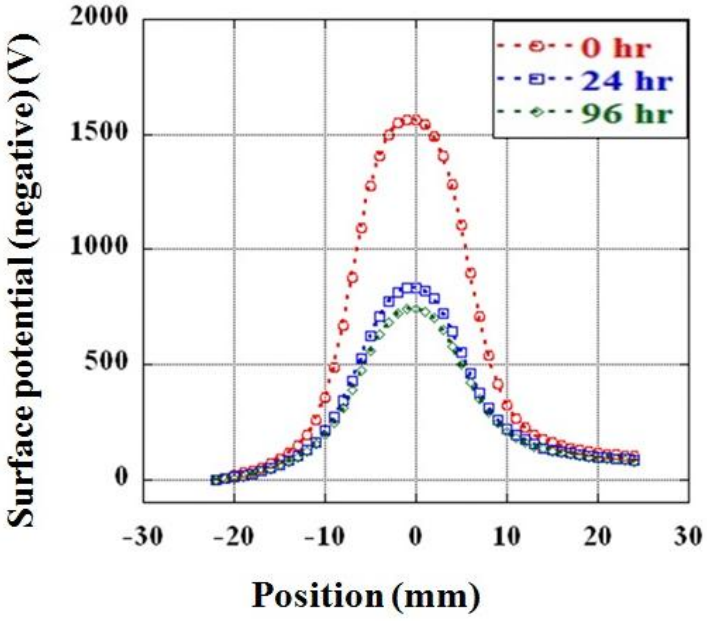

(b) Surface potential decay of virgin sample along Y- axis

Figure 4.14: Surface potential decay of virgin polyimide along the X-axis and Y-axis measured using a surface potentiometer.

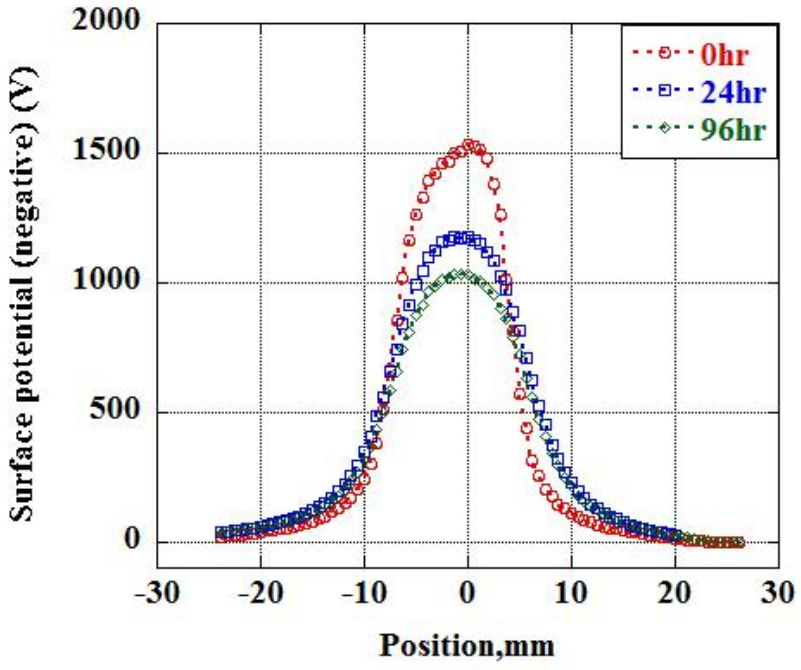

(B1) Surface potential decay of AO-exposed sample along X-axis

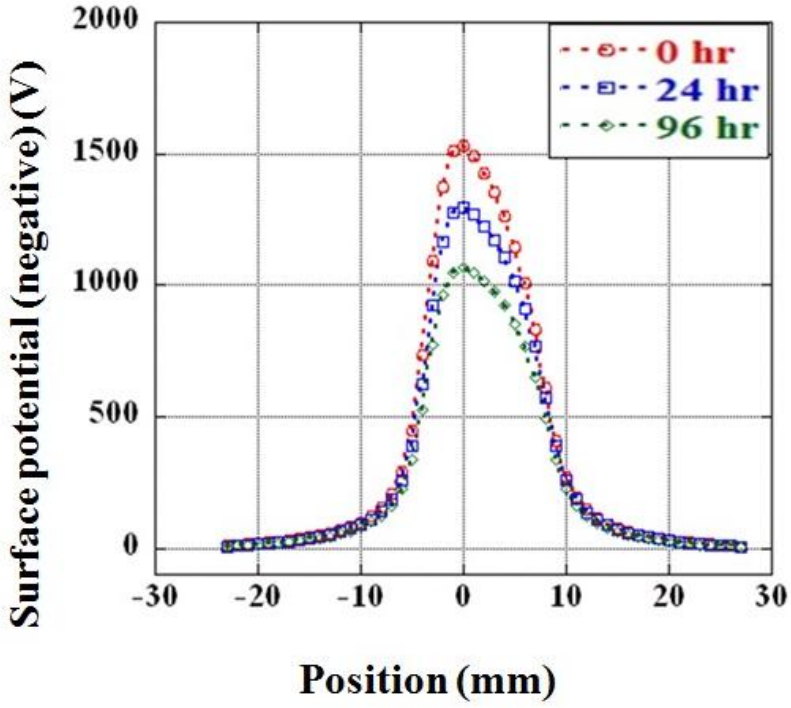

(B2) Surface potential decay of AO-exposed sample along Y-axis

Figure 4.15: Surface potential decay of AO-exposed polyimide along the X-axis and Y-axis measured by using a surface potentiometer.

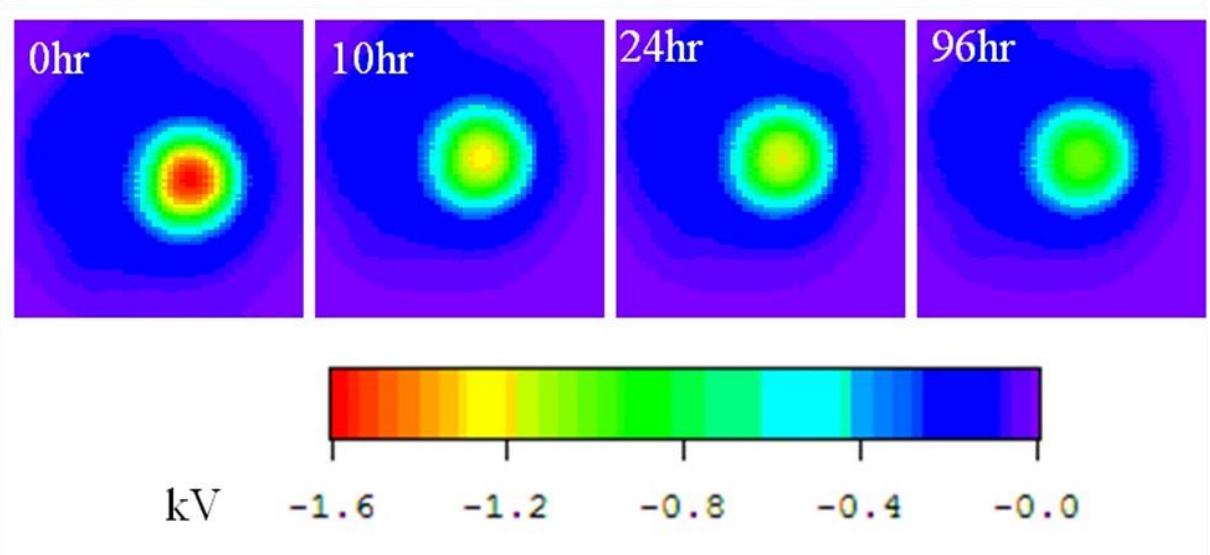

a. Virgin polyimide

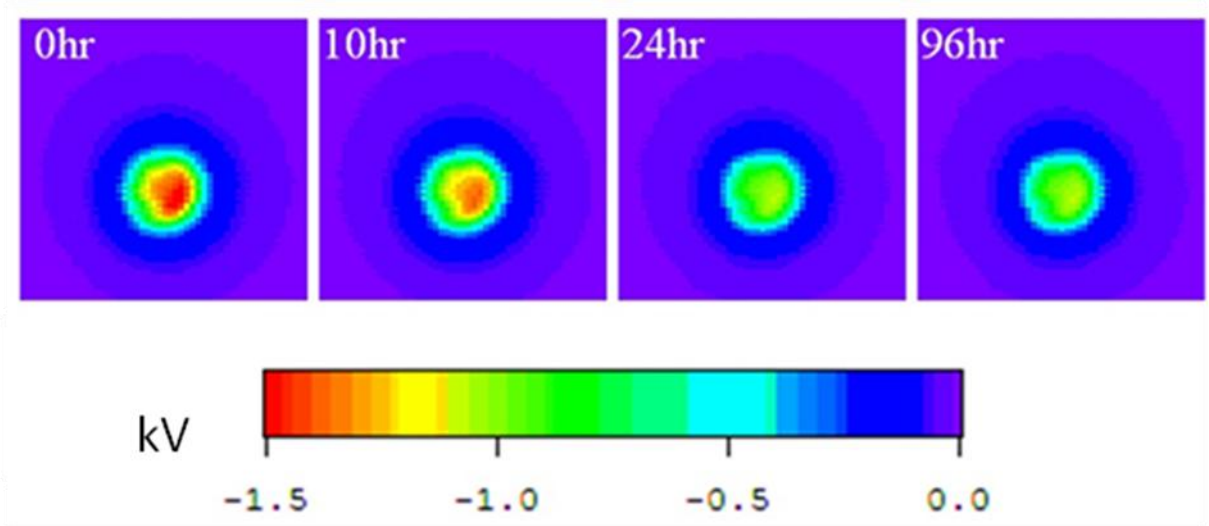

b. AO-exposed polyimide

Figure 4.16: Two dimensional surface views of potential drop with time for virgin sample and AO-exposed sample, respectively, measured by using a surface potentiometer.

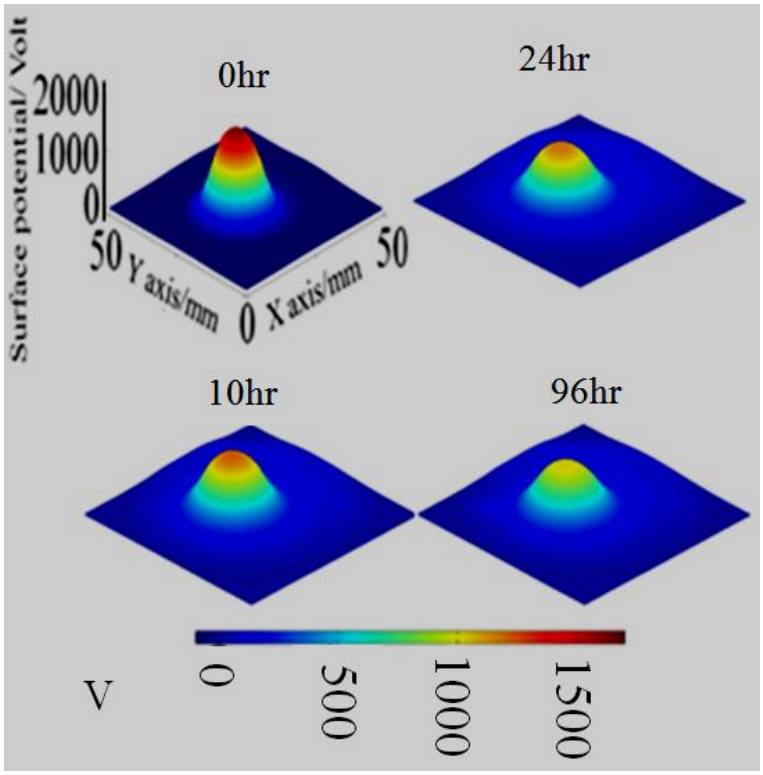

a. Virgin polyimide

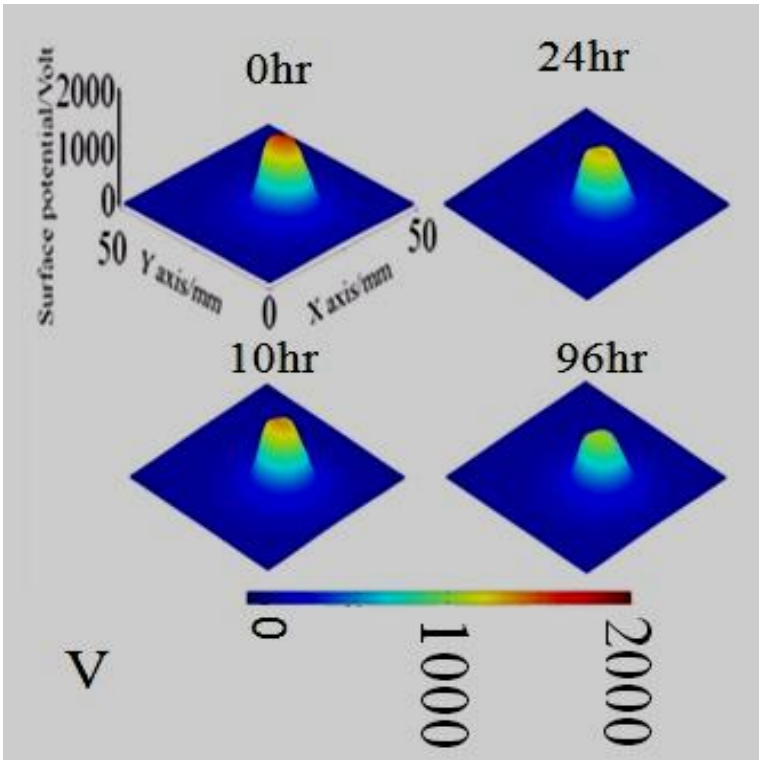

b. AO-exposed polyimide

Figure 4.17: Three dimensional view of potential drop with time for (a) virgin polyimide and (b) AO exposed polyimide measured by using a surface potentiometer.

4.2.2 Determination of surface and volume resistivity

The resistivity measurement experiments were performed for virgin and AO-exposed polyimide samples. Three experiments were performed for the virgin sample with the hole size in the beam modifier plate of 5mm, 10mm, and 10mm respectively for exposing the corresponding area at the centre of sample to the electron beam directly. One of the experiments was performed for the AO-exposed sample with the hole diameter size of 10mm in the beam modifier plates.

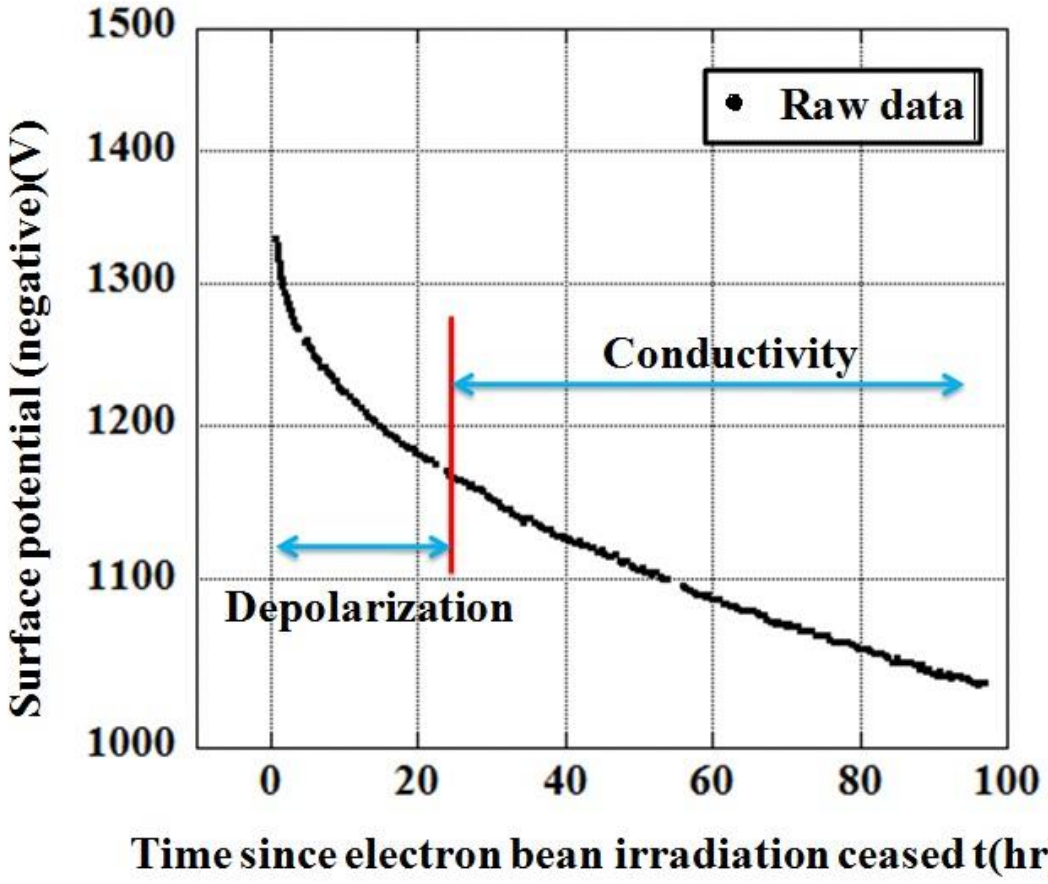

Figures 4.18: Temporal profile of the potential at the centre of the test samples.

The initial surface potential drop is due to polarization-depolarization phenomenon. After a certain time, the process of polarization-depolarization ends. After initial polarization-depolarization phenomenon finishes further drop in surface potential is due to the electron propagating outward towards peripheral electrode and through the bulk of materials. After a

certain time, the flows of electron from the sample centre to the peripheral electrode and trough the bulk materials become steady. We consider beginning of this time as 24hours since the electron beam irradiation stopped as shown in Figure 4.18. In this graph x-axis is time in hours and y-axis is the potential fall on log scale. This area of conductivity is called "dark current conductivity" and is assumed to be constant and independent of time.

After 24hours since the electron beam stopped, the potential decay profile was fitted by Eq. [5], chapter 2. We used the potential profile, along y axis passing through the centre, at 24hours as initial condition and solved Eq. [5] numerically until 96hours. The numerical profile at 96hours was compared with the experimental data. We varied the surface and volume resistivity in Eq. [5] and looked for a combination of the two values to give the best fit between the simulation and the experiment. For the purpose of analysis, each potential profile, as shown in Figure 4.3, was divided into two sections, one in negative x-axis and other positive Y-axis with the peak potential point as the origin of Y-axis. The numerical technique used to solve Eq. [5] was a finite difference method, where the forward difference and the central difference were used for the temporal and spatial difference respectively. The temporal step was 10seconds and the spatial step was 1mm.

In terms of space application, evaluating the resistivity at the later stage of potential decay gives the safe margin to the prediction of charging in orbit. Until Frederickson *et al.*[10,11] gave warning that the majority of spacecraft charging analysis had been carried out using the resistivity values measured based on conventional methods, such as ASTM D-257 standard[12], where the resistivity value measured after 1minute of voltage application is used as the resistivity. The time of 1minute is still when polarization dominates and the resistivity is underestimated. As shown in the experimental result in Figure 4.6, the charge does not decay as quickly as the initial decay phase where the polarization dominates.

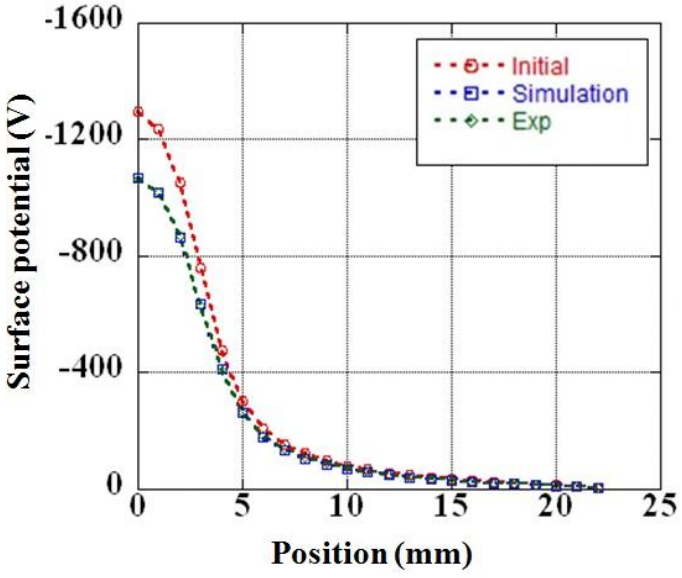

Figure 4.19: Comparison of potential decay between experiment and simulation.

In spacecraft charging, charging of insulator continues for the time scale of seconds to hours. The measurement results shown in the present thesis tell us that the charge can stay for even days after the end of charging event. The remaining charge will be added as the initial charge in the next charging event. To make conservative prediction of the spacecraft charging, it is safer to use the value evaluated in this research. Tables 4.5 and 4.6 list the surface and volume resistivity of virgin and AO-polyimide, respectively.

Table 4.5: Surface resistivity of the virgin and AO-exposed samples.

Sample condition	Exp. No.	Surface resistivity 10^{17} Ω/□	Avg. 10^{17}Ω/□	Sd. Deviation 10^{17}Ω/□
Virgin	1	2.8	2.3	0.92
		3.6		
	2	2.8		
		1.8		
	3	1.3		
		1.4		
AO-exposed	4	4.5	5.8	1.8
		7.1		

Table 4.6: List the volume resistivity of the virgin and AO-exposed samples.

Sample condition	Exp. No.	Volume Resistivity $10^{16}\,\Omega$m	Avg. $10^{16}\Omega$m	Sd. Deviation $10^{16}\Omega$m
Virgin	1	1.0	2.2	1.1
		0.89		
	2	2.2		
		2.2		
	3	3.1		
		3.5		
AO-exposed	4	1.8	1.7	0.14
		1.6		

The analysis result for the simulation of equating Eq. [5] and experimental results of potential decay for AO-exposed sample is shown in Figure 4.19. This shows that the theoretical plot and experimental plot match each other, verifying the Eq. [5].

The value of surface resistivity was found in the order of $10^{17}\Omega/\square$, whereas the value of bulk resistivity was found in the order of $10^{16}\Omega$m. The value of surface resistivity was found to increase by a factor of more than 2, whereas the volume resistivity was found to decrease slightly for AO-exposed sample. It shows that AO-exposure affects the value of surface resistivity by a factor of two; this can be attributed to the change in surface morphology. The AO induced change on surface morphology makes the flow of electron difficult. Small decrease in volume resistivity was reasonable considering that the AO-exposure cause the loss of certain amount of thickness of the sample. The increase in the surface resistivity perhaps causes the increase in the depth of the surface potential well, which makes the flow of electron difficult further difficult in insulator. This aspect need to be investigated for further understanding. The small decrease in volume resistivity of AO exposed polyimide is due to the change in thickness of the polyimide due to AO erosion, however, as the thickness

of 25μm was taken for the simulation purpose for both virgin and AO-exposed sample. Thickness change should not affect the volume resistivity in theory.

The higher value of surface and bulk resistivity means that the material can be considered as insulator for the spacecraft simulation. This change in resistivity will not affect the spacecraft charging to a significant limit as the value of resistivity is too high for the electron propagation on the surface.

4.3 Conclusion

- It found that the AO-exposure changes the surface morphology of silver and polyimide.
- It found that the AO-exposure caused loss certain amount of thickness.
- It was found that AO-exposure increases the presence of oxygen and decreases the presence of carbon.
- We found that the surface resistivity of AO-exposed polyimide is more than two times that of virgin polyimide.
- We found that the volume resistivity of polyimide decreases slightly due to AO exposure of 10years equivalent at 800km in altitude due to the change in the thickness of sample.

4.4 References

1. Rooij A. D.: The oxidation of silver by atomic oxygen, product assurance safety department, ESA journal, Vol. 13, 1989, pp. 363-383, http://esmat.esa.int/Atox_on_Ag.PDF

2. Rooij A. D.: Exposure of silver to atomic oxygen, product assurance safety department, ESA document, ESTEC, Noordwijk, The Netherlands,

http://esmat.esa.int/Publications/Published_papers/Exposure_of_Silver_to_Atomic_Oxygen.pdf

3. Chambers A. R., Harris I. L., and Roberts G. T.: Reactions of spacecraft materials with fast atomic oxygen. Materials Letters, Vol. 26, 1996, pp. 121-131.

4. Tagawa, M., Yokota, K., Kishida, K., Okamoto, A. and Minton, T. K.: Energy Dependence of Hyperthermal Oxygen Atom Erosion of a Fluorocarbon Polymer: Relevance to Space Environmental Effects, ACE Appl. Mater. Interface, Vol. 2, No. 7, 2010, pp. 1866-1871.

5. Bank B. B., Groah K. K. de. And Miller S. K.: Low Earth Orbital Atomic Oxygen Interaction with Spacecraft Materials, NASA/TM- 2004-213400, Nov. 2004.

6. Dooling D., and Finckenor M. M.: Material Selection Guidelines to Limit Atomic Oxygen Effects on Spacecraft Surface, NASA/TP- 1999- 209260, June 1999.

7. Wang Pu Sen: A characterization of Kapton polyimide by X-ray photoelectron spectroscopy and energy dispersive spectroscopy, Journal of Materials Sciences, Vol. 23, 1988, pp. 3987-3991.

8. Zeng D. W., Yung K. C. and Xie C. S.: XPS investigation of chemical characteristics of kapton film ablated by a pulsed TEO CO_2 laser, Surface and coating technology, Vol. 153, No. 2-3, 2002, pp. 210-216.

9. Sakurai K., Ezura Y., Morioka Y., Watanabe R., Meguro A., Miyake H., and Nita K.: Temperature Control for Volume Resistivity Measurement, Proceedings of the 6th Spacecraft Environment Symposium, 2009, ISSN 1349-113X, JAXA-SP-09-006, pp. 236-241 (In Japanese).

10. Dennison, J. R., Bruson, J., Swaminathan, P., Wesley, N. and Frederickson, A. R.: Method of High Resistivity Measurement Related to Spacecraft Charging; IEEE transaction on plasma society, Vol. 34, No. 5, 2006, pp. 2204-2218.

11. Frederickson, A. R. and Dennison, J. R.: Measurement of Conductivity and Charge Storage in Insulators Related to Spacecraft Charging, IEEE transactions on nuclear science, Vol. 50, No. 6, 2003, pp. 2284-2291.

12. ASTM D-257-7: Standard Test Methods for DC Resistance or Conductance of Insulating Materials, Developed by Subcommittee: D09.12, DOI: 10.1520/D0257-07.

Chapter 5: Summary

5.1 Conclusion of this study

Our designed facility generates atomic oxygen environment of Lower Earth Orbit having velocity 8-12 km/sec and comparatively higher flux for the quick degradation of surface materials. AO generation was confirmed using emission spectroscopy. AO velocity and hence energy was measured by using TOF technique. AO flux and fluence were measured using silver-coated QCM and polyimide-coated QCM. The local fluence per pulse was of the order of $2x10^{19}$atoms/m^2 at a distance of 0.4m from the nozzle. These oxygen atoms interact with the surface materials and cause the change in surface morphology and hence surface properties. The material degradation experiments were carried out and the change in surface morphologies and properties of materials was studied. It was found using SEM images that the surfaces of silver and polyimide were affected due to interaction with atomic oxygen. The SEM image's change in case of silver is due to the formation of silver oxide on surface because of the reaction with atomic oxygen. The change in surface morphology of polyimide is due to removal of materials from the surface.

The investigations of surface charge decay on polyimide using the discussed electrode configuration has been found suitable for surface and volume resistivity measurement. The mathematical formulation discussed earlier also shows good agreement with experimental data. It has been observed that the AO-exposure causes the increase in surface resistivity by a factor of more than two and does causes a decrease in volume resistivity by smaller factor for the given AO fluence. Since the surface resistivity is dependent on surface structure, its values have been affected by AO exposure. The change in the value of volume resistivity is attributed to the loss in thickness of the materials due to AO-exposure. Spacecraft charging simulation tools, like MUSCAT should use the same value of volume resistivity and change

value of surface resistivity for simulating charging environment at the end of satellite life as it is used in the beginning of life simulation.

5.2 Future Works

There are some issues that should be investigated in future regarding the improvement of this study, which can be summarized as follows:

In order to simulate the atomic oxygen environment more similar like LEO, the energy distribution of generated AO inside chamber will be controlled.

In resistivity measurements, we should increase the number of samples by changing the AO exposure fluence to quantify the change of surface resistivity. Other spacecraft insulator materials shall also be tested to see the differences among the materials.

The detailed analysis of the surface to investigate the mechanism of resistivity change will also be necessary.

Appendix

1. Introduction to MSIS-E-90

NASA website provides the service for the calculation of different gases species concentration. One can download data from this website for the atomic oxygen density with respect to altitude and solar condition. The link for website is

http://omniweb.gsfc.nasa.gov/vitmo/msis_vitmo.html

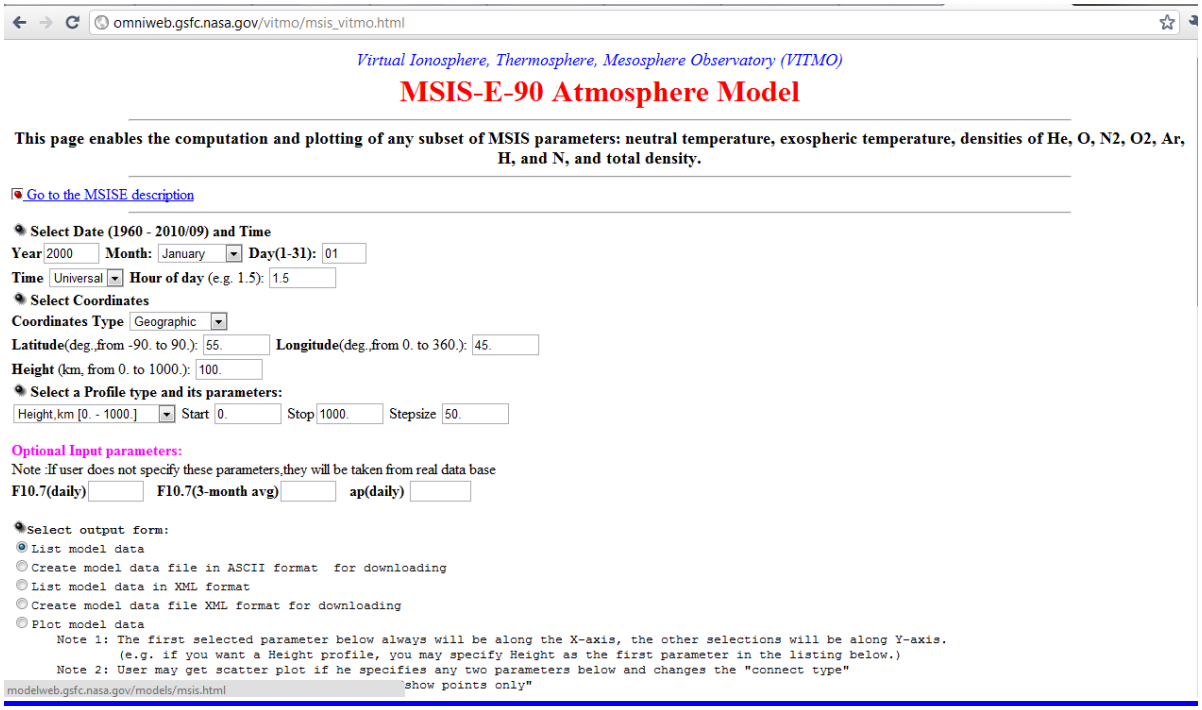

From this source we get the density profile for the different orbits of LEO. We convert this density profile in flux of atomic oxygen after multiplying with the orbital velocity of satellite. This gives the flux for the given orbit in LEO.

2. Calculation of Flux/Fluence using Kapton

The AO fluence was calculated using the following formula:

$F = \Delta M / \rho A E_y$

Where,

F = AO fluence (atoms/cm^{2}s),

ΔM = Mass loss of the Kapton sample (g),

ρ = The density of Kapton (g/cm^3),

A = Sample surface area (cm^2) and

Ey = The erosion yield of Kapton (Ey = 3.0 x 10^{24} cm^3/atom).

3. Calculation of Flux/ Fluence using silver

- Effective mass gain for X pulse = Y g/cm^2
- Mass gain for one pulse = Y/X g/cm^2

  = X/Y g/cm^2
- Mole gain = (X/Y) g/cm^2 / 16 grammole^{-1}

  = (X/ 16Y) molecm-^{2}
- Molecular gain = (X/16Y) mole x 6.023 x 10^{23} atoms/mole

  = (6.023 x 10^{23} x X/ 16 Y) atoms cm^{-2}

Flux = (6.023 x 10^{23} x X/ 16 Y) atomscm $^{-2}$ per shot

Fluence = Flux x No. of pulse shot used